Joris Tiebosch

# Photon-bunching in ground-based submillimeter-wave astronomy

TU Delft

# Photon-bunching in ground-based submillimeter-wave astronomy

By

J.P. Tiebosch

in partial fulfilment of the requirements for the degree of

**Bachelor of Science**
in Applied Physics

at the Delft University of Technology,
to be defended publicly on Monday February 14, 2022, at 9:00 AM.

| | | |
|---|---|---|
| Supervisor: | Dr. A. Endo | |
| Thesis committee: | Prof. dr. J.J.A. Baselmans, | TU Delft |
| | Prof. Dr. A.F. Otte, | TU Delft |
| | Dr. M. Rybak, | TU Delft |

An electronic version of this thesis is available at http://repository.tudelft.nl/ and https://joristiebosch.github.io/thesis/

TU Delft

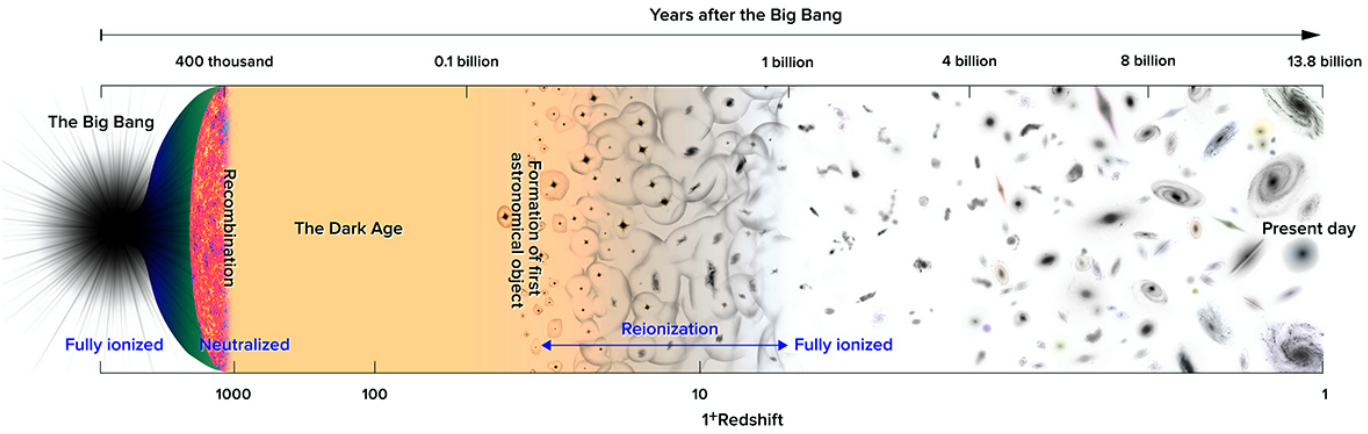


*Figure 1.1. Looking back into history through redshift. The DESHIMA spectrometer is mainly interested in the reionization era of the universe. Image taken from [1]*

# Abstract

In order to investigate the forming of galaxies, astronomers look back in time using (sub)-mm observations. DESHIMA (the Deep Spectroscopic High-Redshift Mapper) is a 347 channel superconducting spectrometer with spectral resolution $R = \frac{\nu}{\Delta\nu} = 500$ that operates in the range of $220\ \mathrm{GHz}$ to $440\ \mathrm{GHz}$ and can therefore accurately measure the frequency of spectral lines in order to calculate redshift $z$.

This report investigates the sensitivity of DESHIMA-like spectrometers by investigating photon noise due to Poisson and bunching effects. It gives a broad overview of photon statistics and explains, through an analogous model, that photon bunching occurs due to an underlying change in the probabilistics, rather than the act of detecting itself. After that I investigate photon and quasiparticle recombination noise for a DESHIMA-like spectrometer with Lorentzian filters and find a closed form equation for Noise Equivalent Power per channel for a constant power spectral density arriving at the filters.

$$\mathrm{NEP}_\tau^2 = \frac{1}{\tau}\left(h\nu\eta\mathrm{PSD}\Delta\nu + \frac{2}{\pi}\eta^2\mathrm{PSD}^2\Delta\nu + \frac{4\Delta_{\mathrm{Al}}}{\eta_{\mathrm{pb}}}\eta\mathrm{PSD}\Delta\nu\right) \tag{1.1}$$

where $\eta$ is $\pi/4$ times the peak hight of the Lorentzian, the average transmission over the $\mathrm{FWHM}$ of the Lorentzian. Previously the bandwidth of the filters was assumed to be negligible, resulting in an overestimation of the bunching. Because the photons that are impinging on the detector span a bigger bandwidth, the bunching is a factor of $\pi/2$ smaller than previously approximated.

This $\mathrm{NEP}_\tau$ is defined at an integration time of $\tau = 0.5\ s$. For other integration times this is scalable through:

$$\mathrm{NEP}_\tau = \frac{1}{\sqrt{2\tau}}\mathrm{NEP}_{\tau=0.5\mathrm{s}} \tag{1.2}$$

This will however only hold while the integration time is much bigger than the coherence time $\tau \gg t_{\mathrm{coh}}$. Because of the correlation between photons arriving shorter than a coherence time apart, the scaling of the $\mathrm{NEP}_\tau$ drops in cases when $\tau \gg t_{\mathrm{coh}}$.

Finally I propose and describe modifications to the sensitivity model DESHIMA uses. The following features have been be improved and added:

### Integrate over the entire power spectrum when calculating photon noise

I use an integral expression for photon noise found in the literature and integrate over it using a Riemann sum to calculate the photon noise per channel. This improves accuracy, in particular in local extrema, for example at frequencies close to the emission lines of water and oxygen, where the loading of the side bands smooths out the $\mathrm{PSD}$ at the center frequency.

### Use arbritatry filter designs loaded from a file

I design the modifications in such a way that an arbitrary filtershape can be loaded in and the sensitivity can be calculated from it. These can include lab measurement and simulations based on the full circuit model, both varying wildly from perfect Lorentzians. This enables a more robust estimation of the instrument performance on sky.

### Improve estimations of the quantities that express sensitivity

Finally I will transform the calculated $\mathrm{NEP}$ to quantities like the noise equivalent flux density $(\mathrm{NEFD})$ to show the sensitivity of the system in an astronomical measurement. This was previously done by approximating the $\mathrm{PSD}$ as flat over the filter channel, but I have improved on this by taking the entire range of the filter into account for both continuum and spectral sources separately. For calculating the sensitivity of line emissions the $\mathrm{NEP}$ can also be compared to frequency-integrated signal power at the detector, to be calculated separately.

I compare the proposed modifications to the old model, which has previously been compared with measurement results, and use it to validate the changes. Other than the previously mentioned factor of $\pi/2$ for the bunching term and the smoothing out in local extrema, the modified simulation results are similar to the old model. This is because the Lorentzian filters have a small bandwidth $\nu \gg \Delta\nu$, such that the previous narrowband approximation held for most non-extreme cases.

The figures in this thesis are interactive. That means that you can drag over an area to zoom as well as toggle traces on and off and hover over them to inspect the data.

1. [1]D. R. Wilkins and S. J. Crass, “Institute of Astronomy,” *ALMA detects the most distant oxygen ever | Institute of Astronomy*. University of Cambridge, Jun-2016 [Online]. Available at: https://www.ast.cam.ac.uk/content/alma.detects.most.distant.oxygen.ever

# Introduction

Introduction to Radio Astronomy, Spectrometers and DESHIMA

Jan 7, 2022 • 10 min read



The ultimate weapon in the arsenal of a historian just might be a time machine. While historians can infer a lot from written texts and archaeological digs, no substitute can outperform being in the past and observing. Unfortunately for historians, a time machine has yet to be invented. Astronomers, however, are more fortunate in this field.

Around the turn of the century, new physics was being invented to explain previous observations and conclusions. As a result, it was understood that the speed of light was finite and moreover a constant, independent of the speed of the observer, which Albert Einstein postulated in 1905[1]. It logically follows that the arriving light from distant stars and galaxies is reaching us from the past.

Since light is a wave traveling through the expanding universe, it undergoes Doppler shift and therefore cosmological objects that move away from the observer undergo a shift in the frequency of light. This is known as redshift, because the expanding wavelength means that visible light would shift towards the red end of the spectrum. Just 12 years after Einstein's discovery, American Astronomer Vesto Slipher [2] discovered the redshift of distant galaxies and with it cosmological spectroscopy was born.

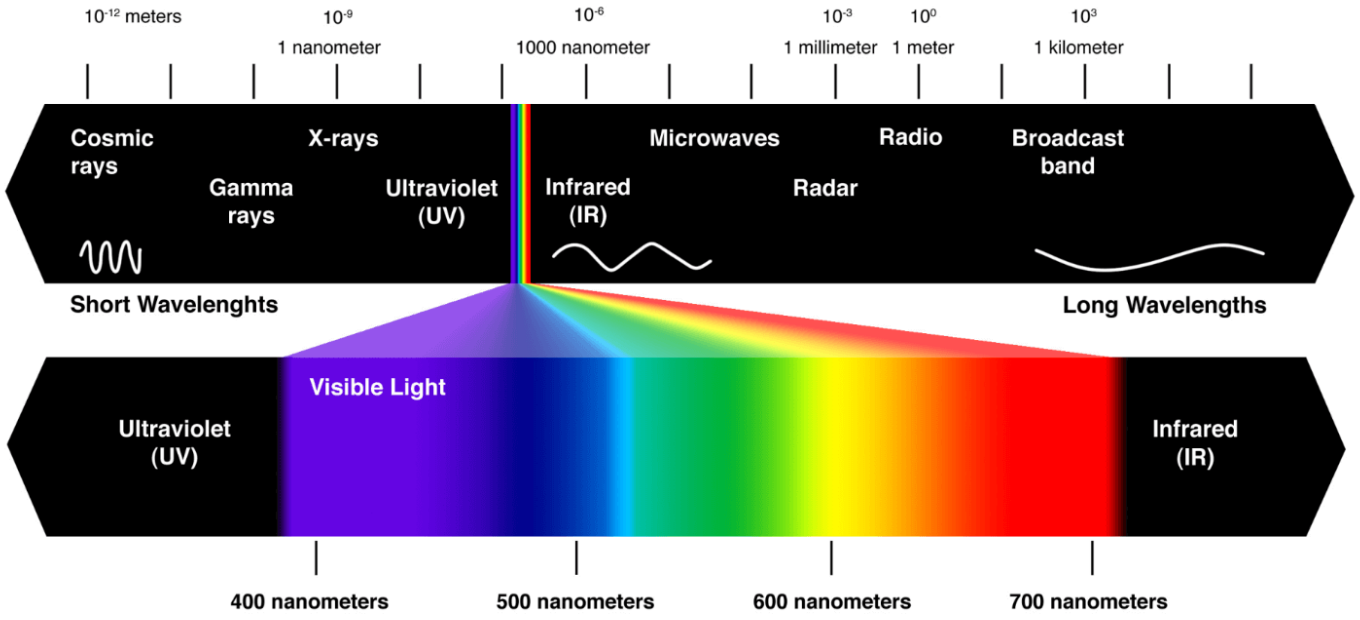


*Figure 2.1. A part of the light spectrum. Visible light is expanded to show the different colors. Note how red light in the visible spectrum has a longer wavelength, giving redshift its name. Image taken from [3]*

Combining these effects gives us a sort of astronomical time machine: looking far out into the cosmos means looking into the past where the universe was much younger. However, just pointing a telescope at the night sky poses a few problems.

## Cosmological formation

Understanding how stars and galaxies form out of a uniformly gaseous universe is one of the largest areas of research in modern physical cosmology. The physical processes by which these happen might be well understood, but the amount of possible initial values of these processes are so vast that they can have wildly different outcomes[4]. Looking at these events occurring in the distant universe (and therefore distant past) is therefore important to further the understanding of the forming of the universe.

Unfortunately, much of the formation of these cosmological bodies happens inside thick dust clouds which are opaque to visible light and are therefore investigated using what is called sub-millimeter astronomy: astronomy ranging from $100\ \mu\mathrm{m}$ to about $1\ \mathrm{mm}$. In frequency terms, following

$$f = \frac{c}{\lambda} \tag{2.1}$$

this corresponds with about $150\ \mathrm{GHz}$ to $1500\ \mathrm{GHz}$.

*Figure 2.2. The Messer-16 nebula, dubbed "The Eagle", captured by the Hubble Space Telescope is an example of a dust cloud that is opaque to visible light. Image taken from [5]*

## Redshift

As mentioned before, the redshift of light gives us the opportunity to calculate the relative speed and therefore distance and age of astronomical sources. By the term "redshift", I mean the following formal

definition [6]

$$1 + z = \frac{f_{\text{emit}}}{f_{\text{obs}}} \tag{2.2}$$

where $z$ denotes redshift and $f_{\text{emit}}$ and $f_{\text{obs}}$ denote the emitted and observed frequency of a signal respectively. In order to calculate redshift we therefore need to know both frequencies.

## Emitted frequency

Quantum mechanics tells us that the electron configuration in atoms exist in quantized states. That is to say: they can move between defined states, but not in the continuum inbetween. When an atom moves from one configuration to a higher state energy is absorbed, when it moves to a lower state energy is emitted. These quantized energy states give way to what is known as spectral lines, where a specific wavelength is known to be emitted by specific atoms.

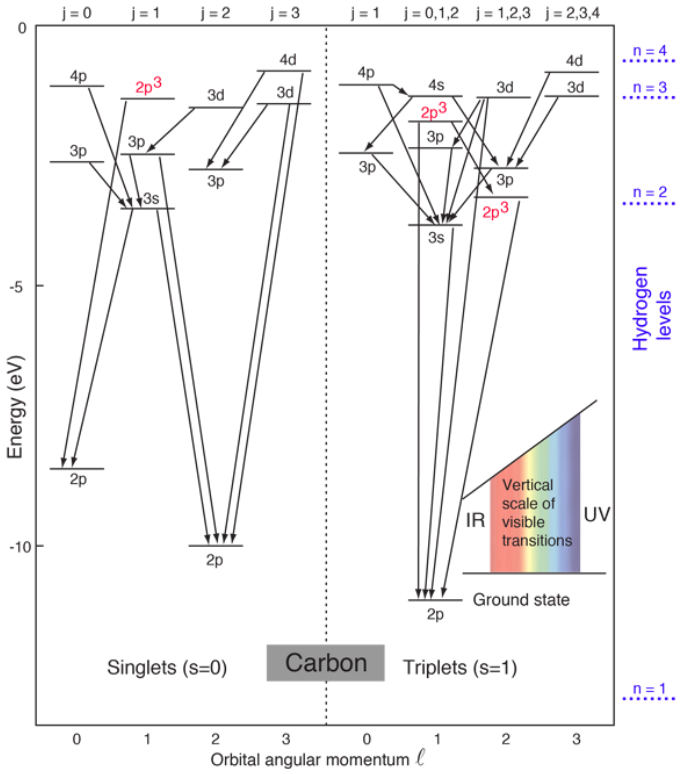


*Figure 2.3. A few energy states of carbon. Note how higher energy gaps result in shorter wavelengths. Image taken from [7]*

The energy gaps shown are to wide to emit photons in the submillimeter wavelength range DESHIMA operates in, however *fine structure* spectral lines are in the correct wavelength gap. This is the splitting of two similar states due to spin and relativistic effects. Another mechanism by which molecules emit spectral lines is due to the shifting in quantized rotational states. The various states astronomical sources split between are well known and therefore can be tracked to measure redshift.

This becomes clear when we look at the spectral flux density $E_{e,\nu}$ of a galaxy, simulated with the Python module `galspec` [8].

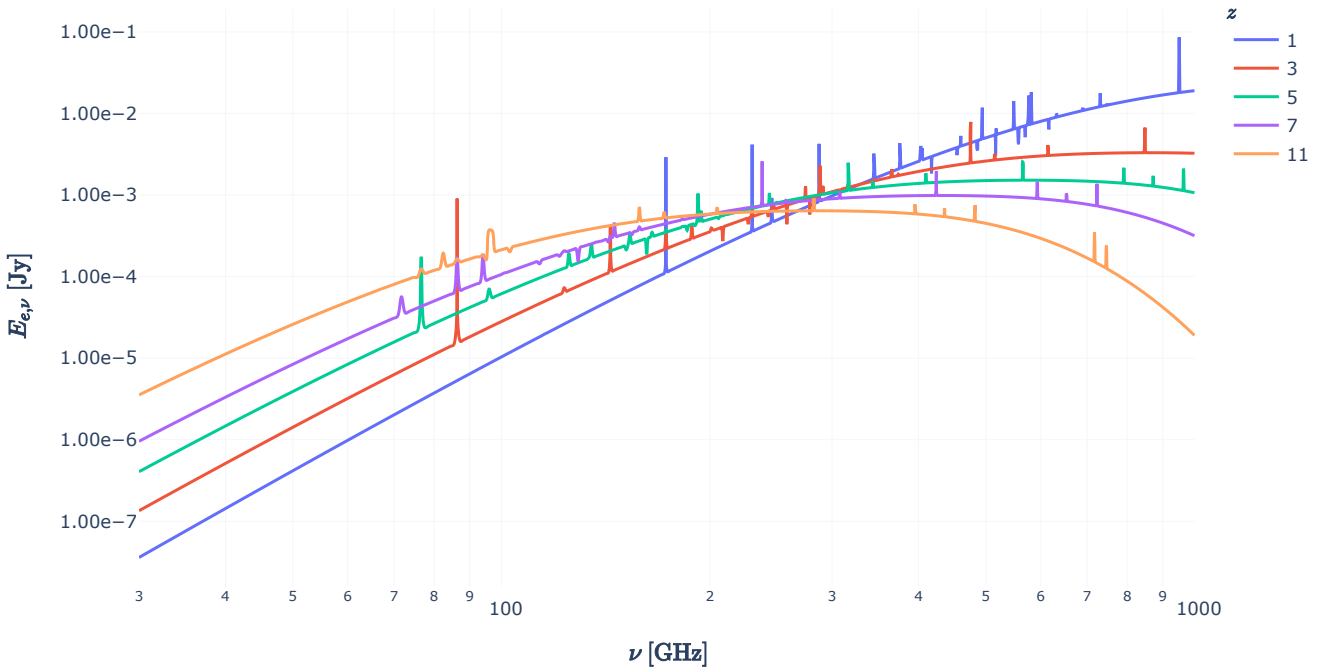


*Figure 2.4. The spectral flux density of a simulated galaxy with different redshifts. Here the spectral flux is given in units of Jansky, which is equivalent to $10^{-26}$ $WM^{-2}Hz^{-1}$*

From the figure it is clear that with higher $z$ the peaks move further to the left, towards lower frequencies and therefore longer wavelengths. If one were to look for peaks in incoming signal and measure the wavelength at which these peaks occur, the redshift and thus age of a galaxy can be detected. Besides these clear spikes in the flux density, the galaxy also emits broad spectrum thermal noise, originating from the black-body emission of interstellar dust.

## Observed frequency

In order to know the wavelength of these spectral lines at our detection point, we need to measure the specific frequency of an incoming photon in a spectrometer. This can be done using a *Coherent Heterodyne receiver*, except that these devices work to a bandwidth of about $36\ \mathrm{GHz}$[9], much lower than the spectral range we are interested in as shown above.

Traditional photon detectors, at their core, work by converting an incoming photon into a charge or current, which means that the specific momentum, energy or frequency of the photon is lost. A way around this is to move the incoming photons depending on their wavelength, such as what happens in an optical prism.

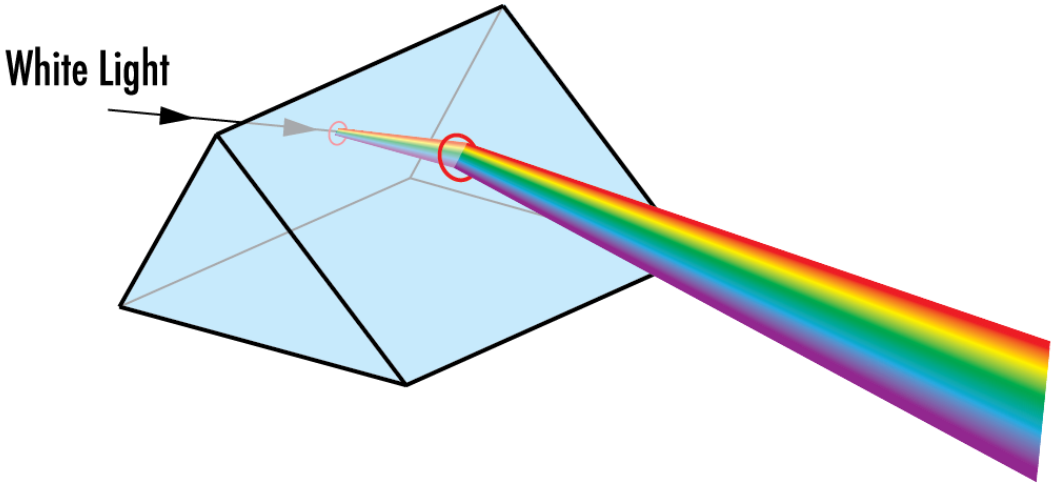


*Figure 2.5. When a photon enters the prism, its angle changes depending on its wavelength. Image taken from [10]*

This is how a lot of spectrometers work, but due to the long wavelengths and wide redshift range $(1 + z \approx 1 - 10)$[11] of the signals involved in galaxy spectroscopy this approach is cumbersome. The long wavelengths and range means that the spectrometer needs to physically large and to reduce the noise they need to be cooled, making the entire system even larger. This means that these devices are inherently not scalable to multiple pixels.

## DESHIMA

DESHIMA, short for the Deep Spectroscopic High-Redshift Mapper, is a spectrometer developed by a joint team of researchers from various institutions including the TU Delft and SRON that takes another approach[11][12]. DESHIMA uses a series of bandpass filters on a superconducting chip to direct incoming photons into bins, where they are detected by Microwave Kinetic Inductance Detectors (MKIDs). The advantage of this approach is that the spectrometer itself is really small, taking up just a few squared centimeters and is therefore easily scalable to $> 100$ spectrometer pixels[11].

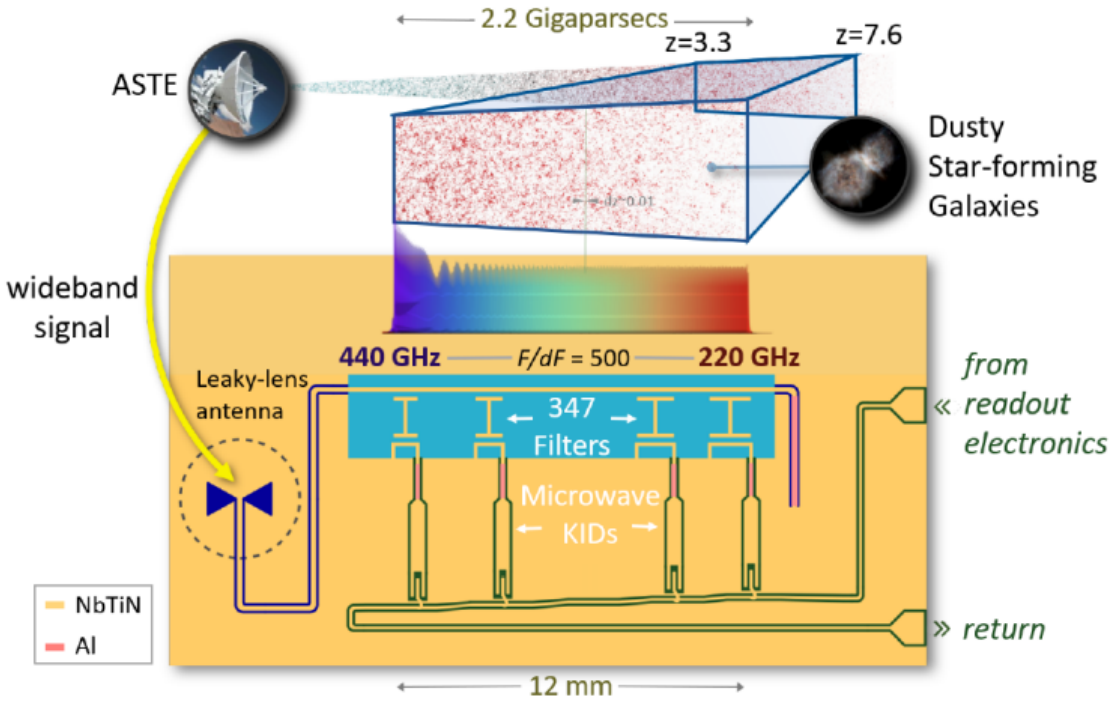


*Figure 2.6. A schematic overview of the DESHIMA 2.0 chip. Image taken from [13]*

DESHIMA is placed on ASTE, a ground-based sub-millimeter telescope near the ALMA site in the Atacama Desert.

*Figure 2.7. A panoramic shot from the ASTE site in the Atacama Desert. The building on the left is NANTEN-2 whereas the building on the left is ASTE. Image taken from [14]*

## Ground-based submillimeter astronomy

While the ASTE site is high up in the Atacama desert, the telescope still needs to look through some atmosphere when doing observations. Since cosmological object of interest are often far away and therefore very dim, they are much dimmer than the effects from the atmosphere. The atmosphere is almost completely opaque at some frequencies DESHIMA operates in and this loads the antenna dish because it is much hotter and therefore brighter than the astronomical source.

Below the atmospheric loading at the ASTE site is calculated by the software package `deshima-sensitivity` [15] and plotted with a galaxy spectrum synthesized by `galspec`:

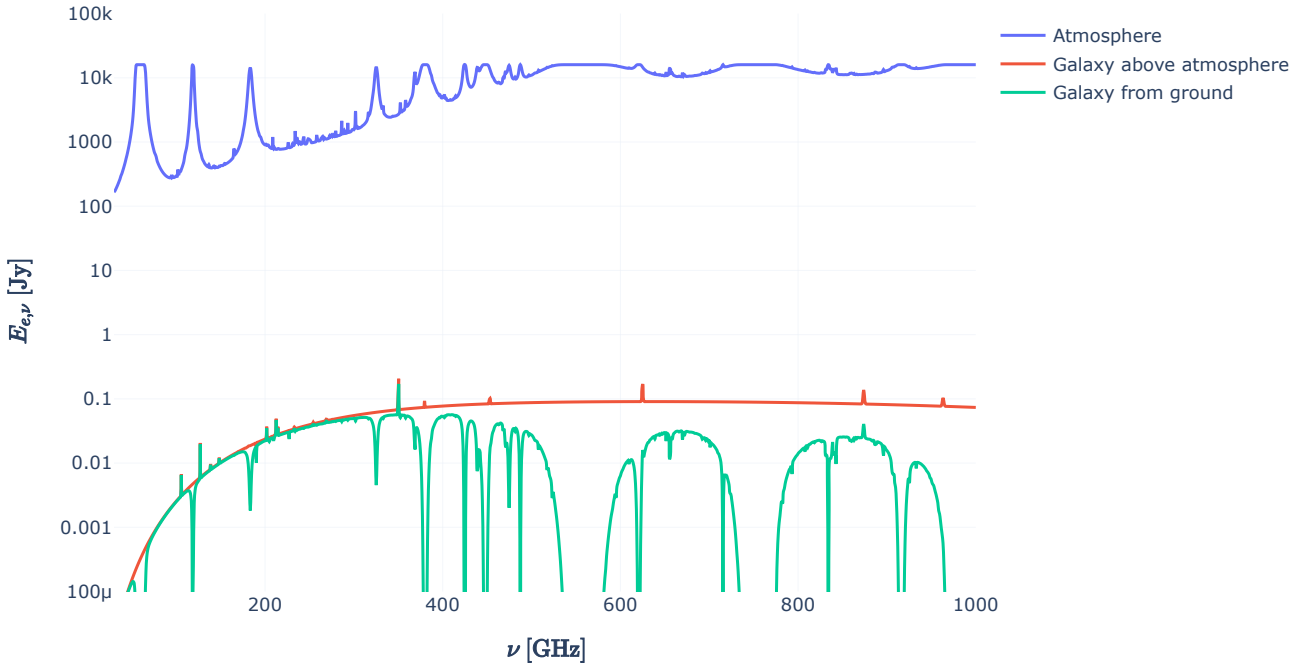


*Figure 2.8. Comparing the spectral flux density of atmospheric loading to loading from an astronomical source. The former is over 3 orders of magnitude brighter. Note how the atmospheric transmission means that for some frequencies the spectrum is barely usable.*

The atmosphere is over 3 orders of magnitude brighter than the galaxy spectrum before the latter is attenuated. After the atmospheric attenuation the difference is even bigger. Therefore modeling the expected loading from the atmosphere and the entire chain from antenna to detector is important to be able to do measurements and to find the signal within the noise. `deshima-sensitivity` [15] was designed to do this, but takes some approximations that were deemed too reductive.

## This Project

The current version of `deshima-sensitivity` does not take filter profiles into consideration when calculating the power received on each channel. It samples the power spectral density calculated to be at the filter's center frequency and multiplies this with the filter bandwidth, creating a crude box filter. While this approach holds for flat power spectra, it doesn't quite hold for spectra like the one above.

In this project I will modify the existing `deshima-sensitivity` package to more accurately resemble the DESHIMA 2.0 filter profiles and therefore the spectrometer as a whole. In order to do so, I will first need to dive into the DESHIMA system in more depth and then give an overview of *photon statistics* and the associated photon noise. Finally I will model the system and compare it with previous versions of `deshima-sensitivity`.

# Bibliography


1. [1]A. Einstein, "Zur Elektrodynamik bewegter Körper," *Annalen der Physik*, vol. 322, no. 10, pp. 891–921, 1905, doi: 10.1002/andp.19053221004.
2. [2]V. M. Slipher, "Radial velocity observations of spiral nebulae," *The Observatory*, vol. 40, pp. 304–306, 1917, doi: 10.1002/andp.19053221004.
3. [3]A. Lemke, "The visible light spectrum," *Once Inc.* Aug-2020 [Online]. Available at: https://www.once.lighting/visible-light-spectrum/
4. [4]A. Blain, "Submillimeter galaxies," *Physics Reports*, vol. 369, no. 2, pp. 111–176, Jan. 2002, doi: 10.1016/s0370-1573(02)00134-5.
5. [5]R. Garner, "Messier 16 (The Eagle Nebula)," *NASA*. NASA, Oct-2017 [Online]. Available at: https://www.nasa.gov/feature/goddard/2017/messier-16-the-eagle-nebula
6. [6]A. Endo, "Session 2 | Line Emission and Cosmological Redshift ," *EE3350TU Introduction to Radio Astronomy*. Nov-2020.
7. [7]R. Nave, "Carbon Energy Levels," *hyperphysics.phy*. [Online]. Available at: http://hyperphysics.phy-astr.gsu.edu/hbase/Atomic/carbon.html
8. [8]T. Bakx and S. Brackenhoff, "galspec v0.2.6," *pypi.org*. Open Source, Nov-2020 [Online]. Available at: https://pypi.org/project/opensimplex/
9. [9]A. J. Baker, *From z-machines to ALMA: (sub)millimeter spectroscopy of galaxies: proceedings of a workshop held at the North American ALMA Science Center of the National Radio Astronomy Observatory in Charlottesville, Virginia, United States, 12-14 January 2006*. Astronomical Soc. of the Pacific, 2007, p. 375.
10. [10]E. Optics, "Introduction to Optical Prisms," *Edmund Optics*. [Online]. Available at: https://www.edmundoptics.eu/knowledge-center/application-notes/optics/introduction-to-optical-prisms/
11. [11]A. Endo *et al.*, "First light demonstration of the integrated superconducting spectrometer," *Nature Astronomy*, vol. 3, no. 11, pp. 989–996, 2019, doi: 10.1038/s41550-019-0850-8.
12. [12]A. Endo *et al.*, "Wideband on-chip terahertz spectrometer based on a superconducting filterbank," *Journal of Astronomical Telescopes, Instruments, and Systems*, vol. 5, no. 03, p. 1, 2019, doi: 10.1117/1.jatis.5.3.035004.
13. [13]E. et al. Huijten, "TiEMPO: Open-source time-dependent end-to-end model for simulating ground-based submillimeter astronomical observations," *Millimeter, Submillimeter, and Far-Infrared Detectors and Instrumentation for Astronomy X*, 2020, doi: 10.1117/12.2561014.

14. [14]D. R. Jacobsen, “Atacama Submillimeter Telescope Experiment complex, Chile.” English Wikipedia, 06-Jul-2008 [Online]. Available at: https://commons.wikimedia.org/w/index.php?curid=60009729
15. [15]A. Endo and A. Taniguchi, “deshima-sensitivity v0.3.0,” *pypi.org*. Open Source, Jun-2021 [Online]. Available at: https://pypi.org/project/deshima-sensitivity/

# DESHIMA

A short overview of the DESHIMA spectrometer, the optical chain and the physics behind the detectors

Jan 6, 2022 • 8 min read



In 2017, as part of the first light campaign, the first DESHIMA device was proven to work as expected when mounted to the ASTE telescope[1], but was limited in scope. The chip had just 49 channels and a spectral resolution of $\nu/\Delta\nu \approx 380$, with a spectral range of $327\ \mathrm{GHz}$ to $377\ \mathrm{GHz}$. This proof of concept led to the development of DESHIMA 2.0 and the Science Verification Campaign[2]. With 347 channels in the range of $220\ \mathrm{GHz}$ to $440\ \mathrm{GHz}$ and a spectral resolution of $\nu/\Delta\nu \approx 500$, DESHIMA 2.0 is much more capable. Besides the obvious bandwidth and channel upgrades, the sensitivity has also been increased four to eight fold [3]. In this thesis I will be discussing DESHIMA 2.0, but it is entirely applicable to any DESHIMA-type spectrometer.

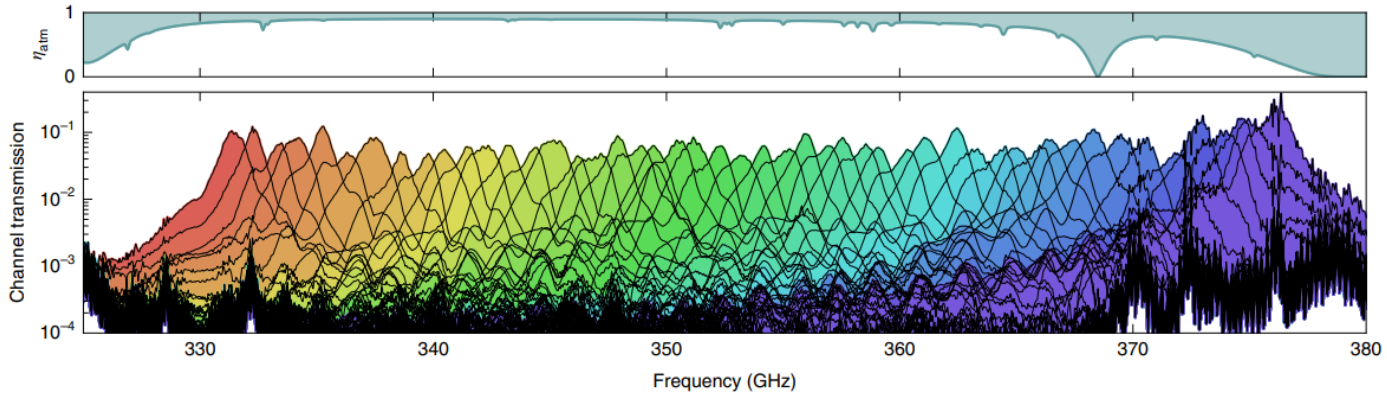


*Figure 3.1. The 49 filter channels and their transmission as measured from the original DESHIMA. Image taken from [1]*

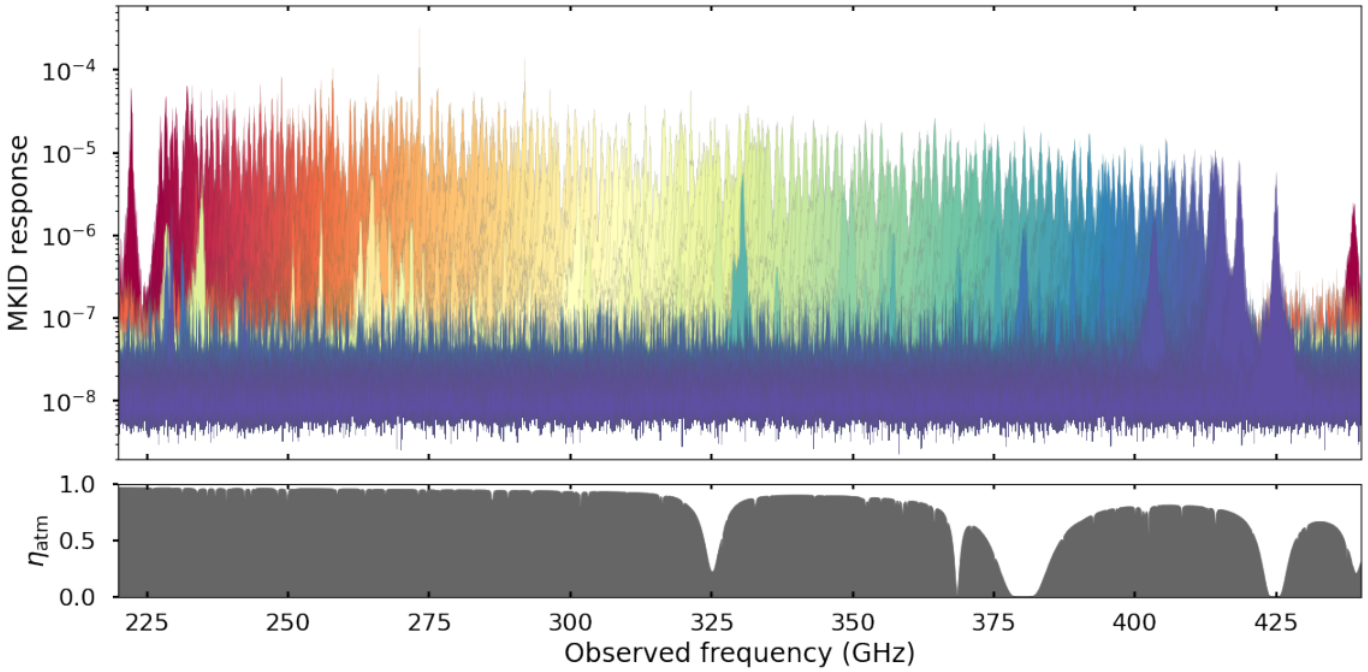


*Figure 3.2. The 347 filter channels and their transmission as measured on DESHIMA 2.0. Image taken from [2]*

## The Optical Chain

As mentioned, DESHIMA is installed on the ASTE radio-telescope in the Atacama desert. This means that the light from distant galaxies travels through the atmosphere towards the dish of the telescope, where it gets reflected to the secondary mirror. The set of primary and secondary mirror is called a Cassegrain reflector and focuses the signal.

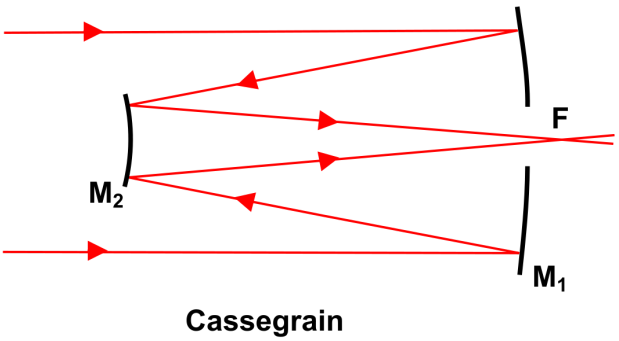


*Figure 3.3. A schematic drawing of a Cassegrain reflector. Image taken from [4]*

After the incoming signal has been focused, it passes a set of mirrors in the telescope cabin and then passes through a window into the cryostat. At a temperature of $4\,\mathrm{K}$ the light passes through a low-pass filter, a third set of mirrors and a polarizer, until reaching the spectrometer chip at a temperature of $120\,\mathrm{mK}$.

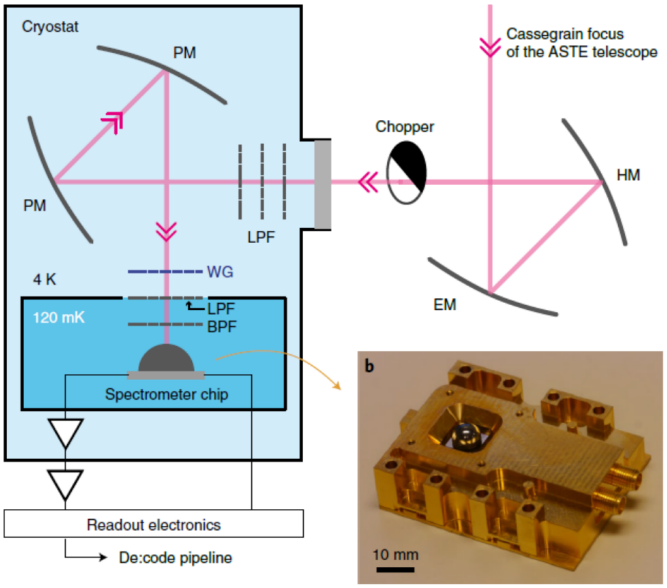


*Figure 3.4. The optical chain of the DESHIMA 1.0 spectrometer. After passing through the Cassegrain reflector, the light hits an ellipsoidal mirror (EM), a hyperbolic mirror (HM), a low-pass filter (LPF), two parabolic mirrors (PM), a wire grid polarizer (WG) a low pass and band pass filter (LPF, BPF) until it hits the spectrometer. DESHIMA 2.0 has too wide a range to use the band pass filter, so it is omitted. Image taken from [1]*

Every optical component has a corresponding efficiency $\eta_{\text{opt}}$ and transmits only a part of the incoming signal $\text{PSD}_{\text{in}}$ while also adding to that signal its own emission $\text{PSD}_{\text{opt}}$, in a process called a radiative transfer[5]:

$$\text{PSD}_{\text{out}} = \eta_{\text{opt}} \text{PSD}_{\text{in}} + (1 - \eta_{\text{opt}}) \, \text{PSD}_{\text{opt}} \tag{3.1}$$

Here $\text{PSD}$ is the power spectral density expressed in units of $[\text{WHz}^{-1}]$, which for the emission of the optical component is given by Johnson-Nyquist[6]:

$$\text{PSD}_{\text{opt}} \, (\nu, T) = \frac{h\nu}{e^{h\nu / k_B T} - 1} \tag{3.2}$$

which depends on both temperature and frequency. Therefore the radiative transfer of the optical chain needs to be calculated across the frequency spectrum for every component at its temperature. This means that the total optical chain is a series of radiative transfers. For a simple two mirror system this is the following

$$\text{PSD}_{\text{in}} \rightarrow \text{M1} \rightarrow \text{PSD}_{\text{intermediate}} \rightarrow \text{M2} \rightarrow \text{PSD}_{\text{out}} \tag{3.3}$$

To simplify the calculations, efficiencies of components at the same temperature can be taken together

$$\begin{aligned} \text{PSD}_{\text{out}} &= \eta_2 \text{PSD}_{\text{intermediate}} + (1 - \eta_2) \, \text{PSD}_{\text{opt}} \\ &= \eta_2 \left( \eta_1 \text{PSD}_{\text{in}} + (1 - \eta_{\text{opt}}) \, \text{PSD}_{\text{opt}} \right) + (1 - \eta_2) \, \text{PSD}_{\text{opt}} \\ &= \eta_1 \eta_2 \text{PSD}_{\text{in}} + \eta_2 \, (1 - \eta_1) \, \text{PSD}_{\text{opt}} + (1 - \eta_2) \, \text{PSD}_{\text{opt}} \\ &= \eta_1 \eta_2 \text{PSD}_{\text{in}} + \eta_2 \text{PSD}_{\text{opt}} - \eta_1 \eta_2 \text{PSD}_{\text{opt}} - \eta_2 \text{PSD}_{\text{opt}} + \text{PSD}_{\text{opt}} \\ &= \eta_1 \eta 2 \text{PSD}_{\text{in}} + (1 - \eta_1 \eta 2) \, \text{PSD}_{\text{opt}} \end{aligned} \tag{3.4}$$

At ASTE, the atmosphere is around $273 \, \text{K}$ and the cabin is $290 \, \text{K}$. as mentioned before the cold optics and the chip are $4 \, \text{K}$ and $120 \, \text{mK}$ respectively. If we plot the $\text{PSD}_{\text{opt}}$ for the different components along with the power a galaxy transmits to a telescope dish with a diameter of $10 \, \text{m}$, we get the following figure:

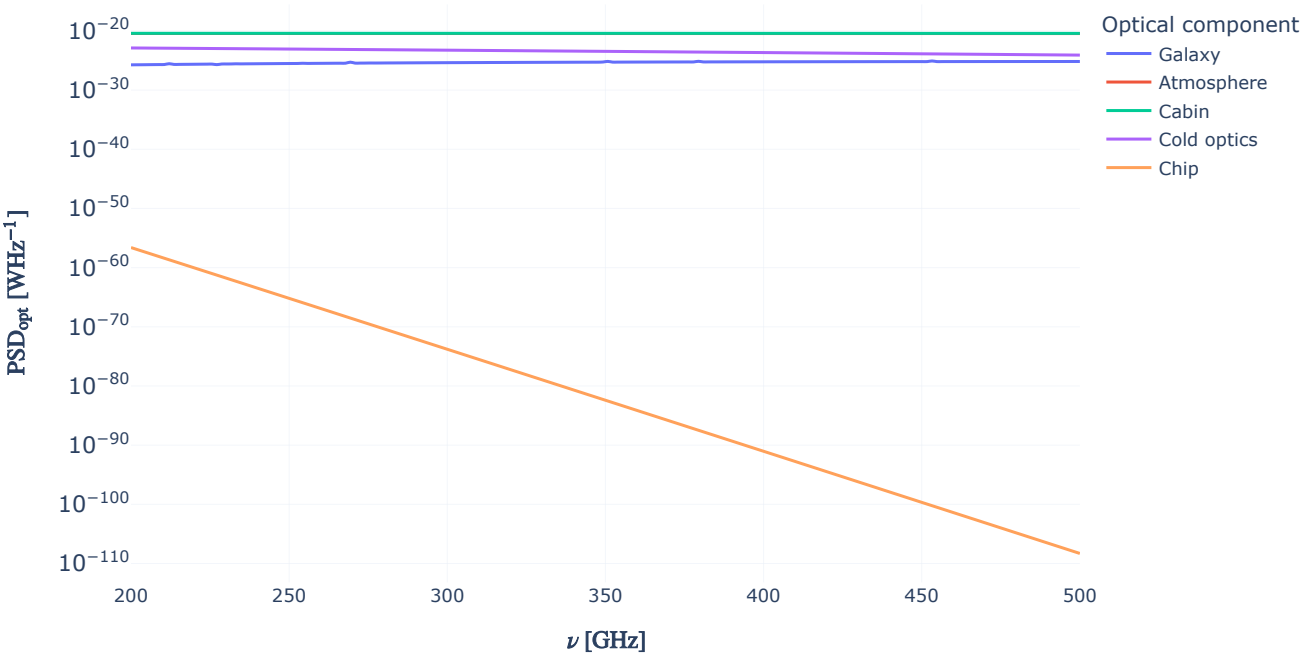


*Figure 3.5. Besides the PSD emitted by the chip, the optical components are much brighter than the astronomical source. Take note that the atmosphere and the cabin are almost at the same temperature and therefore have almost the same PSD.*

As is clear from the figure, the efficiency of all but the chip really matter in the range DESHIMA measures in, which is why they need to be modeled carefully in `deshima-sensitivity`. In order to look at the amount of loading these sections impart on the detector, we can look at the effective power spectral density $\mathrm{PSD_{opt,eff}}$:

$$\mathrm{PSD_{opt,eff}} = \left(1 - \prod_i \eta_i\right) \mathrm{PSD_{opt}} \tag{3.5}$$

with $\eta_i$ the efficiencies of the optical components in the part of the chain that is at the same temperature.

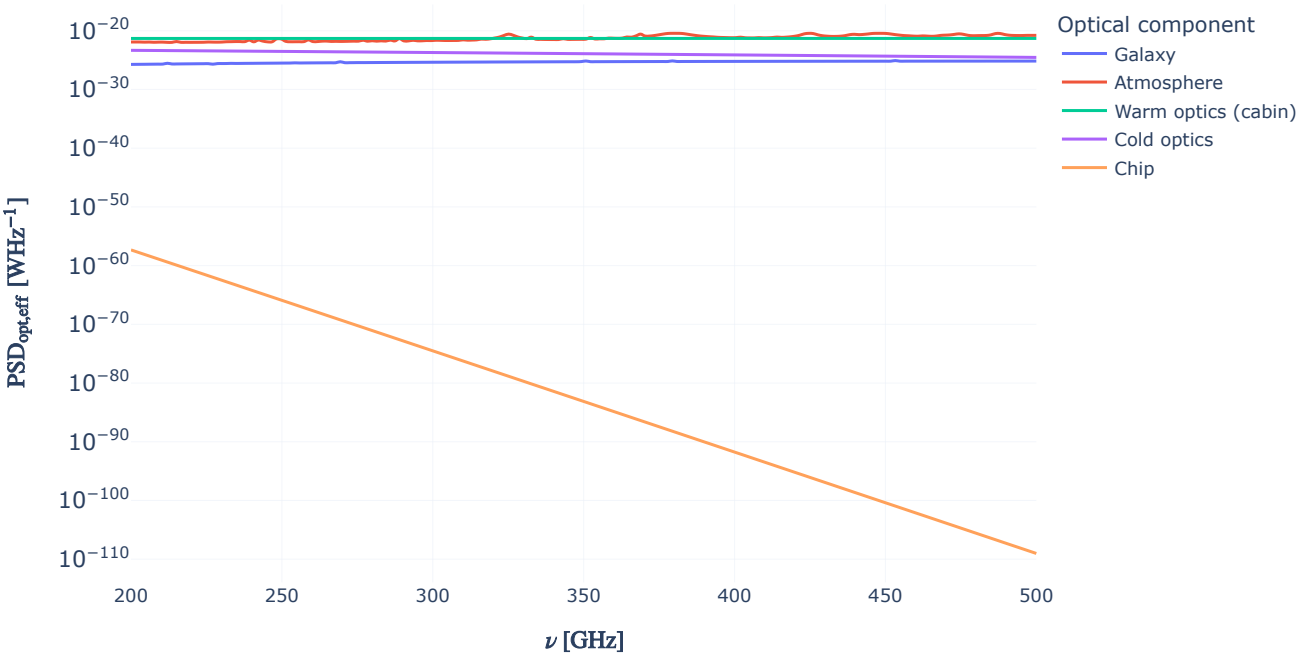


*Figure 3.6. The effective loading from the various optical components. Take note that the simulated galaxy source is still not attenuated*

Because of the faintness of a typical source, everything but the chip is still brighter than the source, while the latter is not even attenuated. From the radiative transfer we have seen that with every optical component the source loses some of its power due to the efficiency of these components, so in actuality the source at the detector would be even less bright.

## The Filterbank

After the optical chain the light is passed to a filterbank containing 347 bandpass filters, with constant spectral resolution $R = \nu/\Delta_\nu = 500$ and a center frequency for the $i^{\text{th}}$ filter given by [7]:

$$\nu_i = \nu_{\min}\left(1 + \frac{1}{R}\right)^i \tag{3.6}$$

with $\nu_{\min} = 220\ \mathrm{GHz}$[3]. This expression ensures that the filter channels are spaced such that the bandwidths of each filters are right next to each other without overlapping, since a constant spectral resolution means the bandwidths get progressively wider as the center frequencies increase.

Due to their spatial efficiency the signal is bandpass filtered by resonators with a Lorentzian pass band[7]. In the figures below a schematic overview of a filter is given and the transmission parameters of this filter are shown.

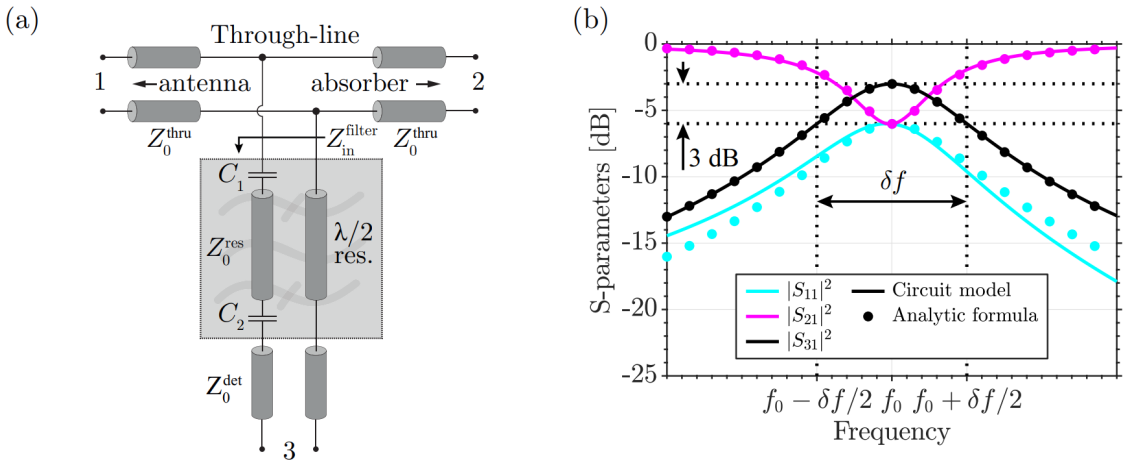


*Figure 3.7. a) A schematic viewing of the filter design. Port 3 is towards the detector. b) The S-parameters of the filter transmission. Here $S_{31}$ is the transmission parameter from the filter input to the detector. Here the solid lines are the simulated circuit and the dots are the analytical approximations. Note the 3dB cutoff point at the bandwidth for the $S_{31}$ transmission. Images taken from [7]*

The transmission from the input to the detector through the filter is given by $|S_{31}|^2$. From [7] we get an approximation for $S_{31}$ around the center frequency of the filter $v_0$ as:

$$S_{31}(\nu) \approx \frac{S_{31}(\nu_0)}{1 + j2Q_l\frac{\nu-\nu_0}{\nu_0}} \tag{3.7}$$

With $j$ the imaginary unit and $Q_l$ the loaded quality factor. This approximation is marked with black dots in the figure above.

In a resonant circuit the quality factor $Q$ is defined as[8]:

$$Q = \frac{\nu_0}{\Delta\nu} \tag{3.8}$$

Therefore, the transmission $|S_{31}|^2$ is given as:

$$|S_{31}(\nu)|^2 \approx \frac{|S_{31}(\nu_0)|^2}{1 + 4Q_l^2\left(\frac{\nu-\nu_0}{\nu_0}\right)^2} = \frac{|S_{31}(\nu_0)|^2}{1 + 4\left(\frac{\nu-\nu_0}{\Delta\nu}\right)^2} = \frac{|S_{31}(\nu_0)|^2}{1 + \left(\frac{\nu-\nu_0}{\gamma}\right)^2} \tag{3.9}$$

with $\gamma = \Delta\nu/2$. This equation describes a Lorentzian with $\gamma$ being the half maximum at half width and $|S_{31}(\nu_0)|^2$ the peak value at $\nu = \nu_0$. As the figure also shows the resonance is tuned such that the bandwidth $\Delta\nu$ is the same as the full width at half maximum. In other words the transmission within the bandwidth is always greater or equal to $50\%$ the peak transmission at the resonance frequency.

Situated after each of these 347 filter channels is a detector to detect the bandpassed signal.

## The Detectors

DESHIMA detects photons using (Microwave) Kinetic Inductance Detectors, or (M)KID for short. These work by exploiting the energy gap in superconductors.

Inside the superconductor electrons are coupled together in Cooper-pairs at energy levels $E_F$. When these pairs get excited, the electrons move as quasiparticles to a higher energy level $E \geq E_F + \Delta_{\text{Al}}$ [9], where $\Delta_{\text{Al}} = 188\ \text{meV}$ the gap energy of an aluminium superconductor[5].

Therefore, if an incoming photon carries enough energy to excite a pair of these electrons, specifically more than $2\Delta_{\mathrm{Al}}$, it increases the number of quasiparticles. This means that the photon needs

$$E = h\nu > 2\Delta_{\mathrm{Al}} \iff \nu \geq \frac{2\Delta_{\mathrm{Al}}}{h} \approx 91\ \mathrm{GHz} \tag{3.10}$$

which is perfect for the $220\ \mathrm{GHz}$ to $440\ \mathrm{GHz}$ range we are interested in.

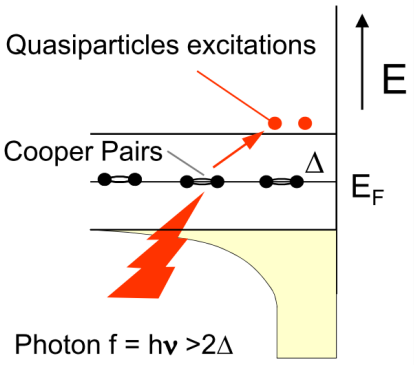


*Figure 3.8. When an incident photon has enough energy to overcome the energy gap, the cooper pair breaks and generates quasiparticles. Image taken from [9]*

## Resonance Circuit

The cooper pairs decrease the inductance[10], so when these are broken the overall inductance increases. In order to measure this change in inductance, the detector is designed as parallel sets of RLC circuits, designed such that the total frequency of the resonance is in the range of $4 - 6\ \mathrm{GHz}$[2].

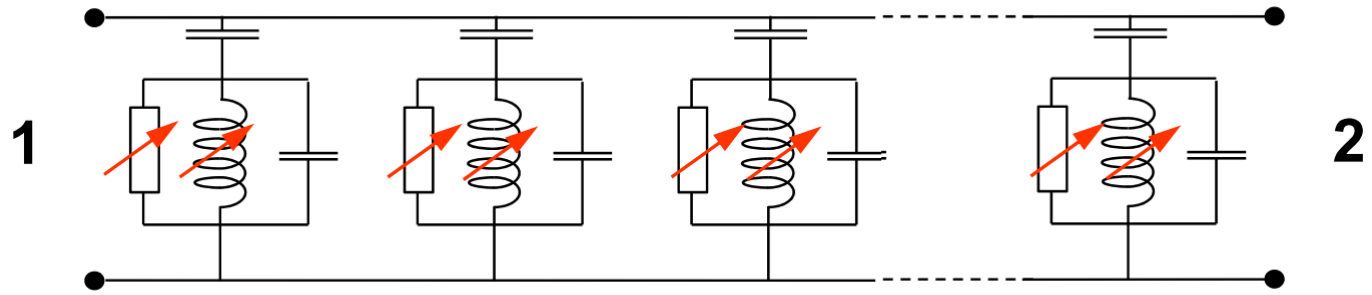


*Figure 3.9. RLC circuits are used to read the change in inductance. Parallel RLC circuits divide the frequency to a range that the read-out electronics can handle. Image taken from [9]*

These circuits are resonant when the reactance of the inductor and the capacitor are equal:

$$X_L = X_C \iff \omega L = \frac{1}{\omega C} \iff \omega_r = \frac{1}{\sqrt{LC}} \tag{3.11}$$

and therefore the resonance gets lowered by a decrease in cooper pairs.

In order to read out the detector, a signal at the resonant frequency is fed into the superconductor. When the resonant frequency decreases, so does the transmission and therefore an increase in power is measured[9].

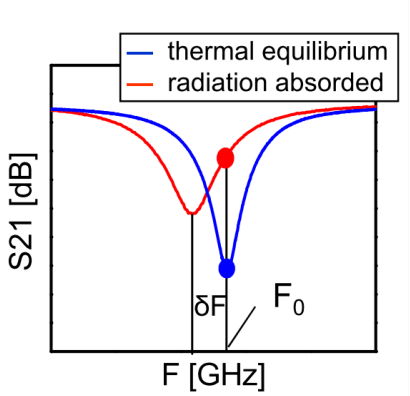


*Figure 3.10. The change in resonance frequency lowers the transmission, therefore increasing the power. This increase in power is measured. Image taken from [9]*

## Bibliography


1. [1]A. Endo *et al.*, "First light demonstration of the integrated superconducting spectrometer," *Nature Astronomy*, vol. 3, no. 11, pp. 989–996, 2019, doi: 10.1038/s41550-019-0850-8.
2. [2]A. Taniguchi *et al.*, "DESHIMA 2.0: development of an integrated superconducting spectrometer for science-grade astronomical observations." 2021.
3. [3]M. Rybak *et al.*, "DESHIMA 2.0: Rapid redshift surveys and multi-line spectroscopy of dusty galaxies." 2021.
4. [4]H. Hahn, "Diagram Reflector Cassegrain." Wikimedia, 01-Apr-2010 [Online]. Available at: https://nl.m.wikipedia.org/wiki/Bestand:Diagram_Reflector_Cassegrain.svg
5. [5]A. Endo and A. Taniguchi, "deshima-sensitivity v0.3.0," *pypi.org*. Open Source, Jun-2021 [Online]. Available at: https://pypi.org/project/deshima-sensitivity/
6. [6]A. Endo, "Session 4 | Photon Noise," *EE3350TU Introduction to Radio Astronomy*. Dec-2020.
7. [7]A. P. Laguna, K. Karatsu, D. Thoen, B. Murugesan rp, A. Endo, and J. Baselmans, "Terahertz Band-Pass Filters for Wideband Superconducting On-Chip Filter-Bank Spectrometers," *IEEE Transactions on Terahertz Science and Technology*, vol. 11, no. 6, pp. 635–646, 2021, doi: 10.1109/tthz.2021.3095429.
8. [8]C. K. Alexander and M. N. Sadiku, *Fundamentals of Electric Circuits*, 7th ed. McGraw-Hill Education, 2021.
9. [9]J. Baselmans, "Kinetic inductance detectors," *Journal of Low Temperature Physics*, vol. 167, no. 3-4, pp. 292–304, 2012, doi: 10.1007/s10909-011-0448-8.
10. [10]R. Meservey and P. M. Tedrow, "Measurements of the Kinetic Inductance of Superconducting Linear Structures," *Journal of Applied Physics*, vol. 40, no. 5, pp. 2028–2034, 1969, doi: 10.1063/1.1657905.

# Photon Statistics

Photon Statistics and the unintuitive way photons behave when they arrive sparsely

Jan 5, 2022 • 16 min read



Because of the inherent probability quantum mechanics entails, photons arriving at some detector follow statistical properties. In this chapter I will discuss these *Photon Statistics* and the unintuitive way photons behave when they arrive sparsely.

## Photon Noise

In order to quantify the sensitivity of a DESHIMA type spectrometer, we need to know the amount of noise that is generated by the aforementioned atmospheric and optical loading and compare this to the signal that an observation will impart on the detector. For our purposes this noise consists of photon noise and quasiparticle recombination noise, the first of which can be split up into two categories: thermal noise and shot noise.

> *An observed astronomical object also emits random photons that reach the detector, therefore contributing to photon noise[1]. While this won't be included in the model, as the model is designed such that it calculates the noise when off-source, the following topics in this chapter are equally valid for photon noise emitted and caused by the astronomical source.*

### Thermal Noise

In radio receivers, a big part of the noise is generated by thermal agitation of electrons. In most uses this can be classified as white noise:the power is constant across its frequency spectrum [2], but in extremely high frequencies or low temperatures this approximation doesn't hold. The power $P$ transmitted by the noise is given as Johnson-Nyquist Noise and is approximated for small bandwidths $\Delta\nu$ as[3]:

$$P = \int_{\nu_0}^{\nu_1} \frac{h\nu}{e^{h\nu/k_BT} - 1} d\nu \approx \frac{h\nu}{e^{h\nu/k_BT} - 1} \Delta\nu = P_\nu \Delta\nu \tag{4.1}$$

With $P_\nu$ the power spectrum in $[\mathrm{WHz}^{-1}]$. Plotting the normalized ($P_\nu/k_BT$) power spectrum supports my earlier statements that, in most cases, thermal noise can be approximated as white

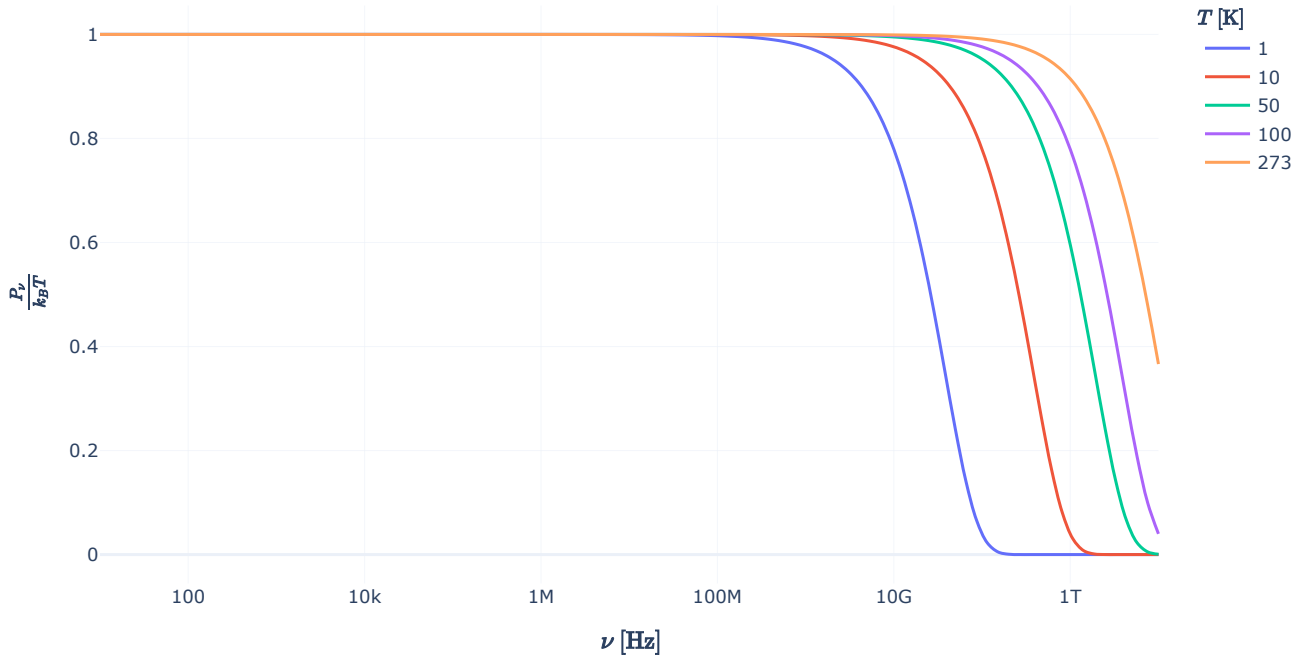


*Figure 4.1. Comparing the normalized Johnson-Nyquist noise for different temperatures shows that it is white for low frequencies*

Unfortunately, this white noise approximation starts to break down in atmospheric temperature for the DESHIMA range. Once more, it is also not the only form of noise we have to deal with.

## Shot noise

When the source is very dim, photons arrive one at a time. This means that we are dealing with shot noise[1]. Here the detection rate of a photon is characterized by Poisson statistics and the famous Poisson distribution [4]:

$$f(x) = \frac{\lambda^x e^{-\lambda}}{x!} \tag{4.2}$$

Hence we also call this noise Poisson noise.

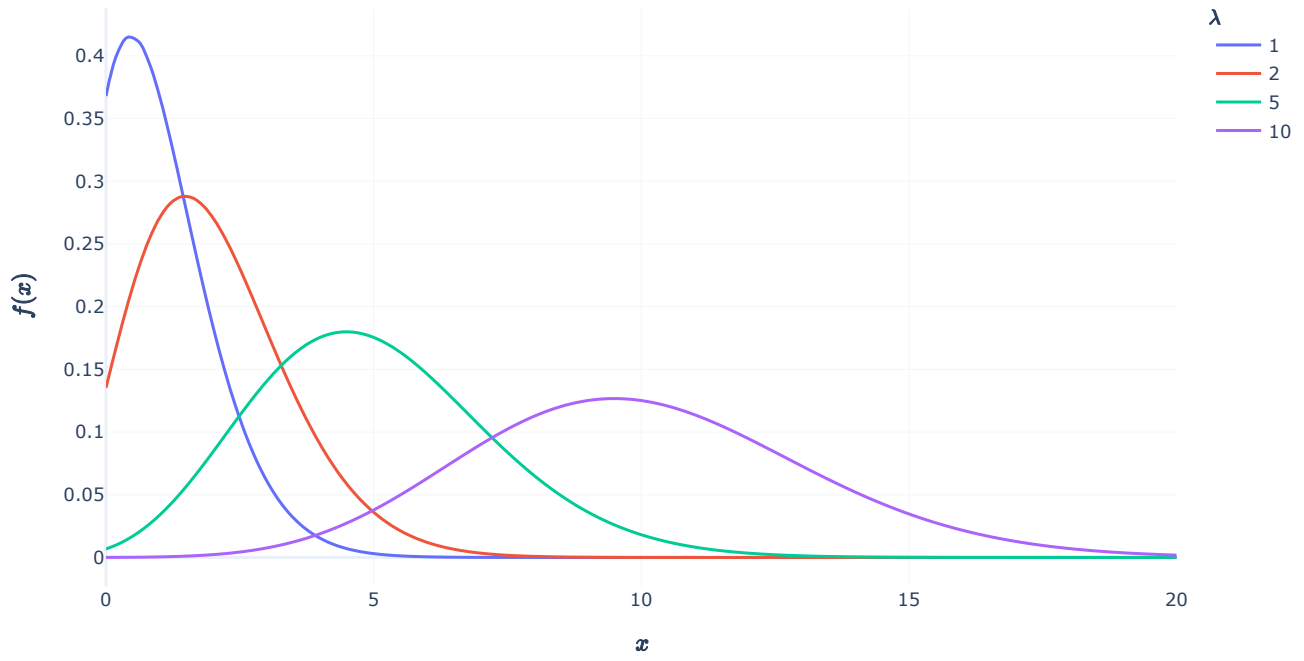


*Figure 4.2. Typical Poisson curves for different parameters.*

## Uncertainty

From Poisson statistics we know that the uncertainty $\sigma_N$ over some number of counts or occurrences $N$ is equal to the square root of the number of counts, since it's an uncorrelated process [1][4]. Because our power arrives with single photons hitting the detector, the power follows the same uncertainty

$$\sigma_N = \sqrt{N} \tag{4.3}$$

$$\sigma_P \propto \sqrt{P} \tag{4.4}$$

However, if we look at Johnson-Nyquist noise and approximate for lower frequencies we get[1][3]:

$$P \approx \frac{h\nu}{e^{h\nu/k_BT} - 1}\Delta\nu \approx k_BT\Delta\nu \tag{4.5}$$

$$\sigma_P \propto P \tag{4.6}$$

Hence we have found two proportionality relations for the uncertainty, which is it?

### Particle-Wave duality

The seemingly paradoxical nature of this uncertainty can be explained as a caveat of the particle-wave duality. In the wave domain the Johnson-Nyquist noise dominates, whereas in the particle domain we get mainly Poisson noise. The general case of the uncertainty in the *rate* of photons arriving within a detection time of $\tau$ is[5][6]:

$$\sigma_{\text{ph}} = \frac{1}{\sqrt{\tau}}\sqrt{n^2 + n} \tag{4.7}$$

with $n$, the photon number, being the number of photons arriving per time per bandwidth. Here both extremes are more obvious: for $n \gg 1$ we get the thermal noise from the wave domain and for $n \ll 1$ the Poisson uncertainty falls out.

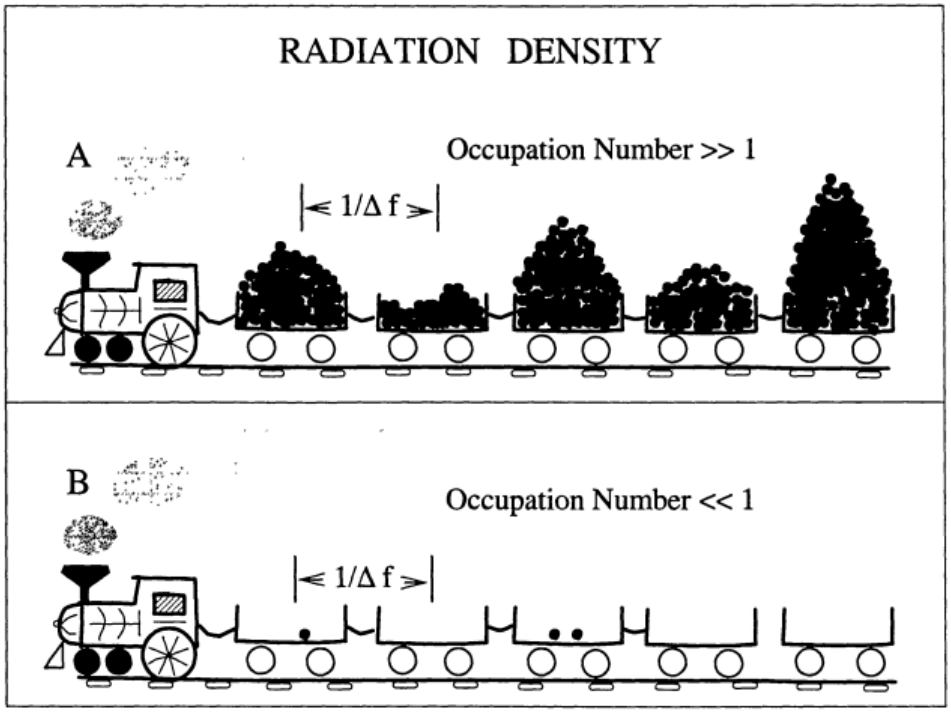


*Figure 4.3. An analogy for the detection of photons in the particle and wave limit. Image taken from [1]*

The photon number for a thermal blackbody radiator is given by the Bose-Einstein equation [7][6]

$$n_{\mathrm{th}}(\nu, T) = \frac{1}{e^{h\nu/k_B T} - 1} \tag{4.8}$$

Which means that in the region between $220\ \mathrm{GHz}$ and $440\ \mathrm{GHz}$ the photon occupation number is neither fully in the wave limit nor the particle limit.

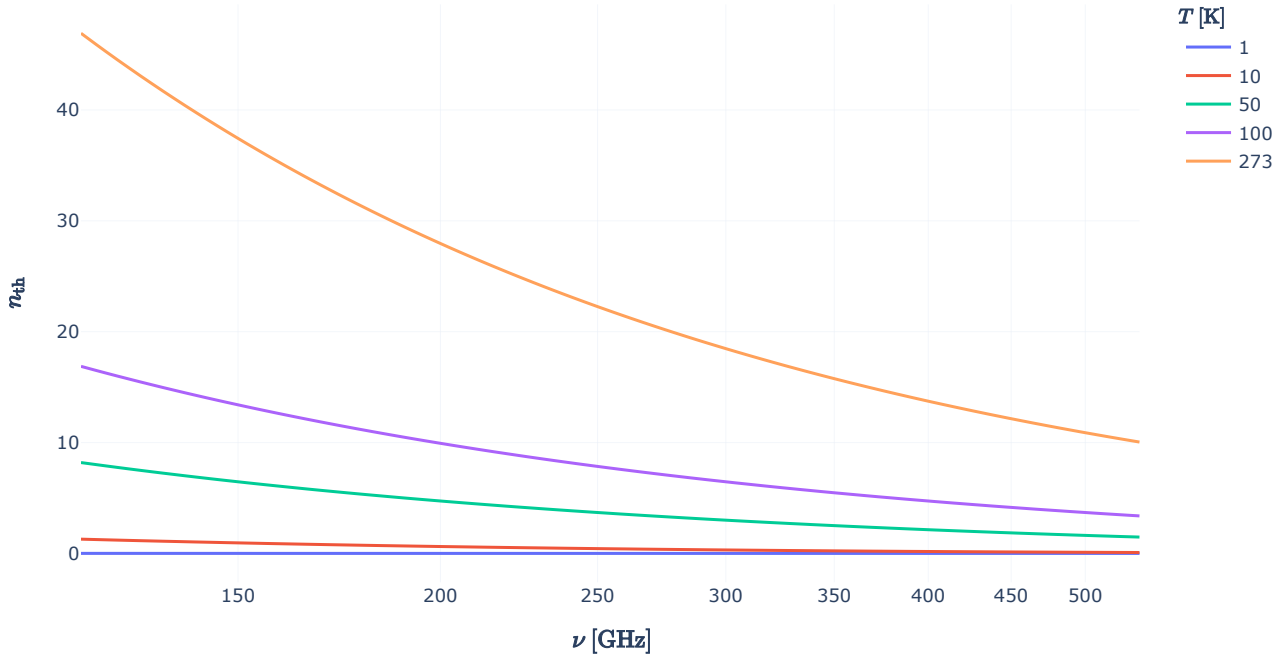

*Figure 4.4. The photon number for different temperatures is neither fully in the wave limit nor fully in the particle limit in the DESHIMA range*

In the wave domain, where the photon number is higher, photons tend to come clumped together in a process known as photon bunching[6], which explains the increase in noise.

## Photon Bunching

Quantum Electrodynamics has taught us that photons behave stochastically, so it is reasonable to assume that photon detection also occurs randomly. While this is (obviously) true to some degree, in the previous section I stated photons can arrive 'clumped' together at the detector in a phenomenon known as photon bunching. This means that detecting one photon will result in a higher chance of another photon being detected within a specified time, called the coherence time $t_{\mathrm{coh}}$ [6]. In this chapter I will first present an intuitive, *qualitative* explanation as to why photon bunching occurs. Then I will go deeper into the mathematics and quantum mechanics of photon bunching and the specific case of the DESHIMA system.

### An analogy

To understand photon bunching, first think of photons arriving at the detector like raindrops falling on a piece of paper. While it's raining with constant intensity, the chance of a raindrop falling on a specific area within, say, the next second (expressed by $P(\mathrm{drop})$) is constant. In the figure below I have set $P(\mathrm{drop}) = 0.3$:

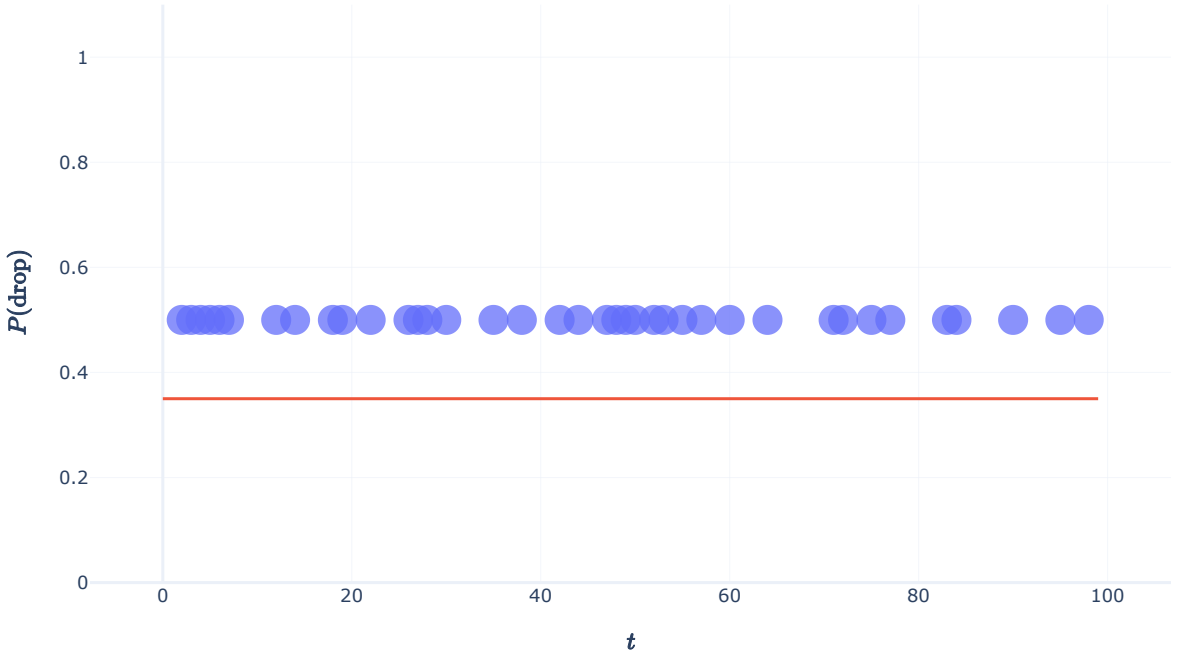


*Figure 4.5. Plotting occurrences and the underlying probability for a constant chance.*

The raindrops fall uncorrelated: every second a new chance of $P(\mathrm{drop})$ means a raindrop falling from the sky might land in our defined area. This is how unbunched, or random, photons behave.

Now let's assume the chance of a raindrop occurring is not constant over time, but rather varies relatively slowly over time. This could be because of varying wind speeds or varying intensity in the rain, but whatever the case the rain drops are no longer uncorrelated. There are moments of high intensity, where the chance of a raindrop is high and similarly there are moments of low intensity. I have simulated this using open simplex noise [8] in the following graph.

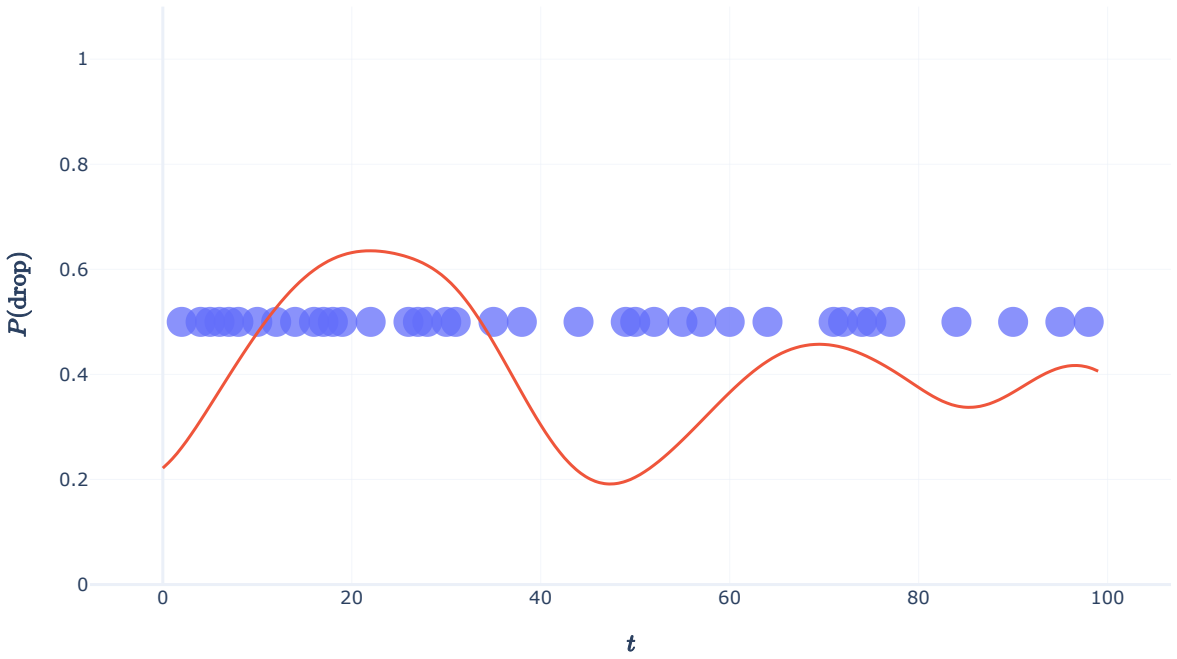


*Figure 4.6. Plotting occurrences and the underlying probability for a varying chance.*

As is clear from the graph, the raindrops are clumped together. This is the same underlying principle as photon bunching in photons from astronomical sources. The random motion of the exciting atoms, for example Brownian motion, means that the intensity also fluctuates over time[6]. It is therefore not the act of detecting a photon that increases the chance of another detection, but rather an underlying change in probability of detecting, easily explained by probabilistics.

This means that at the point where a raindrop falls or a photon gets emitted, it is still a simple stochastic process. Should our sampling interval be much smaller than the time over which the rain varies, we'd still see 'stochastic regions', where the probability function stays roughly constant, like in the first example. This is illustrated in the graph below with stretched noise:

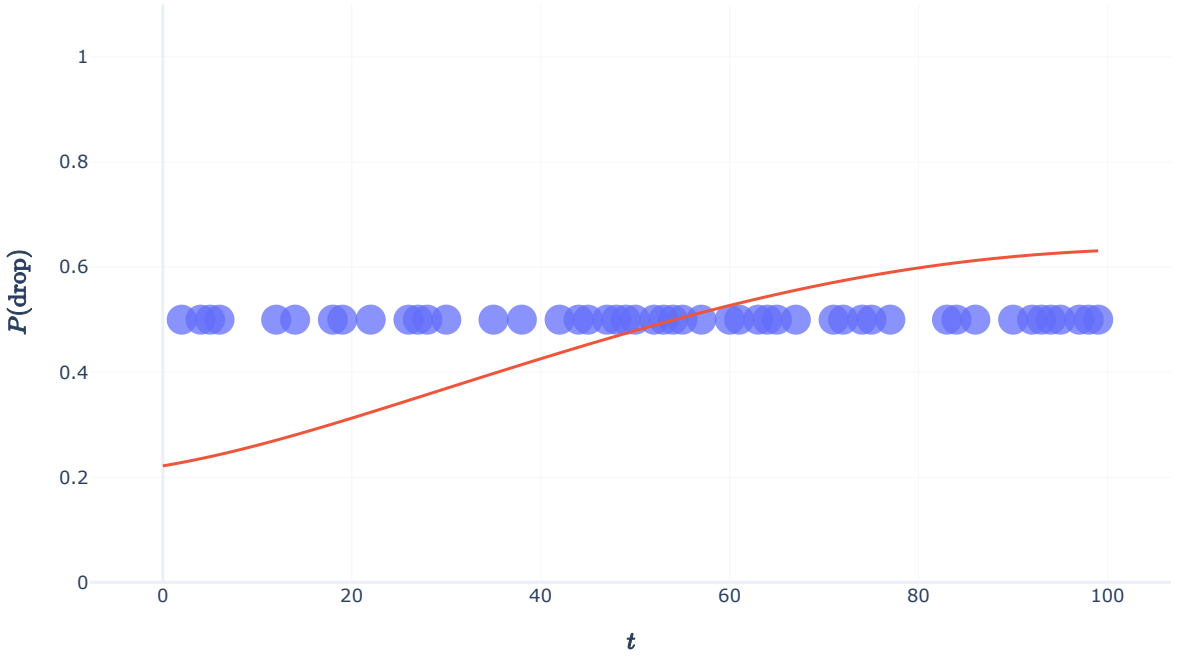


*Figure 4.7. Plotting occurrences and the underlying probability for a slowly varying chance.*

The droplets appear less bunched, because the time scale in which the measurements take place is much smaller than the time scale in which the intensity changes. The very first example I spoke about, of raindrops falling at a constant intensity, is a situation in which this discrepancy occurs. Of course it won't rain forever and when the rain dies down the chance of a raindrop falling is *much* lower than while it's still raining. So while the droplets look purely random when it rains, they aren't over the course of the entire day. I will call this behavior *bunched (slow timescale)*, because the sampling time is much faster than the coherence time, which I shall later elaborate on further.

Let's also take a look at what happens when the sampling time is much slower than the underlying probability fluctuations.

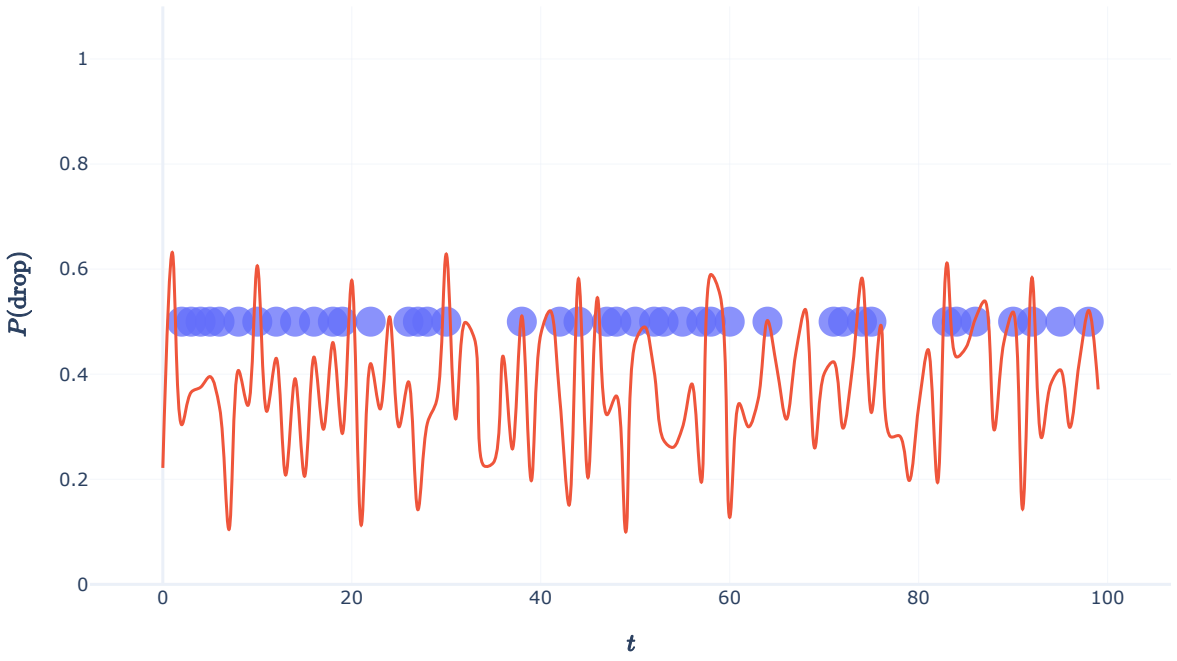


*Figure 4.8. Plotting occurrences and the underlying probability for a quickly varying chance.*

As expected, the detection rate looks much like the first detection rate with constant $P\left(\mathrm{drop}\right)$. Although the underlying probability changes, it changes too fast between detections for bunching to occur.

### Intermezzo: Antibunching

While this report focuses on photon bunching, the opposite also occurs in, for example, single photon sources [9]. Now that I have discussed a framework with which to explain photon bunching, I thought it would be remiss to leave out an explanation for antibunching.

As one would expect, in antibunching the opposite of bunching happens: detecting a raindrop would mean that, at least for the next period of time, the chance of a raindrop falling becomes smaller. A good allegory for this is a dripping faucet. A small flow of water exits the faucet and, due to surface tension, pools up in a small droplet at the end. As the droplet gets bigger, the chance of it falling increases, but once it drips down it takes all water with it and the process starts anew.

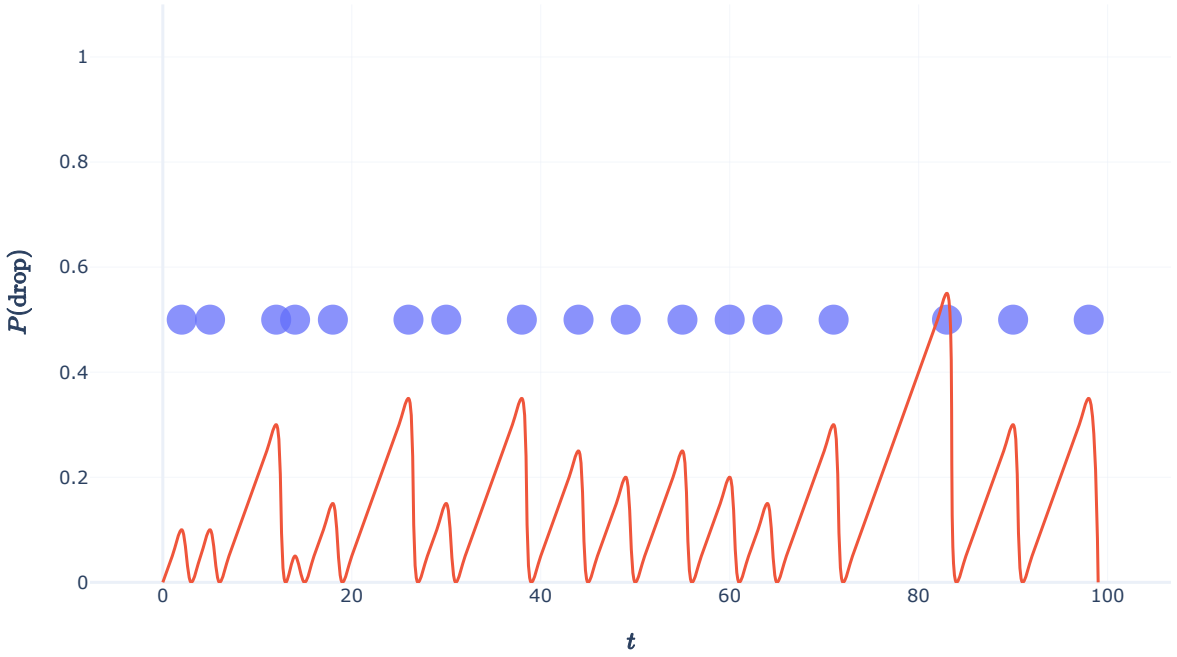


*Figure 4.9. An analogy for anti-bunching.*

This behavior corresponds with antibunching behavior in single photon sources[9]. Atoms are excited through an energy pump process. When this energy increases sufficiently they emit a photon and lose energy, ready to get excited again[6].

Again, the detection of such single photons will display antibunching, but it is not the detection that triggers this *cool-down* period, it is the emission.

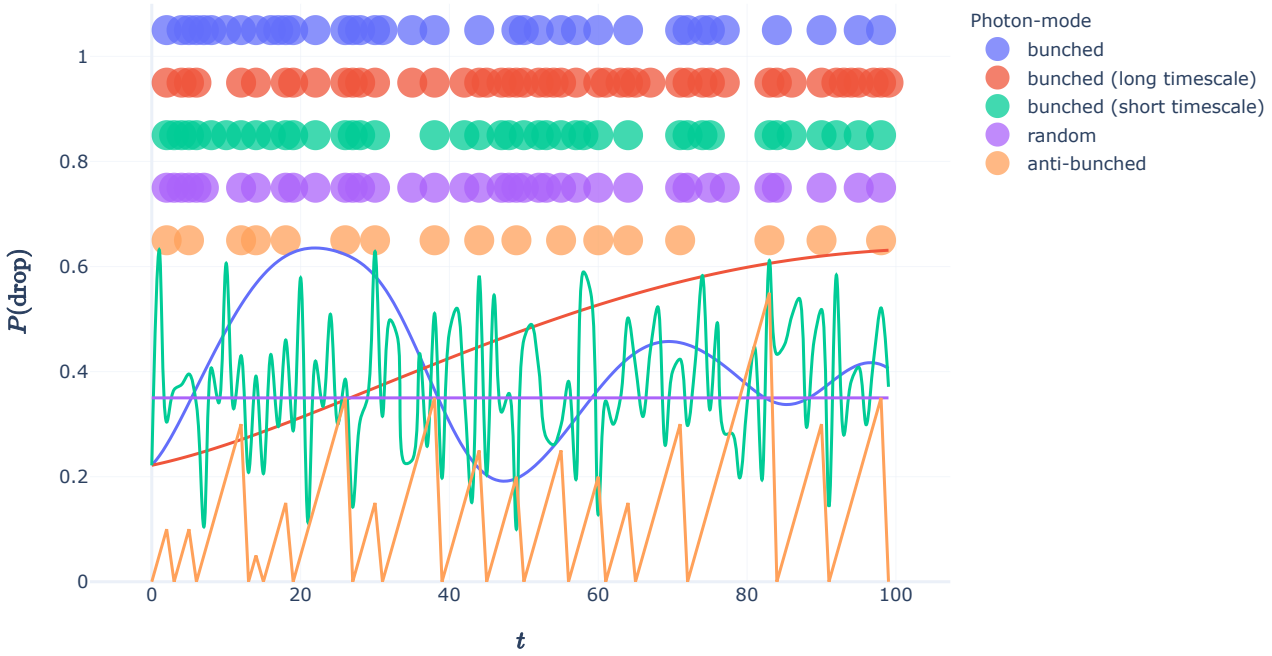

*Figure 4.10. All different probability and occurrences for the discussed probabilities. These are toggleable By selecting modes in the legend.*

## Coherence

If the underlying probability function is unknown (and quantum mechanically it is), how would we be able to quantify whether our detections are bunched. A possible heuristic we can use comes from signal processing. We could take the autocorrelation of the signals and compare them. Since the autocorrelation is the cross-correlation between the signal and a time-shifted copy, we'd likely see the bunched signal display some sort of correlation for a delay that is around the timescale of the oscillations in the probability function. In the figure below I have correlated the detections described above with $t \in [0, 10000]$ and plotted these values for different time delays $h$.

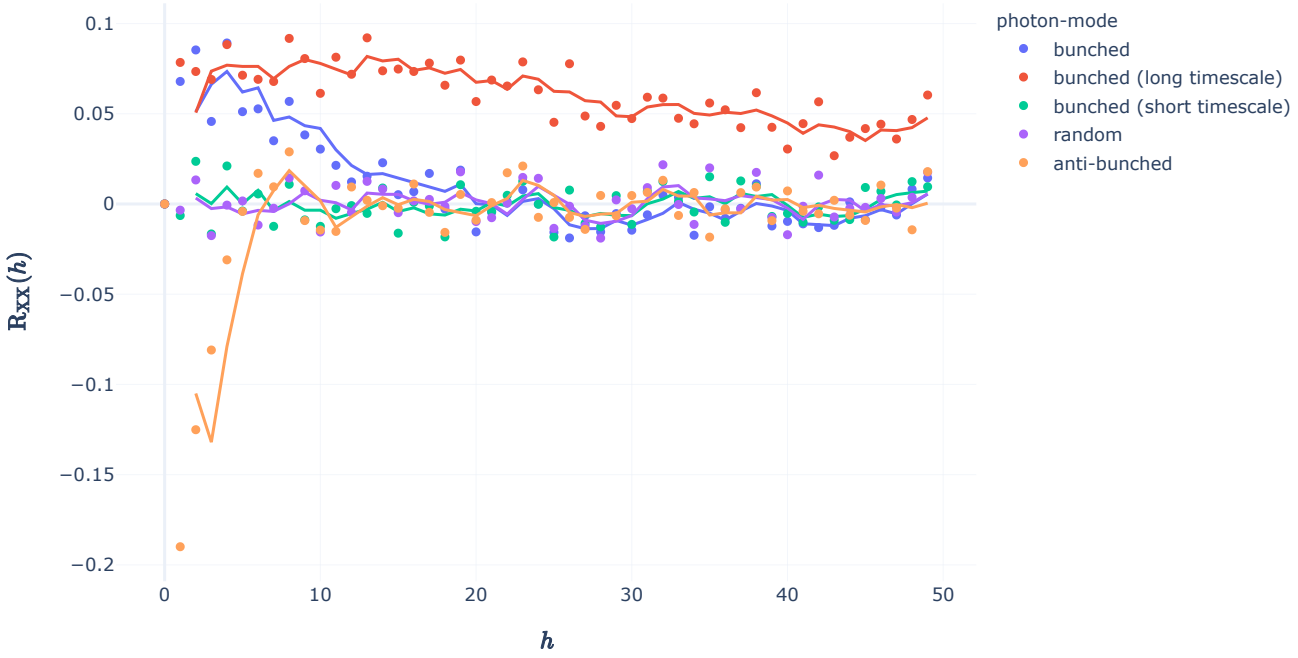


*Figure 4.11. The autocorrelation for the different photon modes.*

As is clear from the graph, the bunched photons show some autocorrelation, with the longer timescale showing longer (bigger time shifts) autocorrelation. This can be explained further by signal analysis. We are working in the discrete domain and smaller sampling steps relative to the variation in the underlying probability will mean more correlation.

What this shows is temporal coherence, a property of light that describes the predictability over a timescale[1].

## Bandwidth

Up until now we have only looked at raindrops as analogous detections, but when talking about photons we need to take frequency into account. Photons obey the Heisenberg uncertainty relation where the uncertainty in position $\Delta x$ and momentum $\Delta p_x$ must obey [1]:

$$\Delta x \Delta p_x = \frac{\hbar}{2} \tag{4.9}$$

Our photons are flying at the detector, so its uncertainty in longitudinal ($z$, towards the detector) position can be equated as it's uncertainty in detection time and it's momentum can be expressed as $h/\lambda$:

$$\Delta z \cdot \Delta p_z = c\Delta t \cdot \frac{h\Delta\nu}{c} = h\Delta t\Delta\nu = \frac{\hbar}{2} \tag{4.10}$$

and finally we arrive at

$$\Delta\nu \propto \frac{1}{\Delta t} \tag{4.11}$$

In other words: a shorter coherence time means more accurate knowledge on where the photons are, meaning their uncertainty in momentum and therefore bandwidth is bigger.

This relation can also be seen experimentally. In Morgan and Mandel's 1966 paper[10], the authors explore the autocorrelation between two different light sources: a $Hg^{198}$ source with a very narrow bandwidth (a) and a tungsten light bulb with a broad spectrum thermal source (b). By designing an apparatus that counts the number of times two photon arrive within a defined time period, they show the autocorrelation of the two light sources

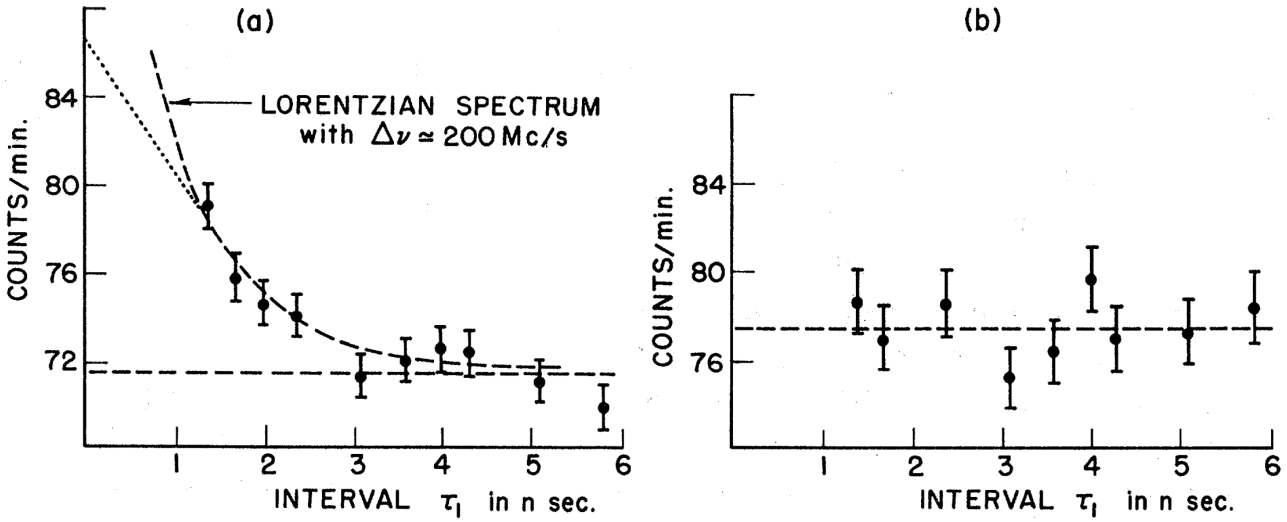


*Figure 4.12. The number of times per second two photons arrived after a specified time delay for a a) $Hg^{198}$ light source and a b) tungsten incandescent light source. Image taken from [10]*

Because the tungsten light has a wide bandwidth, it has a short coherence time and the reverse is true for the $Hg^{198}$ light. Therefore, if we take the short timescale bunched photons as an analogy for the tungsten light and the longer timescale bunched lights as analogous for the mercury light, we get something that looks very similar.

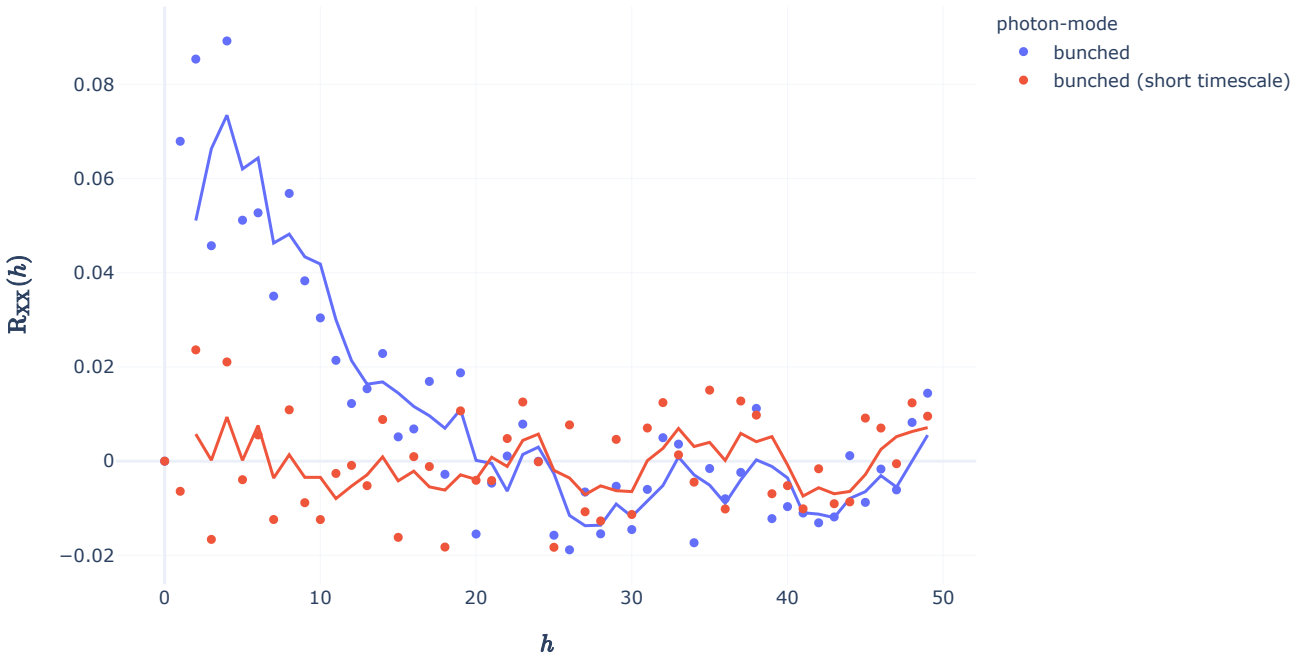


*Figure 4.13. The autocorrelation of just the slow and short bunched timescale photons behave like the spectral and tungsten source respectively.*

With a more thorough understanding of photon bunching, it is time to return to photon noise and discuss noise-equivalent power.

## Noise Equivalent power

The noise equivalent power ($\mathrm{NEP}$) is a way to express the sensitivity of a photon detector. It is defined as *the input signal power that results in a signal-to-noise-ratio of 1 in a 1 Hz output bandwidth*. [11]. For our purposes this means multiplying the uncertainty in photon count $\sigma_{\mathrm{ph}}$ with the photon energy[12] and setting the $\tau$ in eq. $(4.7)$ to $\tau = 0.5\ \mathrm{s}$. From [7] we have an equation for the electrical (detected) photon noise

$$\sigma_{\mathrm{ph}}^2 = \frac{1}{\tau}\int_0^\infty \eta(\nu)n(\nu)\left[1+\eta(\nu)n(\nu)\right]d\nu \tag{4.12}$$

Where $\eta\left(\nu\right)$ is the *quantum efficiency*, which for our purposes is the efficiency of the filter. Multiplying this integral with the photon energy, we get the electrical Noise Equivalent Power added by photon noise for a specified integration time

$$\mathrm{NEP}_{\tau,\mathrm{ph}}^2 = \frac{1}{\tau}\int_0^\infty (h\nu)^2\eta(\nu)n(\nu)\left[1+\eta(\nu)n(\nu)\right]d\nu \tag{4.13}$$

> *This integral implicitly assumes an infinite coherence time, since it integrates over infinitely small bandwidths $d\nu$. Another side effect of this is that photons only bunch with photons that share the exact same frequency. These two paradoxical conclusions make this integral therefore inherently not physical and we will need to make some assumptions in order to work with it.*

If we were to create a perfect box filter, and approximate the photon number as constant over this filter $\eta\left(\nu\right)$ falls out of the integral. Let's first define this box function

$$\Pi_{\nu_0}^{\Delta\nu}(\nu) = \begin{cases} 1 & |\nu - \nu_0| \leq \frac{\Delta\nu}{2} \\ 0 & \text{elsewhere} \end{cases} \tag{4.14}$$

And then set $\eta(\nu) = \eta_0 \Pi_{\nu_0}^{\Delta\nu}(\nu)$. When we assume we have a constant photon occupation number over this range, the equation simplifies to:

$$\begin{aligned} \mathrm{NEP}_{\tau,\mathrm{ph}}^2 &= \frac{1}{\tau} \int_0^\infty (h\nu)^2 \eta_0 \Pi_{\nu_0}^{\Delta\nu}(\nu) n(\nu) \left[1 + \eta_0 \Pi_{\nu_0}^{\Delta\nu}(\nu) n(\nu)\right] d\nu \\ &= \frac{1}{\tau} \int_{\nu_0 - \frac{\Delta\nu}{2}}^{\nu_0 + \frac{\Delta\nu}{2}} (h\nu)^2 \eta_0 n \left[1 + \eta_0 n\right] d\nu \end{aligned} \tag{4.15}$$

Which, for $\Delta\nu \ll \nu$ approximates as:

$$\mathrm{NEP}_{\tau,\mathrm{ph}}^2 = \frac{1}{\tau} (h\nu_0)^2 \eta_0 n \left[1 + \eta_0 n\right] \Delta\nu \tag{4.16}$$

Taking our definition of Noise Equivalent Power $\tau = 0.5\ [\mathrm{s}]$, this results in a Noise Equivalent Power of:

$$\mathrm{NEP}_{\tau=0.5\mathrm{s},\mathrm{ph}} = h\nu_0 \sqrt{2\eta_0 n \left(1 + \eta_0 n\right) \Delta\nu} \tag{4.17}$$

### DESHIMA

In actual measurements the photon occupation number isn't known, but we are able to deduce it from the power spectral density[6]:

$$n_{\mathrm{ph}} = \frac{\mathrm{PSD}}{h\nu} \tag{4.18}$$

Inserting this in the equation for $\mathrm{NEP}$ we get:

$$\mathrm{NEP}_{\tau=0.5\mathrm{s},\mathrm{ph}} = \sqrt{2\eta_0 \mathrm{PSD} h\nu_0 \left(1 + \eta_0 \frac{\mathrm{PSD}}{h\nu_0}\right) \Delta\nu} \tag{4.19}$$

If we assume the $\mathrm{PSD}$ to be flat, for a box filter the power spectrum multiplied by the bandwidth and the efficiency is obviously the power on the detector.

$$P_{\mathrm{KID}} = \eta_0 \mathrm{PSD} \Delta\nu_0 \tag{4.20}$$

rearranging we get:

$$\mathrm{NEP}_{\tau=0.5\mathrm{s},\mathrm{ph}} = \sqrt{2P_{\mathrm{KID}} h\nu_0 + 2\frac{P_{\mathrm{KID}}^2}{\Delta\nu}} \tag{4.21}$$

Which is in agreement with [13].

## Generation-Recombination Noise

Besides photon noise (both Poisson and bunching), another type of noise adds to our $\mathrm{NEP}$: recombination noise. This is a type of noise that occurs in superconductor-based pair-breaking photon detectors. As mentioned before, incoming photons generate quasiparticles in the detector, which later

recombine in a Cooper pair [14]. For our purposes we will take the noise equivalent power of recombination noise $\mathrm{NEP}_{\tau,\mathrm{R}}$ as given by [13]:

$$\mathrm{NEP}_{\tau,\mathrm{R}} = \frac{1}{\sqrt{\tau}}\sqrt{2\Delta_{\mathrm{Al}}\frac{P_{\mathrm{KID}}}{\eta_{\mathrm{pb}}}} \tag{4.22}$$

Even though the amount of quasiparticles generated is proportional to the incoming power, the recombination noise happens randomly and is therefore an uncorrelated process. This means we can add the $\mathrm{NEP}_{\mathrm{R}}$ and $\mathrm{NEP}_{\mathrm{ph}}$ together by quadrature addition, creating a total noise equivalent power given by:

$$\mathrm{NEP}_{\tau=0.5\mathrm{s}} = \sqrt{\mathrm{NEP}^2_{\tau=0.5\mathrm{s},\mathrm{ph}} + \mathrm{NEP}_{\tau=0.5\mathrm{s},\mathrm{R}}{}^2} \tag{4.23}$$

$$\mathrm{NEP}_{\tau=0.5\mathrm{s}} = \sqrt{2P_{\mathrm{KID}}h\nu_0 + 2\frac{P^2_{\mathrm{KID}}}{\Delta\nu} + 4\Delta_{\mathrm{Al}}\frac{P_{\mathrm{KID}}}{\eta_{\mathrm{pb}}}} \tag{4.24}$$

Finally, quasiparticles also generate randomly without any incoming photons, eg when the detector is kept in total darkness[15]. This is called *Generation-Recombination noise* and is negligible compared to the photon noise and photon-induced recombination noise as can be seen in the figure below:

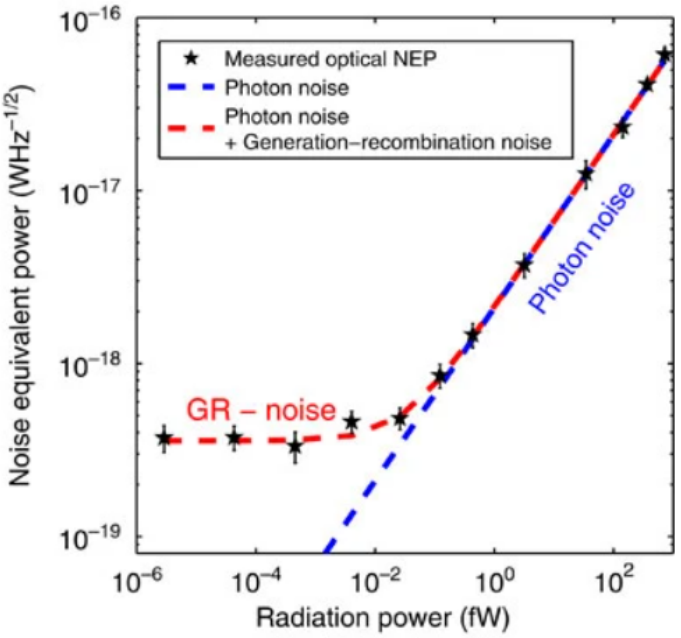


*Figure 4.14. The noise induced by spontaneous Generation and recombination of quasiparticles is negligible compared to photon noise. Image taken from [15]*

Because this effect is negligible, it won't be included in the model.

## Bibliography


1. [1]G. B. Taylor, C. L. Carilli, and R. A. Perley, *Synthesis imaging in radio astronomy II: a collection of lectures from the Sixth NRAO/NMIMT Synthesis Imaging Summer School held at Socorro, New Mexico, USA, 17-23 June 1998*. Astronomical Society of the Pacific, 2008, pp. 671–688.
2. [2]C. S. Turner, “Johnson Nyquist noise - clay’s DSP Page,” *Johnson-Nyquist Noise*. Wireless Systems Engineering, Inc., Jan-2007 [Online]. Available at: http://www.claysturner.com/dsp/Johnson-

Nyquist%20Noise.pdf
3. [3]A. Endo, “Session 4 | Photon Noise,” *EE3350TU Introduction to Radio Astronomy*. Dec-2020.
4. [4]F. M. Dekking, C. Kraaikamp, L. H.P, and L. E. Meester, *A modern introduction to probability and statistics: Understanding why and how*. Springer-Verlag, 2011.
5. [5]A. Endo, “Memo: Poisson limit and bunching limit of photon NEP: Deshima Kibela,” *Memo: Poisson limit and Bunching limit of Photon NEP*. Kibela, Nov-2020 [Online]. Available at: https://deshima.kibe.la/shared/entries/96349e15-acfa-474f-adf8-f21ebe25cda5
6. [6]H. Paul, *Introduction to quantum optics: from light quanta to quantum teleportation*. Cambridge University Press, 2004, pp. 127–153.
7. [7]J. Zmuidzinas, “Thermal noise and correlations in photon detection,” *Applied Optics*, vol. 42, no. 25, p. 4989, 2003, doi: 10.1364/ao.42.004989.
8. [8]K. Spencer and O. S. Community, “opensimplex v0.3,” *pypi.org*. Open Source, Dec-2021 [Online]. Available at: https://pypi.org/project/opensimplex/
9. [9]M. Krottenmüller, “Photon Statistics,” *Technische Universität München*. May-2013 [Online]. Available at: https://www.mpq.mpg.de/5020834/0508a_photon_statistics.pdf
10. [10]B. L. Morgan and L. Mandel, “Measurement of Photon Bunching in a Thermal Light Beam,” *Physical Review Letters*, vol. 16, no. 22, pp. 1012–1015, 1966, doi: 10.1103/physrevlett.16.1012.
11. [11]P. L. Richards, “Bolometers for infrared and millimeter waves,” *Journal of Applied Physics*, vol. 76, no. 1, pp. 1–24, 1994, doi: 10.1063/1.357128.
12. [12]S. Leclercq, “Discussion about Noise Equivalent Power and its use for photon noise calculation,” 2007 [Online]. Available at: https://www.iram.fr/ leclercq/Reports/About_NEP_photon_noise.pdf
13. [13]A. Endo *et al.*, “First light demonstration of the integrated superconducting spectrometer,” *Nature Astronomy*, vol. 3, no. 11, pp. 989–996, 2019, doi: 10.1038/s41550-019-0850-8.
14. [14]P. J. de Visser, “Quasiparticle dynamics in aluminium superconducting microwave resonators,” Mar. 2014, doi: 10.4233/uuid:eae4c9fc-f90d-4c12-a878-8428ee4adb4c.
15. [15]P. J. D. Visser, J. J. A. Baselmans, J. Bueno, N. Llombart, and T. M. Klapwijk, “Fluctuations in the electron system of a superconductor exposed to a photon flux,” *Nature Communications*, vol. 5, no. 1, 2014, doi: 10.1038/ncomms4130.

# The Model

Designing the model

Jan 4, 2022 • 13 min read



The original `deshima-sensitivity` code follows the following flowchart

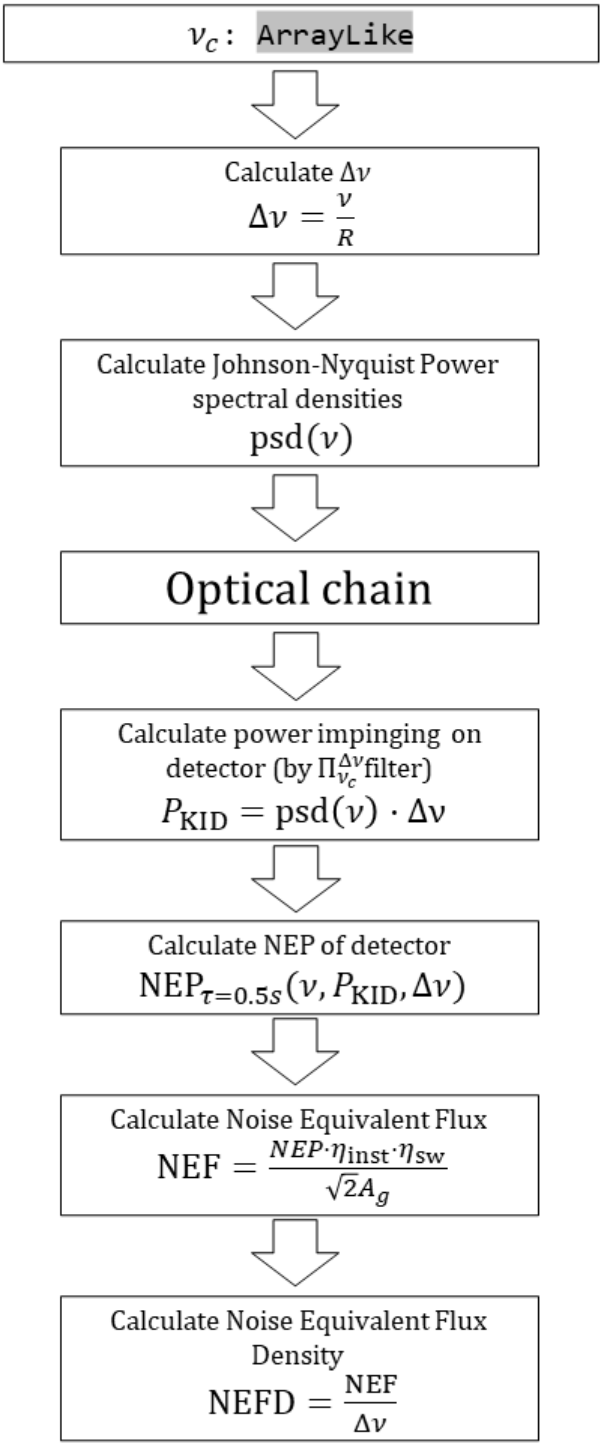


*Figure 5.1. A flowchart showing the design of the old version of the model.*

The optical chain described in the flowchart consists of serial transmission calculations from 1 medium to another. This entire chain of stacked transformations of the spectral input power can be regarded as a single affine transformation of the input and is independent of the bandwith or amount of frequency bins. It will remain unchanged throughout the proposed modifications.

The power impinging on a detector for a specific filter bin is calculated by taking the spectral flux density at the center frequency $\nu_c$ and multiplying this with the bandwith $\Delta\nu$. This matches the model of the previous described box filter, assuming the flux density $\mathrm{psd}$ is flat over the entire bandwith. This is not the case however, as we shall see.

## Filter distribution

1 filter channel has so far been approximated as a perfect box integral, which is physically inaccurate. As we have seen, the actual filter shapes are more closely described by a Lorentzian curve

$$\eta(\nu) = \frac{A\gamma^2}{(\nu - \nu_0)^2 + \gamma^2} \tag{5.1}$$

Where $\gamma$ is the half-width at half maximum (HWHM) value, for DESHIMA given as

$$\gamma = \frac{\nu_c}{2R} \tag{5.2}$$

with $R = 500$ the spectral resolution. As we have seen previously our box filters were defined by an efficiency constant labeled $\eta_0$. Together with the bandwidth, this describes the transmission of the box filter. If we define the full width at half maximum for the Lorentzian as the bandwidth of the Lorentzian, we would like to define the $A$ parameter such that the area of this $\mathrm{FWHM}$ is exactly the same as the area of the box filter.

$$\eta_0 2\gamma = \int_{\nu_0-\gamma}^{\nu_0+\gamma} \frac{A\gamma^2}{(\nu - \nu_0)^2 + \gamma^2} d\nu = \frac{\pi}{2}\gamma A \Leftrightarrow A = \frac{4}{\pi}\eta_0 \tag{5.3}$$

Meaning our filters are given by

$$\eta(\nu) = \frac{4}{\pi}\frac{\eta_0\gamma^2}{(\nu - \nu_0)^2 + \gamma^2} \tag{5.4}$$

For atmospheric loading, which as you might recall is the main source of the noise, the channel is of course loaded over the entire filter spectrum: both in and out band. For a constant $\mathrm{PSD}$ this means that the corresponding box approximation can simply be widened so as to enclose the same area as the full band of the filter. For a Lorentzian this is as simple as widening the effective bandwidth with a constant:

$$\int_{-\infty}^{\infty} \frac{A\gamma^2}{(\nu - \nu_0)^2 + \gamma^2} d\nu = \pi\gamma A = 2\int_{\nu_0-\gamma}^{\nu_0+\gamma} \frac{A\gamma^2}{(\nu - \nu_0)^2 + \gamma^2} d\nu \tag{5.5}$$

Meaning that the full band effective bandwidth is exactly twice the in band effective bandwidth.

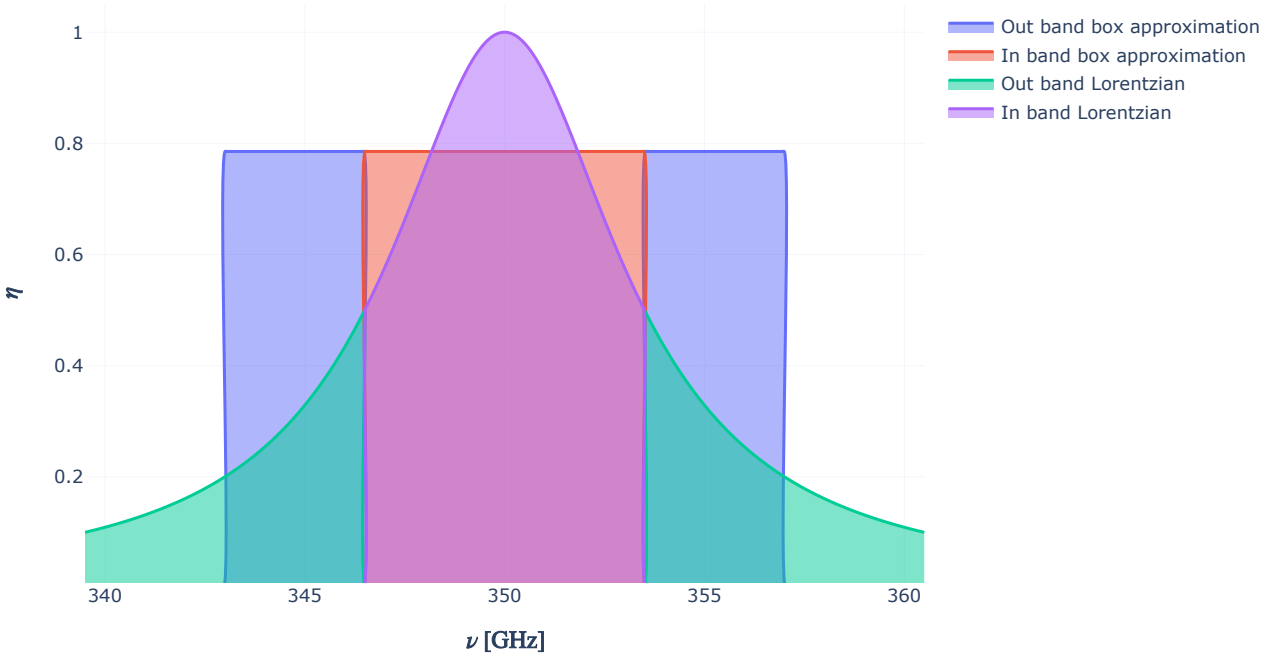


*Figure 5.2. The different sections of the Lorentzian filter. The box approximation and the corresponding part of the Lorentzian have the same area.*

## Noise Equivalent Power

Redoing the calculation of the noise equivalent power for a flat $\mathrm{PSD}$, but with proper Lorentzian filters $\eta(\nu)$ this time, results in:

$$\begin{aligned}
\mathrm{NEP}^2_{\tau=0.5\mathrm{s,ph}} &= 2\int_0^\infty h\nu\eta(\nu)\mathrm{PSD} + \eta^2(\nu)\mathrm{PSD}^2 d\nu \\
&= 2\mathrm{PSD}\int_0^\infty h\nu\eta(\nu)d\nu + 2\mathrm{PSD}^2\int_0^\infty \eta^2(\nu)d\nu \\
&\approx 8\mathrm{PSD}h\nu_0\eta_0\gamma + \frac{16}{\pi}\mathrm{PSD}^2\eta_0^2\gamma \\
&= 4\mathrm{PSD}h\nu_0\eta_0\mathrm{FWHM} + \frac{8}{\pi}\mathrm{PSD}^2\eta_0^2\mathrm{FWHM}
\end{aligned} \tag{5.6}$$

where an approximation is used for the first term, assuming $\Delta\nu \ll \nu$. Because the calculations are done for a constant $\mathrm{PSD}$, the filter gets loaded across the full band, meaning the effective bandwidth $\Delta\nu = 2\mathrm{FWHM}$. Putting this in the equation for the $\mathrm{NEP}_{\tau=0.5\mathrm{s,ph}}$ yields:

$$\begin{aligned}
\mathrm{NEP}_{\tau=0.5\mathrm{s,ph}} &= 2\mathrm{PSD}\eta_0\Delta\nu h\nu_0 + \frac{4}{\pi}\mathrm{PSD}^2\eta_0^2\Delta\nu \\
&= 2P_{\mathrm{KID}}h\nu_0 + \frac{4}{\pi}\frac{P^2_{\mathrm{KID}}}{\Delta\nu}
\end{aligned} \tag{5.7}$$

Which means the second term, the bunching term, is a factor of $\pi/2$ smaller than is the case for narrow-bandwidth approximation described in [1] and used in [2]. This can be explained because the full Lorentzian has a non-negligible width and therefore the approximation of $\nu \gg \Delta\nu$ from [1] doesn't

hold. In other words the photons impinging on the detector span a bigger bandwidth than previously approximated and therefore bunch less.

## Non-flat Power Spectrum Densities

We know the $\mathrm{NEP}$ is proportional to the $\mathrm{PSD}$ impinging on the detector, and we have also seen that the atmospheric loading is a much bigger contribution to the spectral flux density than any astronomical source. Let's take a look at how this atmospheric loading varies over the bin width. In the figures below the actual target frequency channels from DESHIMA 2.0 are taken and compared to the atmospheric model measured at ASTE, taken from `deshima-sensitivity`.

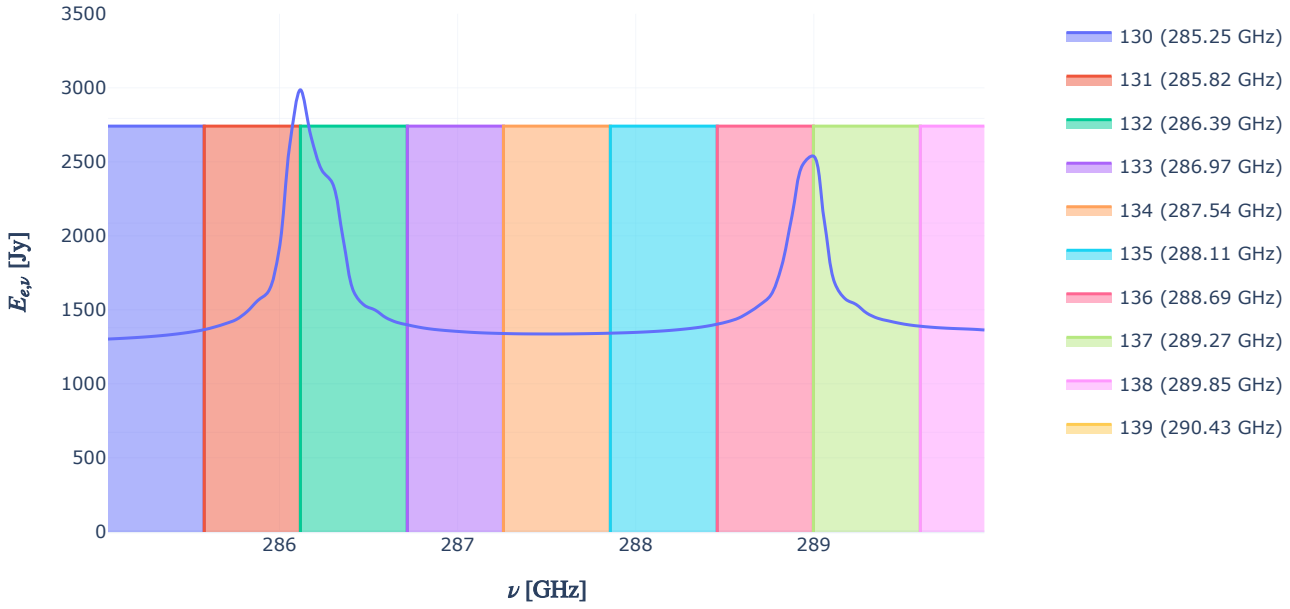


*Figure 5.3. A non-flat power spectral density overlayed over box filters. The out of band loading is not calculated.*

For the channels where the atmospheric loading is reasonably constant over the bandwidth this approximation is fine, however when the spectral flux density peaks to twice it's local background level the box filters are obviously a poor approximation for reality. The atmospheric loading is averaged over the bandwidth before being multiplied with it in the current version of `deshima-sensitivity`, in essence integrating it over the box filter. However, this crude approximation clearly fails when looking at the actual Lorentzian filters.

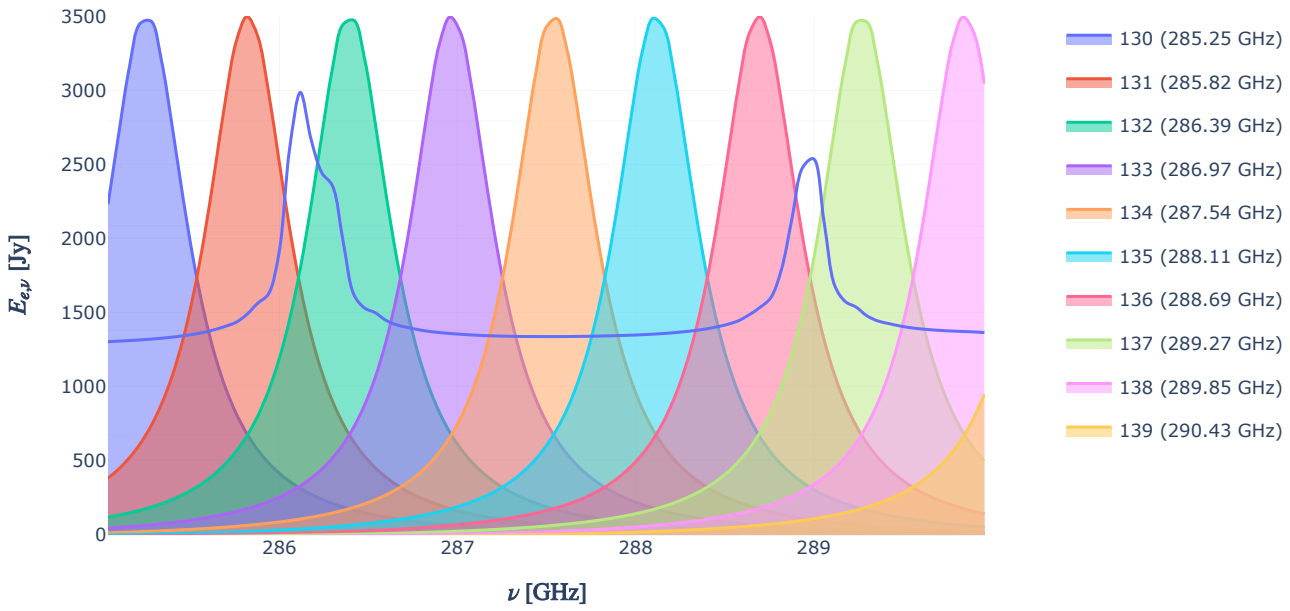


*Figure 5.4. A non flat power spectral density overlayed over Lorentzian filters. Here filters are loaded out of band.*

The peak at $286.1\ \mathrm{GHz}$ is obviously loading channel 131 and 132, but due to the wide profile of a Lorentzian even 130 and 133 are receiving energy from the peak in flux density.

The total power impinged on the detector can be approximated by calculating the spectral power arriving at the detector not just at the center frequencies of the bins $\nu_0$, but by expanding the number of frequencies calculated to some amount of *integration bins* and calculating the spectral power at these frequencies. For an integration frequency $\nu_i$ and a channel $j$, the effective power loading by that frequency on that channel is given by:

$$P_{\mathrm{KID},i,j} = \eta\left(\nu_i, j\right) \mathrm{PSD}\left(\nu_i\right) \Delta\nu_i \tag{5.8}$$

with $\Delta\nu_i$ the bandwidth for that frequency. The total power impinged on a filter channel $P_{\mathrm{KID},j}$ is then given by:

$$P_{\mathrm{KID},j} = \sum_i P_{\mathrm{KID},i,j} = \sum_i \eta\left(\nu_i, j\right) \mathrm{PSD}\left(\nu_i\right) \Delta\nu_i \tag{5.9}$$

To make this more visual, take a look at the figure below

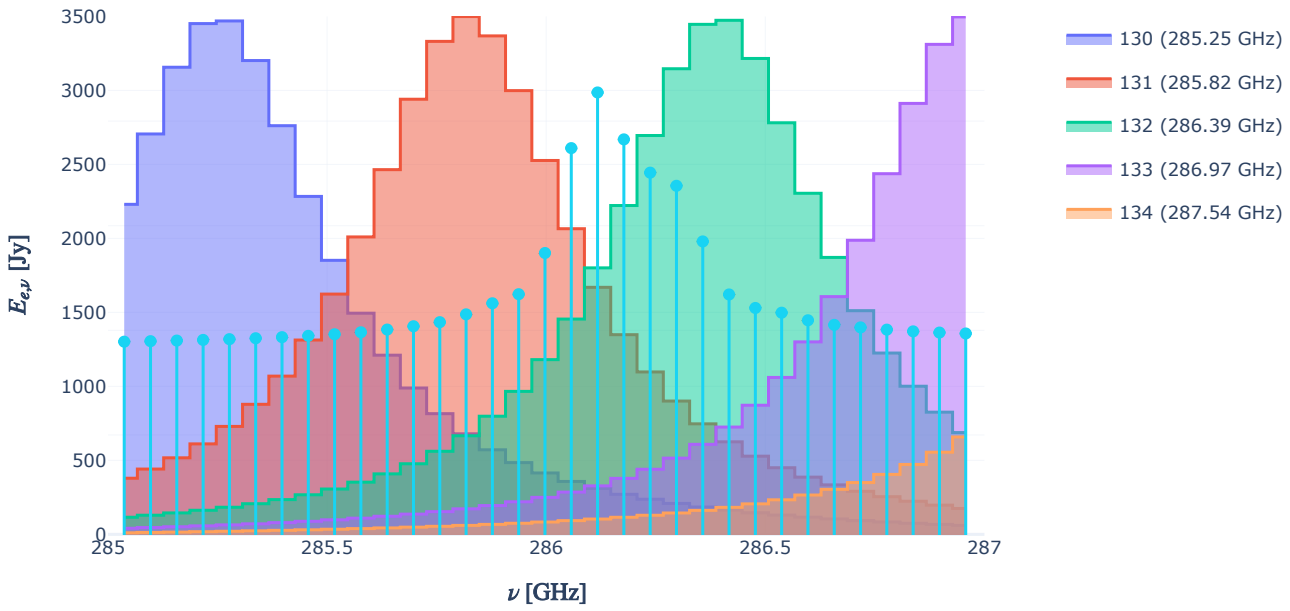


*Figure 5.5. A stem plot of the power spectral density overlayed over binned Lorentzian filters.*

The calculated flux spectrum arriving at the filter will be calculated as is done in the current version of the `deshima-sensitivity` package, but using a finer frequency resolution. This spectrum will then arrive at the filter, where for each channel a weighted sum will be taken over all integration bins, resulting in a total power impinged on the detector.

## Noise Equivalent Power

As seen, the photon noise equivalent power for a single DESHIMA channel $\mathrm{NEP}_{\tau=0.5\mathrm{s,ph},j}$ is given by[1]:

$$\mathrm{NEP}^2_{\tau=0.5\mathrm{s,ph},j} = 2\int_0^\infty h\nu\eta\left(\nu, j\right)\mathrm{PSD}\left(\nu\right) + \eta^2\left(\nu, j\right)\mathrm{PSD}(\nu)^2 d\nu \tag{5.10}$$

Again taking the filter efficiency $\eta\left(\nu_i, j\right)$ and $\mathrm{PSD}$ constant over a single integration frequency, and multiplying $\mathrm{PSD}$ with the bandwidth to get the power impinged by an integration bin on the channel $P_{\mathrm{KID},i}$ we can easily take the Riemann sum of this integral as

$$\mathrm{NEP}^2_{\tau=0.5\mathrm{s,ph},j} = 2\sum_i \left(h\nu_i P_{\mathrm{KID},j,i} + \frac{P^2_{\mathrm{KID},j,i}}{\Delta\nu_i}\right) \tag{5.11}$$

The recombination noise $\mathrm{NEP}_\mathrm{R}$ is given by

$$\mathrm{NEP}^2_{\tau,\mathrm{R},j} = \frac{1}{\tau}2\Delta_\mathrm{Al}\frac{P_{\mathrm{KID},j}}{\eta_\mathrm{pb}} = \frac{1}{\tau}2\Delta_\mathrm{Al}\frac{\sum_i P_{\mathrm{KID},j,i}}{\eta_\mathrm{pb}} \tag{5.12}$$

Which results in a total $\mathrm{NEP}_{\tau=0.5\mathrm{s}}$ of

$$\mathrm{NEP}_{\tau=0.5\mathrm{s},j} = \sqrt{2\sum_i \left( h\nu_i P_{\mathrm{KID},j,i} + \frac{P^2_{\mathrm{KID},j,i}}{\Delta\nu_i} \right) + 4\Delta_{\mathrm{Al}} \frac{\sum_i P_{\mathrm{KID},j,i}}{\eta_{\mathrm{pb}}}} \tag{5.13}$$

## Photon Bunching

But what about photon bunching? I have shown that the coherence time and the bandwidth are inversely proportional. By decreasing the size of the integration bins we have also decreased the bandwidth and therefore increased the coherence time.

Now the $\mathrm{NEP}$ is simply *defined* at $\tau = 0.5\ \mathrm{s}$, but in measurements the integration time can vary. The $\mathrm{NEP}$ is scaled accordingly:

$$\begin{aligned} \mathrm{NEP}_{\tau,j} &= \frac{1}{\sqrt{\tau}} \sqrt{\sum_i \left( h\nu_i P_{\mathrm{KID},j,i} + \frac{P^2_{\mathrm{KID},j,i}}{\Delta\nu_i} \right) + 2\Delta_{\mathrm{Al}} \frac{\sum_i P_{\mathrm{KID},j,i}}{\eta_{\mathrm{pb}}}} \\ &= \frac{1}{\sqrt{2\tau}} \mathrm{NEP}_{\tau=0.5\mathrm{s},j} \end{aligned} \tag{5.14}$$

Even though DESHIMA 2.0 samples at a minimum integration frequency of $160\ \mathrm{Hz}$ which results in a integration time of $\tau = 6.25\ \mathrm{ms}$, it still integrates periods orders of magnitude longer than the coherence time [3], meaning that the non-stochastic effects of photon bunching still don't come into play and we can define the noise as described previosuly.

But this scaling doesn't hold indefinitely. I conjecture that at some point the incoming photons are sampled at such a short sampling interval that they become correlated, as we have seen previously. In order to investigate this, let's define 3 bunched signal using open simplex noise[4] as done before along with an uncorrelated signal, where the underlying probability doesn't change, as in the first example of the previous section.

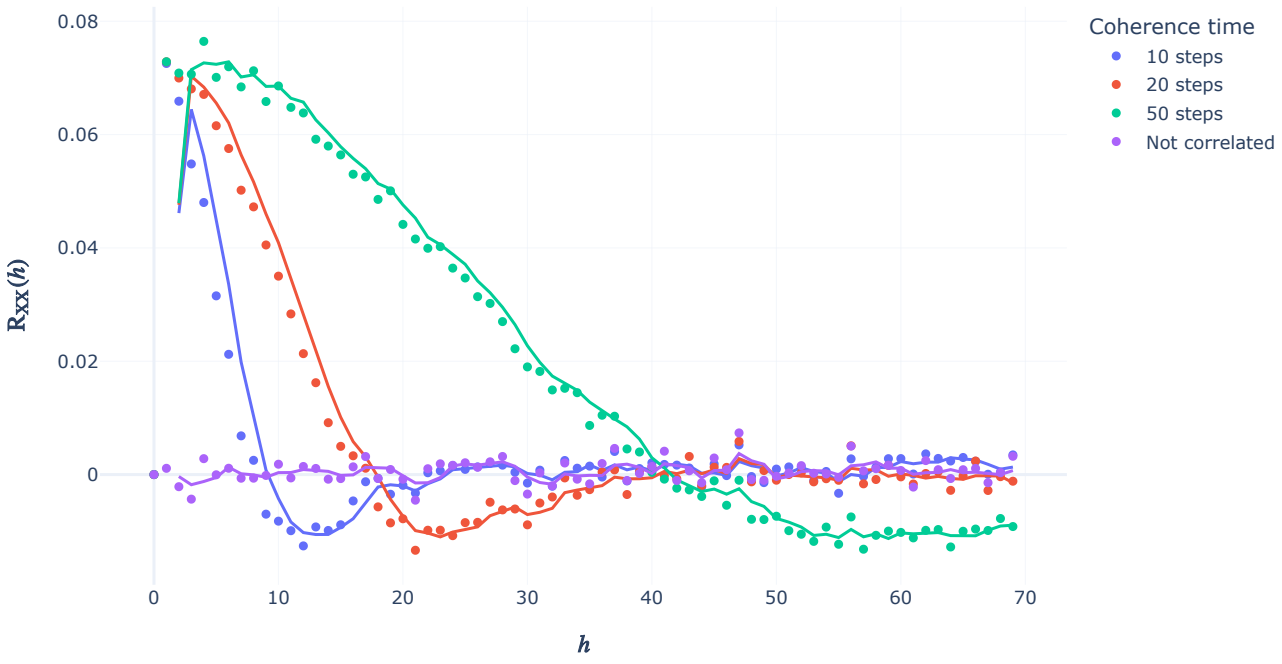

*Figure 5.6. The autocorrelation of three different bunched signals, with coherence times at roughly 10, 20 and 50 steps along with a totally uncorrelated signal.*

Here the signals are generated such that they have a coherence time $t_{\mathrm{coh}}$ of roughly 10, 20 and 50 steps. By sampling these signals at sampling intervals much longer than the coherence time $t_{\mathrm{sample}} \gg t_{\mathrm{coh}}$ we get the same inverse square root relation as we have derived for the $\mathrm{NEP}_{\tau}$. However when the sampling time nears the coherence time this relation no longer holds. Since detections shorter than a coherence time apart are correlated the overall uncertainty drops.

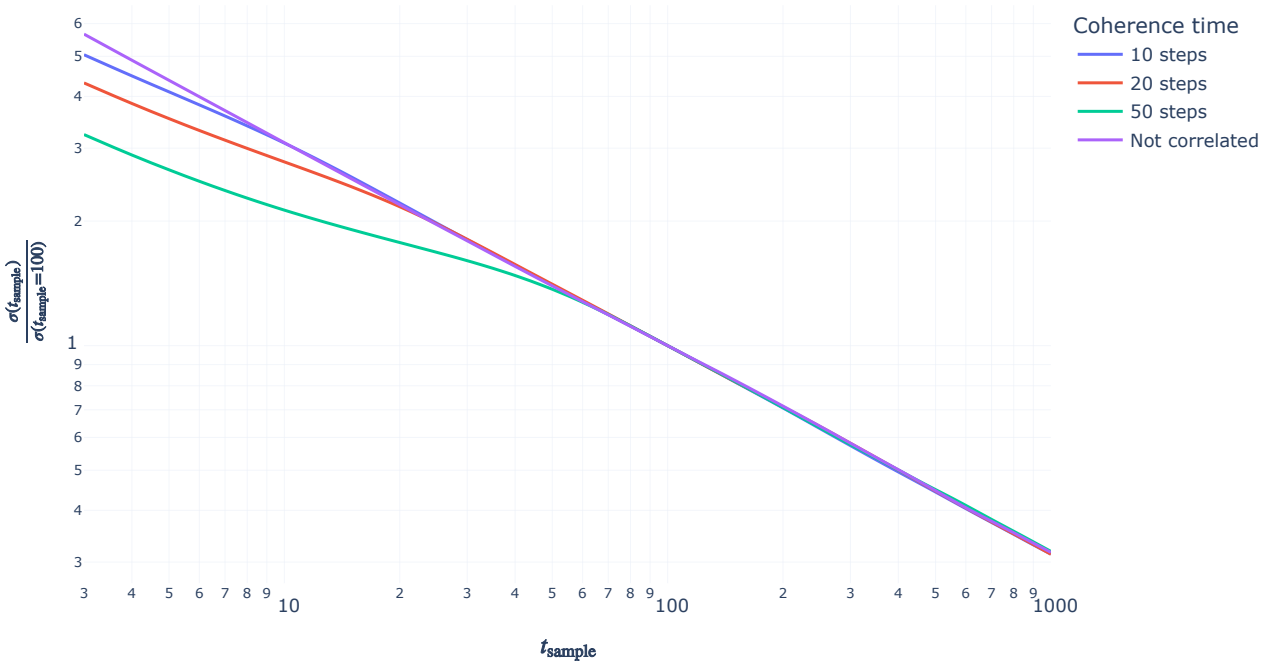


*Figure 5.7. When the sampling time drops below the coherence time the inverse square root relation doesn't hold any longer.*

This result shows the difference between the stochastic and the non-stochastic effects of photon bunching. It is the reason why we can model the bunching term as white noise as long as the integration time $\tau$ stays clear of the coherence time.

## The Filter Matrix

From eq $(5.8)$ we can see that we need a two dimensional function $\eta\left(\nu_i, j\right)$ to go from a one dimensional $\mathrm{PSD}$ to a power spectrum for each filter channel. We do this programmatically by calculating a matrix that takes in a vector containing the $\mathrm{PSD}$ at each integration frequency and use that to calculate the power loading by this $\mathrm{PSD}$ on each channel.

Shown in the figure below is a visualization of how this filter matrix might look like.

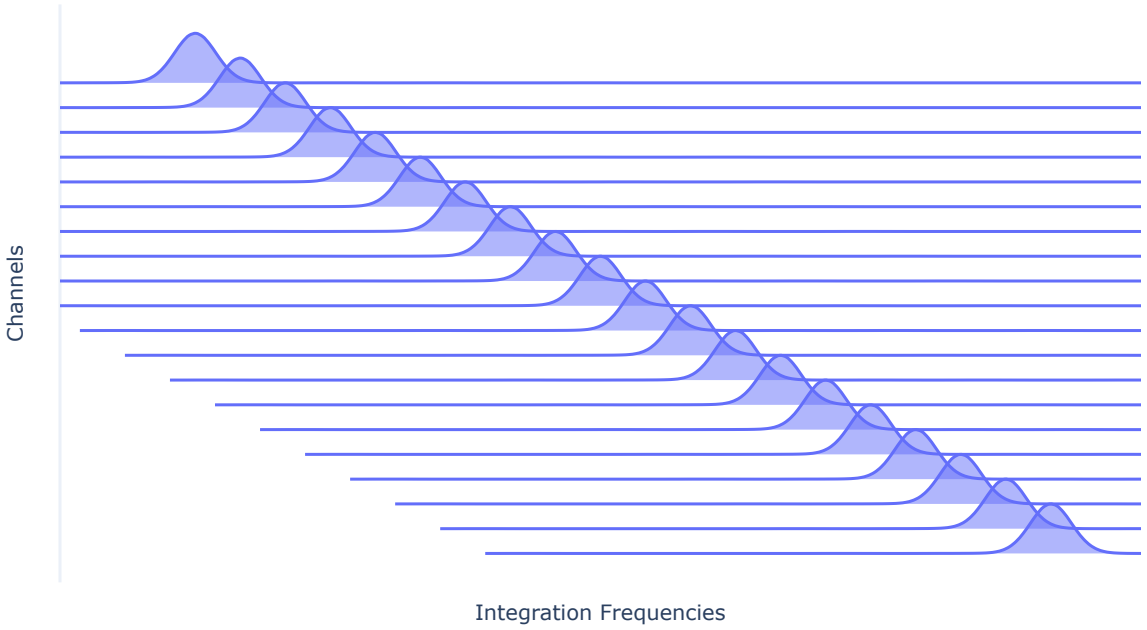


*Figure 5.8. A visual interpretation of the filter matrix. Only 20 channels are shown.*

With this framework in place it is easy to swap out the generated filter with another, more realistic model of the filters. The figure below shows a simulated filter transmission curve for the DESHIMA 2.0 chip.

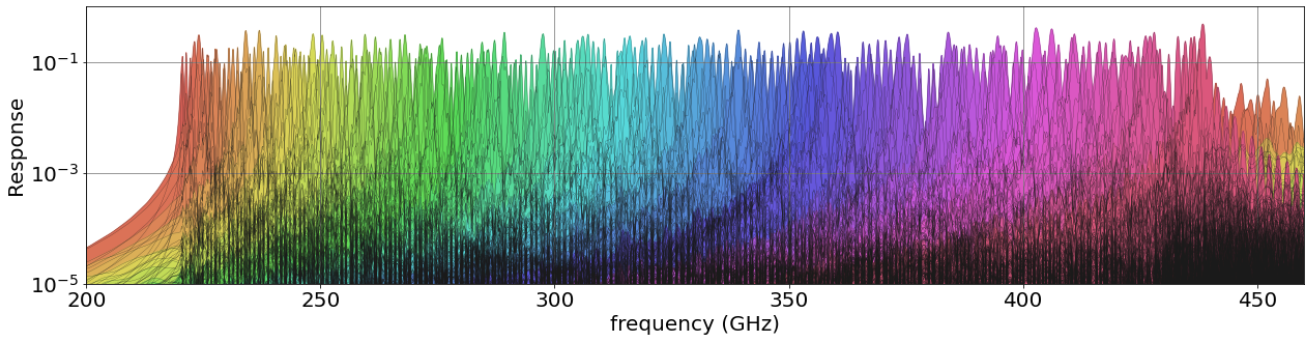


*Figure 5.9. A simulated filter profile of the DESHIMA 2.0 spectrometer*

As you can see, the filters aren't all equally efficient and wide, nor are they perfectly Lorentzian. In the figure below all 346 bins and the corresponding values of $R$ are plotted, with the size corresponding to the transmission.

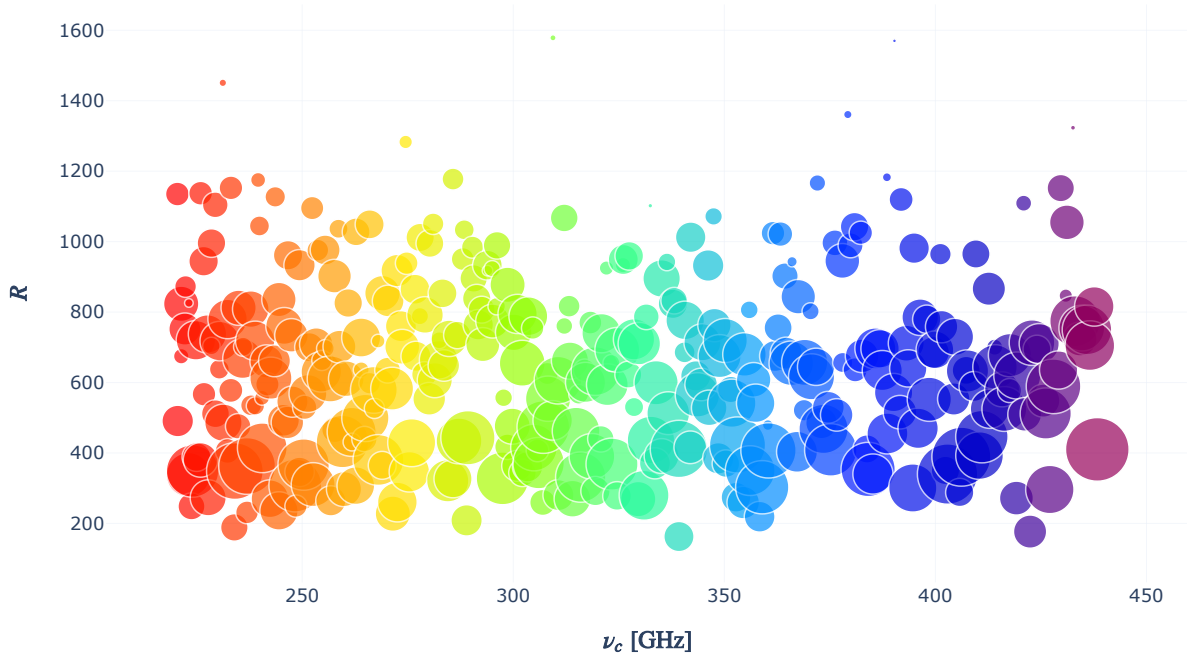


*Figure 5.10. The variations of this simulated filter are clear in this plot. The size corresponds to the transmission. Hover over and the $\chi^2$ parameter of the fit is shown for each channel.*

While using a perfect Lorentzian approximation for the filter profiles for each channel is better than the center frequency sampling that is done now, it might be more advantageous to be able to use simulated or measured profiles. The filter matrix will therefore, depending on the users choice, be either generated via Lorentzian curves or loaded in via a file.

## Transforming the calculated noise

Once the $\mathrm{NEP}$ has been calculated, it needs to be compared to a source in order to calculate the signal to noise. This can be done by generating various signals that are fed through the entire optical chain again and compare the power these impart on the detectors to the $\mathrm{NEP}$ we calculated. Another, crude but nevertheless convenient estimation can be acquired by transforming the noise back into more usable and define the sensitivity of the instrument that way. This model will focus on the latter.

We calculate the *source coupling* through a quantity named the Noise Equivalent (Source) Flux $\mathrm{NEF}$. The $\mathrm{NEF}$ is defined as the flux a source needs to impinge on the detector for it to equal the $\mathrm{NEP}$ in strength and is therefore our sensitivity: a source with a flux lower than the $\mathrm{NEF}$ will be hidden in the noise of the measurement data during an integration time of $1\ s$. Take note that the $\mathrm{NEF}$ is defined for an integration time of $\tau = 1$ s, rather than $\tau = 0.5$ s as is the case for the $\mathrm{NEP}$. The $\mathrm{NEF}$ is given by:

$$\mathrm{NEF} = \frac{\mathrm{NEP}_{\mathrm{inst},\tau=0.5\mathrm{s}}}{\eta_{\mathrm{sw}}\sqrt{2}A_g} = \frac{\mathrm{NEP}_{\tau=0.5\mathrm{s}}}{\eta_{\mathrm{inst}}\eta_{\mathrm{sw}}\sqrt{2}A_g} \tag{5.15}$$

with $A_g$ the area of the telescope, $\eta_{\mathrm{sw}}$ the aggregate efficiency from the source up to and including the window of the cryostat chamber DESHIMA is housed in and $\eta_{\mathrm{inst}}$ the instrument efficiency: the aggregate of all the efficiencies within the cryostat. The first two remain unchanged throughout the

modifications discussed in this chapter, however $\eta_{\text{inst}}$ is dependent on the filter efficiency and is therefore modified.

Since the calculation of the $\text{NEP}_{\tau=0.5\text{s}}$ as in $(5.13)$ collapses the noise equivalent power down to a single value per channel, we can't use the efficiency as calculated for the integration bins to go back through the system in order to calculate the source coupling. Instead there are two different approximations we can take to calculate the source coupling: an in-band and a full band approximation

### In-band Source Coupling

The in-band approximation is used for spectral sources. A spectral source is defined as an object that transmits only within the bandwidth of a single filter channel, where we define the bandwidth as the $\text{FWHM}$

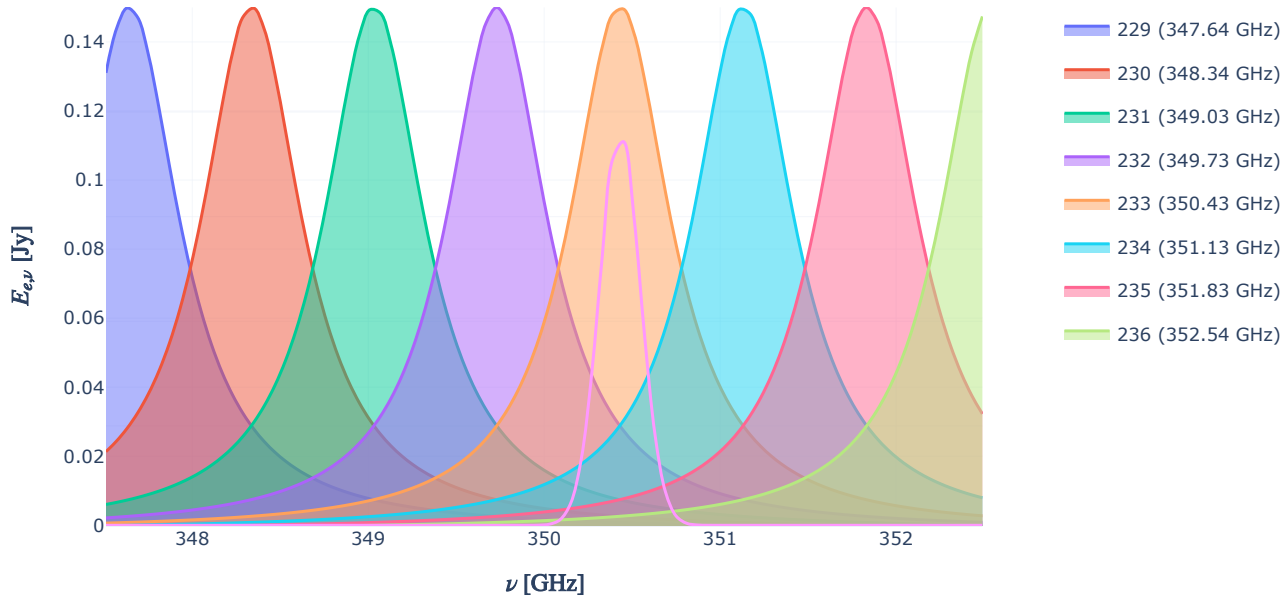


*Figure 5.11. A spectral source is defined as a source that fully fits within the bandwidth of a channel. Shown here for a Lorentzian filter*

In order to get a single value of an efficiency, let's say $\eta_{\text{inst}}$, over the full in-band bandwidth, I take a weighted average over the $\text{FWHM}$ where the weights are given by the filter efficiency $\eta\left(\nu, j\right)$.

$$\eta_{\text{inst,j}} = \frac{\int_{\nu_j-\gamma}^{\nu_j+\gamma} \eta_{\text{inst}}\left(\nu\right) \eta\left(\nu, j\right) d\nu}{\int_{\nu_j-\gamma}^{\nu_j+\gamma} \eta\left(\nu, j\right) d\nu} \tag{5.16}$$

This ensures that the efficiency per channel is normalized such that I can use the box-filter approximation on our way back through the system.

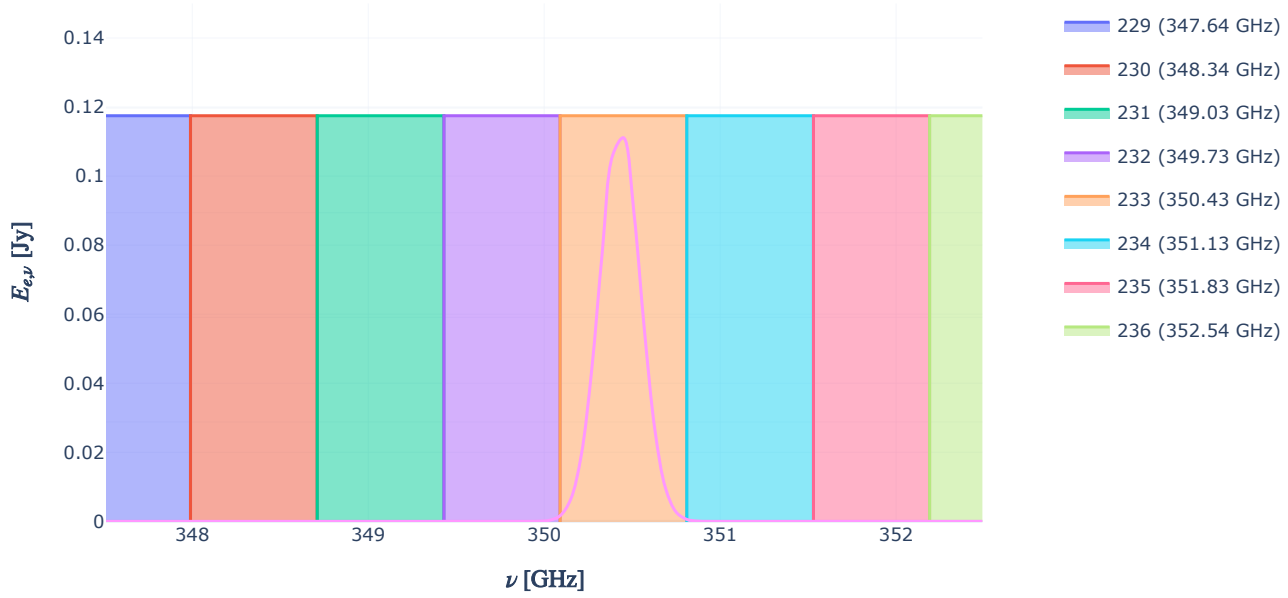


*Figure 5.12. Because spectral sources fit within the bandwidth of a single channel, the box-approximation holds very well.*

## Full-band Source Coupling

Besides spectral sources, astronomical objects also radiate a continuous spectrum, through blackbody radiation:

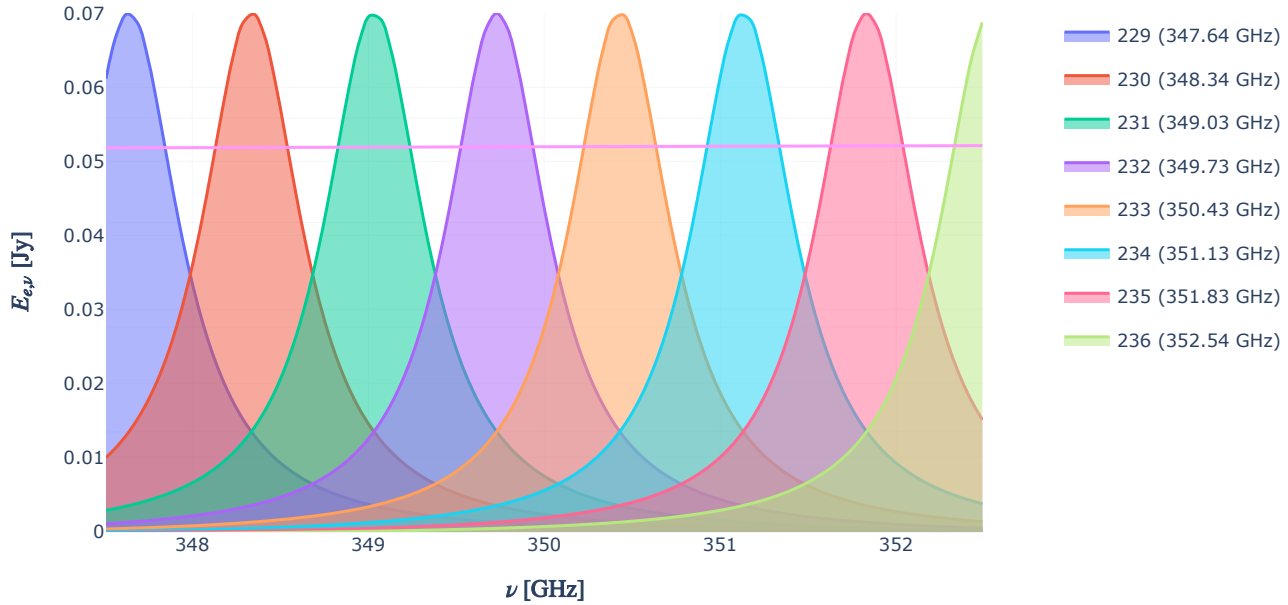


*Figure 5.13. The continuum of blackbody radiation loads the entire channel. Because it varies so slowly over the channel, it can be assumed as constant over a channel and the box filter approximation holds too.*

Because this continuum source is as near as makes no difference constant over the frequency bin, we can model it's transmission by another box-filter, with double the bandwidth of the spectral case, as I have derived previously.

In this case, the efficiencies are calculated using another weighted average, weighted over the full band this time

$$\eta_{\text{inst,j}} = \frac{\int_0^\infty \eta\left(\nu\right) \eta\left(\nu, j\right) d\nu}{\int_0^\infty \eta_{\text{filter}}\left(\nu, j\right) d\nu} \tag{5.17}$$

## The Final Model

Using these two approximations, the NEP can be transformed back through the system and to the sky again as the $\mathrm{NEF}$. In order to transform the $\mathrm{NEF}$ to a flux *density*, we simply divide by the effective bandwidth for either the line or spectral case and get the noise equivalent flux density $\mathrm{NEFD}$.

This means that the total model looks like this:

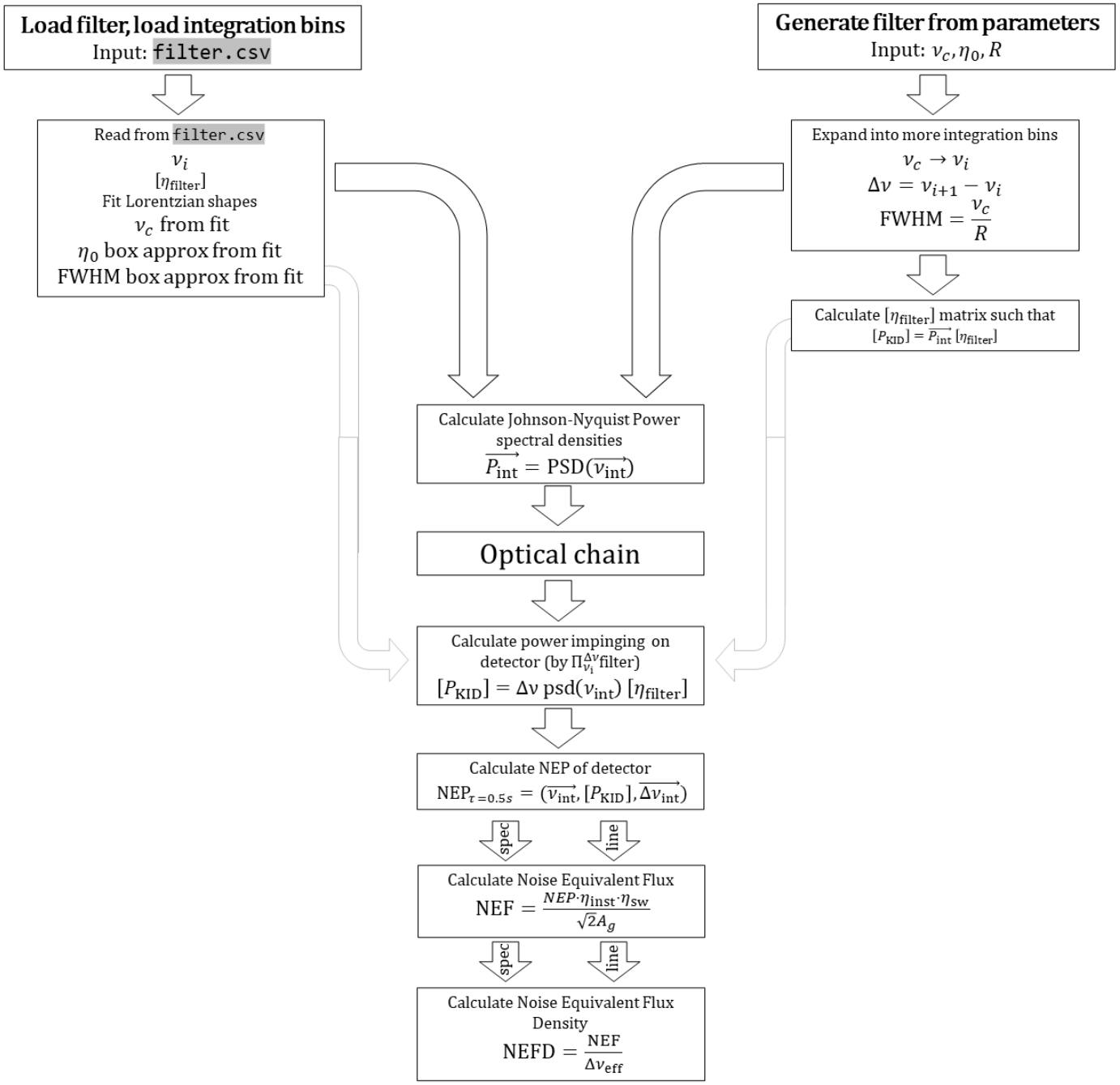


*Figure 5.14. The updated model. Noteworthy changes are the filter and the parallel line and spectral source paths.*

# Bibliography


1. [1]J. Zmuidzinas, "Thermal noise and correlations in photon detection," *Applied Optics*, vol. 42, no. 25, p. 4989, 2003, doi: 10.1364/ao.42.004989.
2. [2]A. Endo *et al.*, "First light demonstration of the integrated superconducting spectrometer," *Nature Astronomy*, vol. 3, no. 11, pp. 989–996, 2019, doi: 10.1038/s41550-019-0850-8.
3. [3]B. L. Morgan and L. Mandel, "Measurement of Photon Bunching in a Thermal Light Beam," *Physical Review Letters*, vol. 16, no. 22, pp. 1012–1015, 1966, doi: 10.1103/physrevlett.16.1012.
4. [4]K. Spencer and O. S. Community, "opensimplex v0.3," *pypi.org*. Open Source, Dec-2021 [Online]. Available at: https://pypi.org/project/opensimplex/

# Results

Looking at the changes and verifying the model

Jan 3, 2022 • 4 min read



To verify the changes made to the model, let's compare it to the old model.

## Impinged Power

The new model calculates the $P_{\mathrm{KID}}$ of the $j$th channel as a Riemann sum approximation of

$$P_{\mathrm{KID},j} = \int_0^\infty \mathrm{PSD}_{\mathrm{filter}}\left(\nu\right) \eta\left(j, \nu\right) d\nu \tag{6.1}$$

whereas the old model approximated this integral as a square filter with width $\Delta\nu = \mathrm{FWHM}$. Therefore the new model takes in a much wider range of the $\mathrm{PSD}$ and is thus expected to be higher in local minima and lower in local maxima of the $\mathrm{PSD}$.

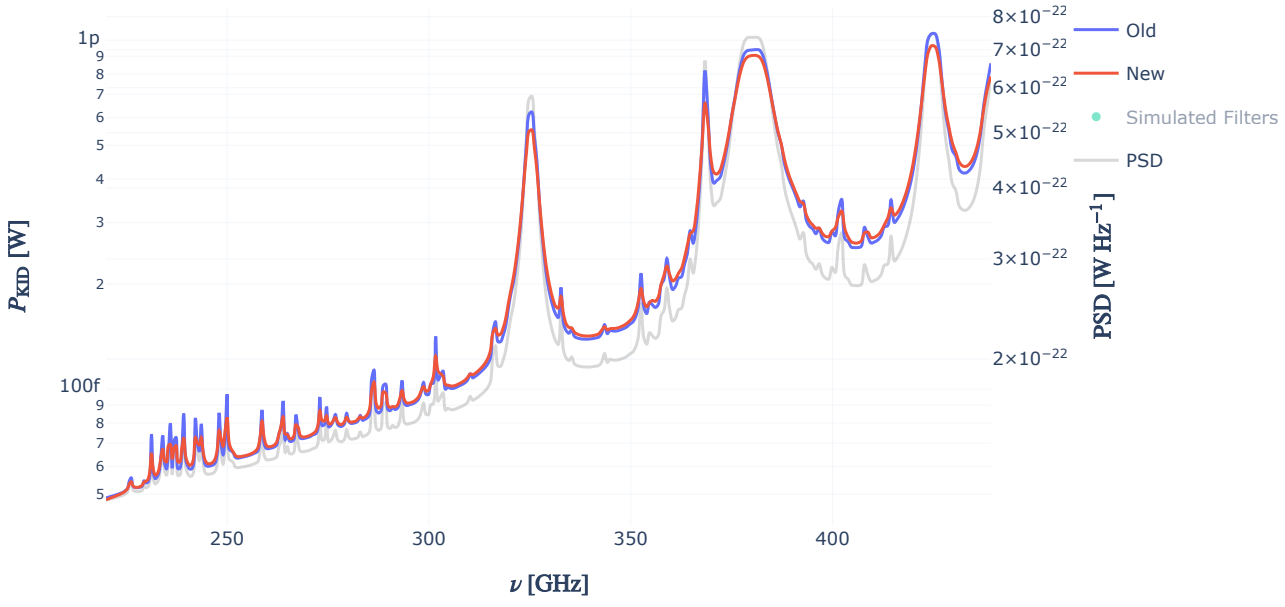

*Figure 6.1. The old and new power per channel, overlayed over the Power spectral density. The left y-axis shows power while the right y-axis shows the PSD. The simulated filters are hidden by default.*

The figure above behaves exactly as expected.

## Noise Equivalent Power

The $\mathrm{NEP}$ is calculated using the Riemann sum of the following integral

$$\mathrm{NEP}_{\tau=0.5\mathrm{s},j} = 2\int_0^\infty h\nu\eta\left(\nu,j\right)\mathrm{PSD} + \eta(\nu,j)^2\mathrm{PSD}^2 + \frac{2\Delta_{\mathrm{Al}}}{\eta_{\mathrm{pb}}}\eta\left(\nu,j\right)\mathrm{PSD}d\nu \qquad (6.2)$$

where the three separate terms are the Poisson term, the bunching term and the recombination term respectively. Plotting this integral yields the following result:

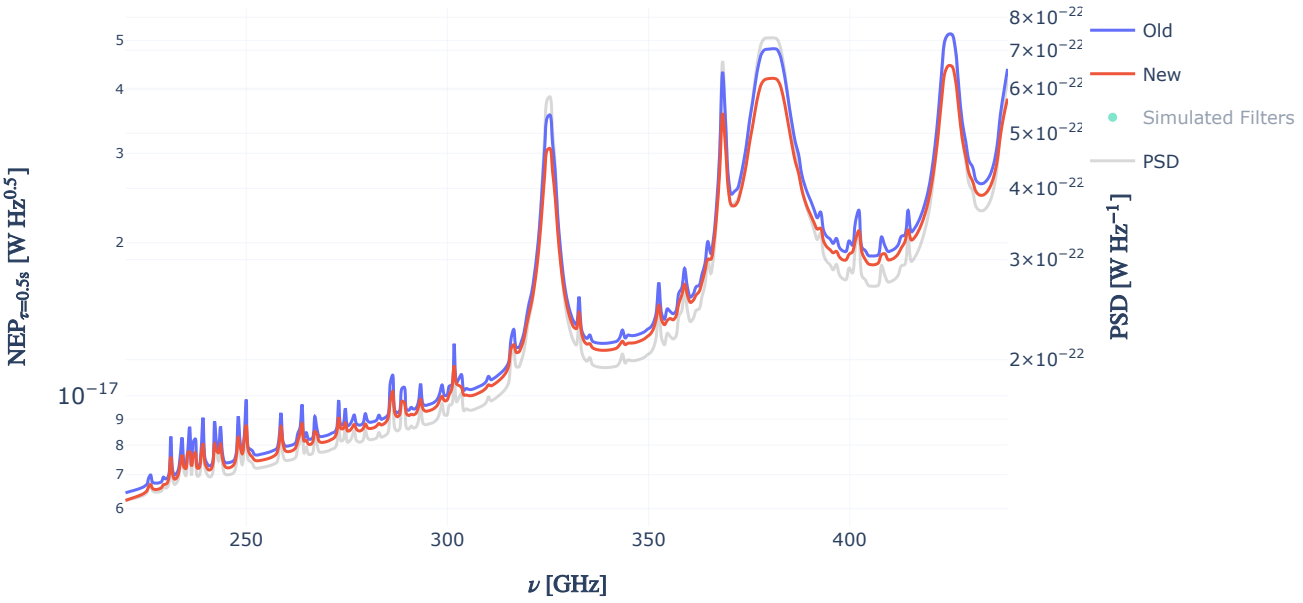


*Figure 6.2. The old and new Noise Equivalent Power per channel, overlayed over the Power spectral density. The left y-axis shows the NEP while the right y-axis shows the PSD. The simulated filters are hidden by default.*

As we can see, and as is expected, the new model has a lower $\mathrm{NEP}$. Plotting the three separate terms, we get the following:

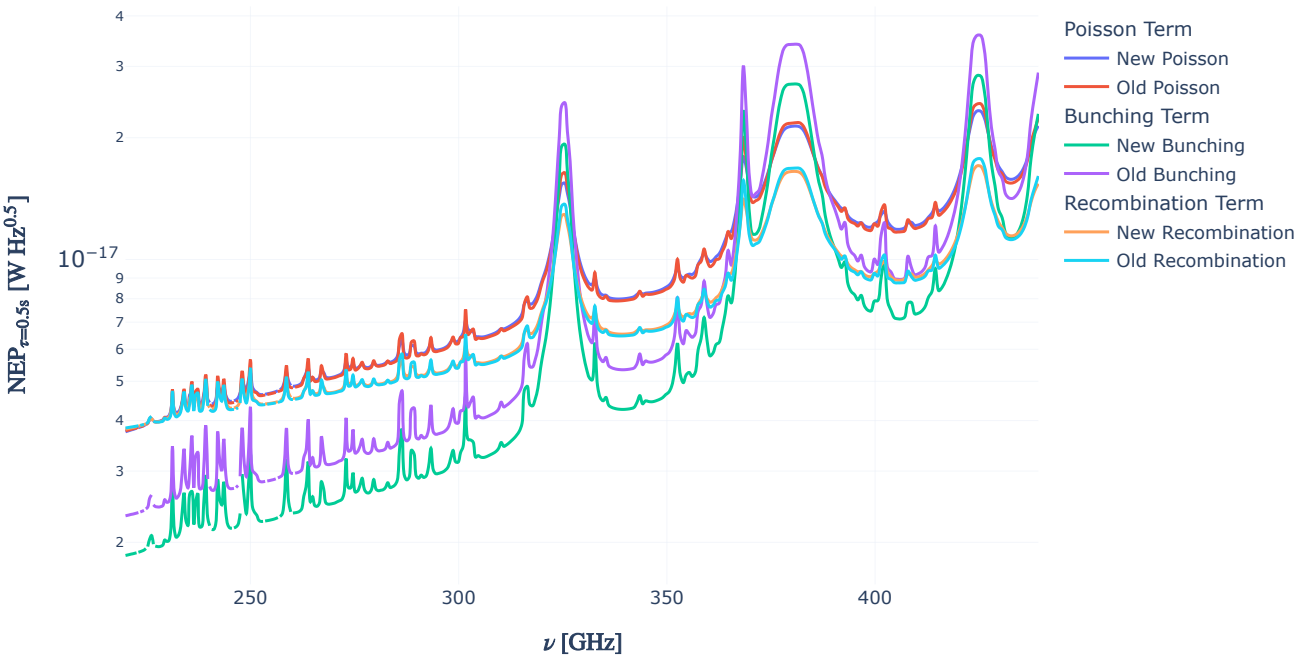


*Figure 6.3. The three terms of the NEP plotted. Toggle in the legend to compare different terms.*

As is clear from the figure, the terms behave as expected, with the new model 'smoothing' over the local extrema in the Poisson and recombination term, but leaving them otherwise unchanged. The bunching term is however smaller in the new model.

### The Bunching Term

As we have seen the old approximation overestimated the bunching term by a factor of $\pi/2$. For a constant $\mathrm{PSD}$ The bunching term is given by

$$\mathrm{NEP}_{\tau=0.5\mathrm{s},j,\mathrm{bunching}} = \frac{8}{\pi}\mathrm{PSD}^2\eta_0^2\mathrm{FWHM} \tag{6.3}$$

Whereas the old model this was given by

$$\mathrm{NEP}_{\tau=0.5\mathrm{s},j,\mathrm{bunching}} = 4\mathrm{PSD}^2\eta_0^2\mathrm{FWHM} \tag{6.4}$$

We can verify this in the following figure, where I have divided the old model by the new model. From our calculations, this should be on average $\pi/2$

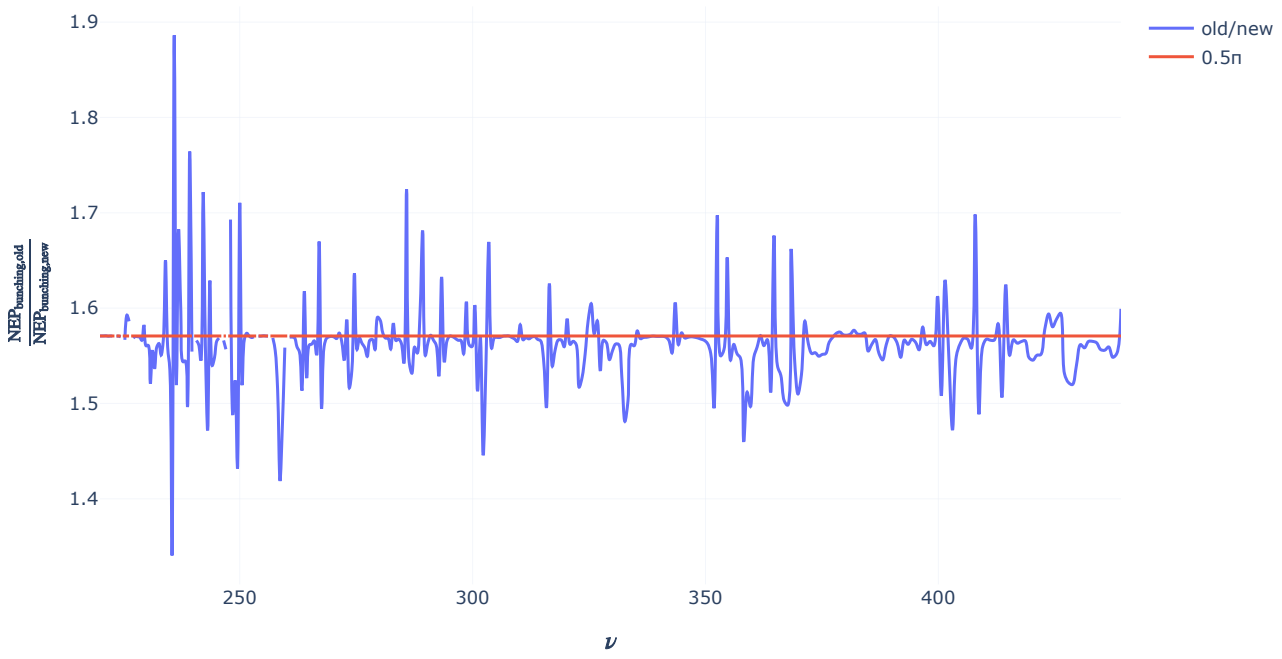


*Figure 6.4. The ratio between the old and new bunching terms. A constant line of half π is plotted as indication.*

## Simulated filterbank

In order to compare the simulated filterbank to the new and old models, it is more advantageous to look at the $\mathrm{NEP}_{\mathrm{inst}}$. Recall that the $\mathrm{NEP}_{\mathrm{inst}}$ is the $\mathrm{NEP}$ divided by the total instrument efficiency: comparing an 'unnormalized' $\mathrm{NEP}$ is deceiving, since a lower noise equivalent power does not necessarily mean a higher signal to noise ratio.

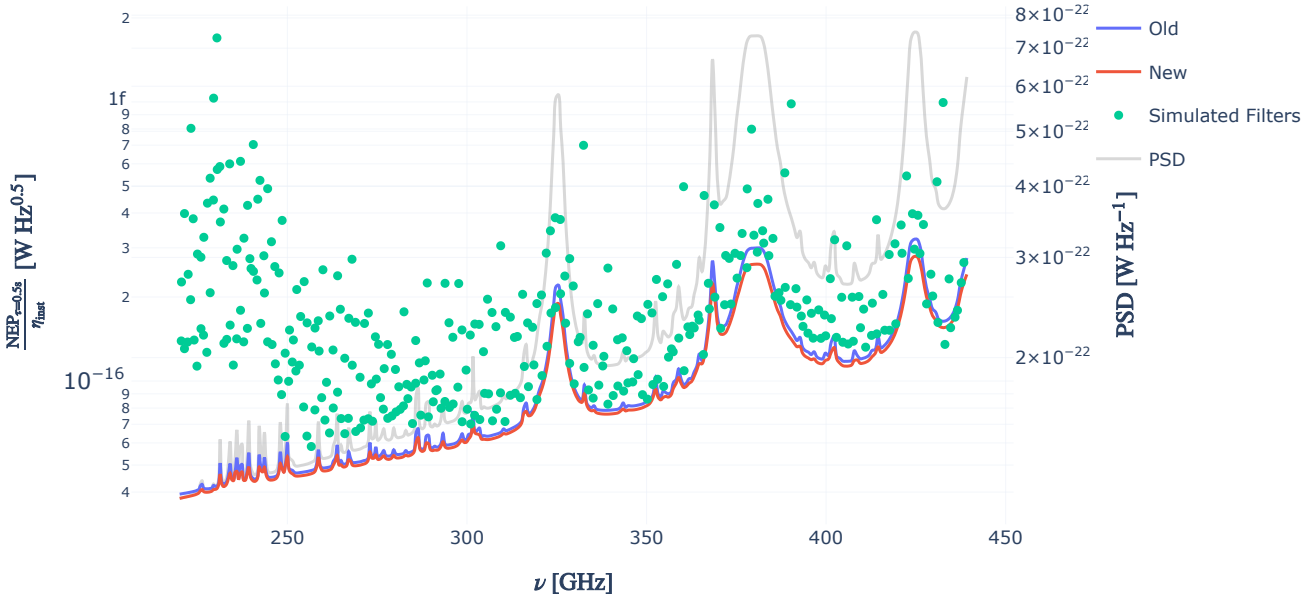

*Figure 6.5. The instrument NEP of the old, new and newly simulated filters. The left y-axis shows the instrument NEP while the right y-axis shows the PSD.*

Since the ideal filter model is generated with parameters which are the target for DESHIMA, the simulated filters behave almost without exception worse than the perfect Lorentzian filters. The outliers have very low transmissions, meaning that in order to improve the sensitivity the transmission needs to increase.

## Noise Equivalent Flux Density

As described in the previous chapter, another modification to the model is the calculation of the $\mathrm{NEFD}$, both for a spectral and a continuum source, with the latter being twice the former.

Let's take a look at $\mathrm{NEFD}_{\mathrm{cont}}$ first.

### The Continuum Case

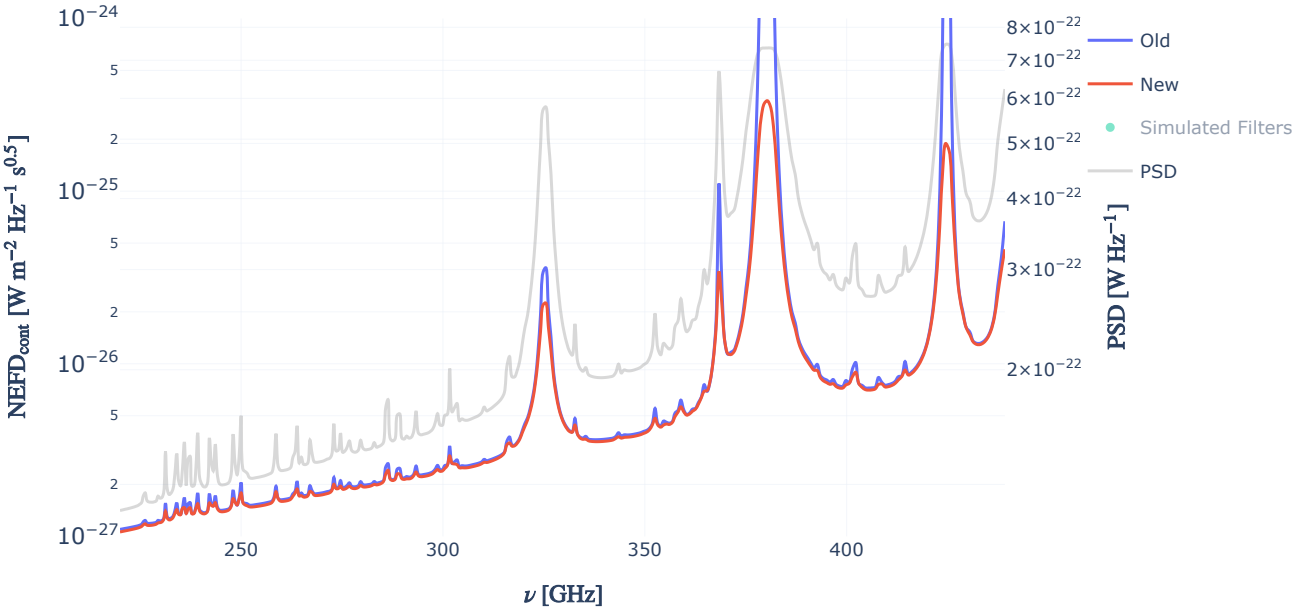


*Figure 6.6. The different Noise Equivalent Flux Density for the continuum case. The left y-axis shows power while the right y-axis shows the PSD.*

Because of the limited sampling range of the old model, the value of $\eta_{\mathrm{sw}}$ is (very close to) zero for channels where the atmospheric transmission is very close to zero. Because the new model takes the wide filters into account, this effect is lowered somewhat, since these channels are still loaded through the fringes of the Lorentzian when the atmosphere is opaque in the center.

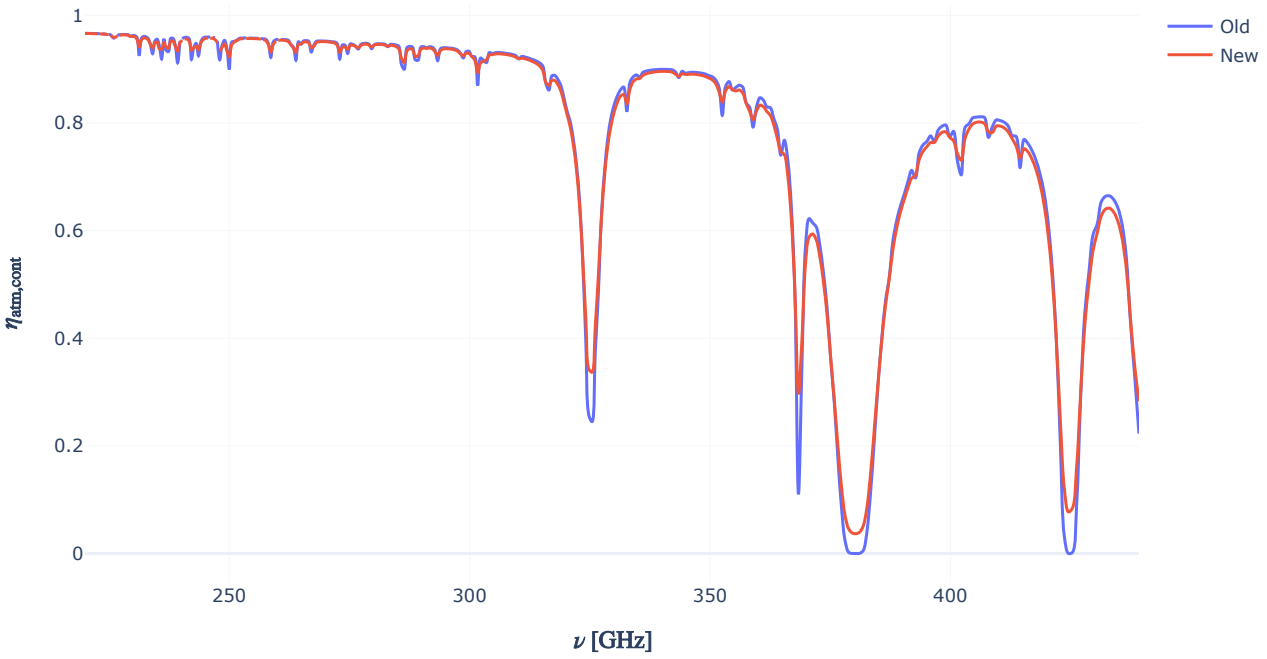


*Figure 6.7. The different atmospheric transmissions over the full filter band.*

## The Spectral Case

For the spectral case this difference is resolved, as spectral sources *by definition* don't load the fringes of a filter channel. This means that the atmospheric transmission isn't smoothed at its extrema.

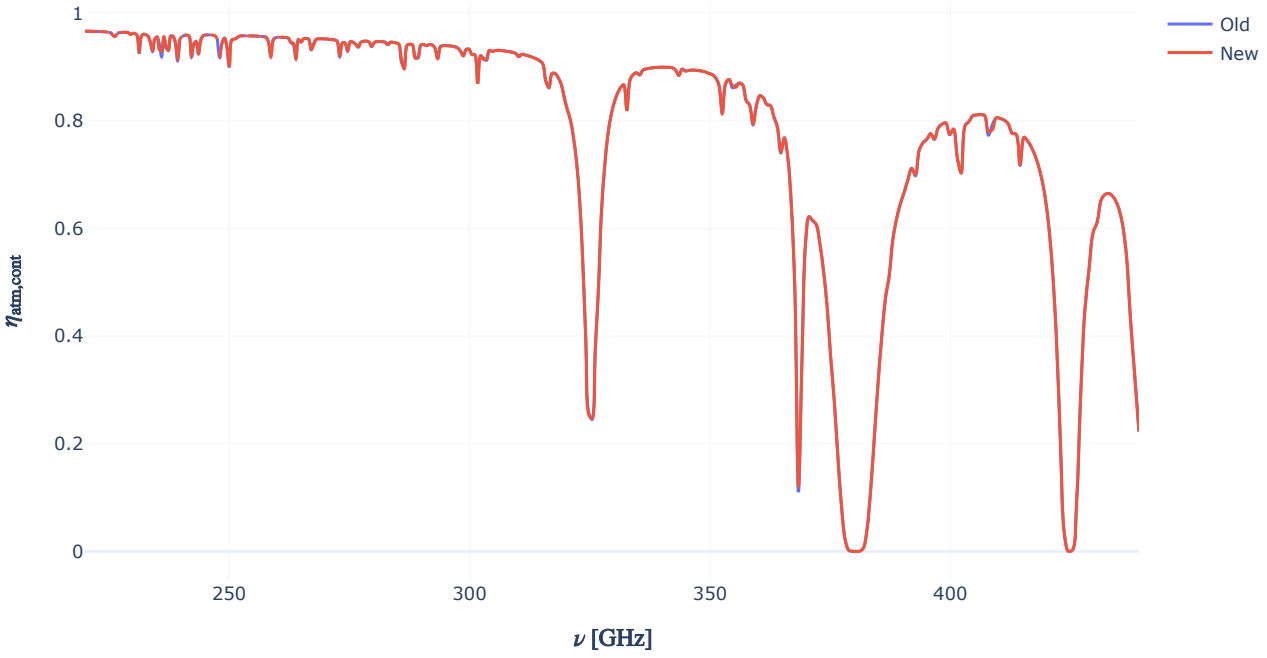


*Figure 6.8. The different atmospheric transmissions over just the bandwidth of the filters.*

This in turn means that the $\mathrm{NEFD}_{\mathrm{spec}}$ also approaches infinity at places where the atmospheric transmission approaches zero.

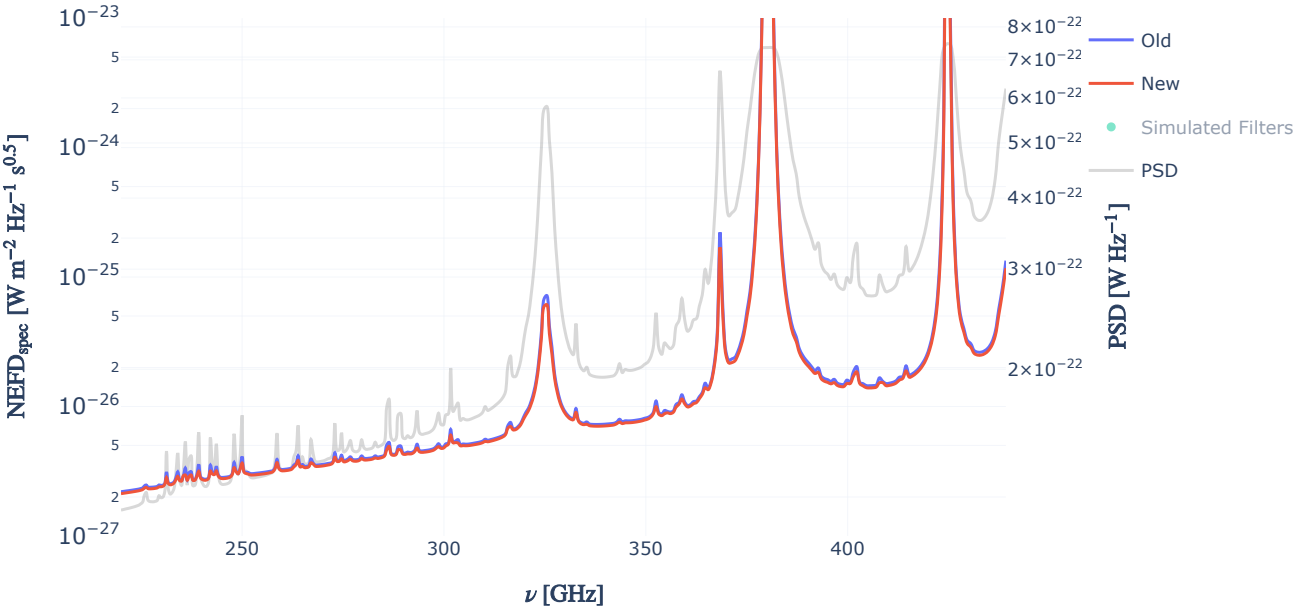


*Figure 6.9. The different Noise Equivalent Flux Density for the spectral case. The left y-axis shows power while the right y-axis shows the PSD.*

# Bibliography

# Conclusion

Concluding the research

Jan 2, 2022 • 4 min read



In the previous chapters I have first explained photon bunching and photon statistics qualitatively and then explored its impact on the DESHIMA spectrometer quantitatively. I have shown a model for the probabilistics behind photon bunching, showing that it is not the detection itself that triggers bunching, but rather a change in the underlying photon probability. I have also discussed the coherence time, defined as the timescale below which the non-stochastic effects of photon bunching take hold. The coherence time is related to the bandwidth by

$$\tau_{\mathrm{coh}} \approx \frac{1}{\Delta\nu} \tag{7.1}$$

After exploring photon statistics, I discussed photon noise induced by both Poisson statistics and photon bunching. The total noise equivalent power induced by photon noise is given by[1]:

$$\mathrm{NEP}^2_{\tau,\mathrm{ph}} = \frac{1}{\tau}\int_0^\infty h\nu\eta\left(\nu\right)\mathrm{PSD} + \eta^2\left(\nu\right)\mathrm{PSD}^2 d\nu \tag{7.2}$$

Whereas the approximation given by [1] and used previously in calculating the sensitivity of the DESHIMA system[2] is found by approximating a very narrow bandwidth ($\nu \gg \Delta\nu$) and then approximating the integral by

$$\mathrm{NEP}^2_{\tau,\mathrm{ph}} = \frac{1}{\tau}\left(h\nu\eta_0\mathrm{PSD}\Delta\nu + \eta_0^2\mathrm{PSD}^2\Delta\nu\right) \tag{7.3}$$

this approximation overestimates the photon bunching effects for a filter $\eta\left(\nu\right)$ with a Lorentzian shape. I have shown that, in the case of a Lorentzian filter and a flat $\mathrm{PSD}$, eq. $(7.3)$ collapses to

$$\mathrm{NEP}^2_{\tau,\mathrm{ph}} = \frac{1}{\tau}\left(h\nu\eta_0\mathrm{PSD}\Delta\nu + \frac{2}{\pi}\eta_0^2\mathrm{PSD}^2\Delta\nu\right) \tag{7.4}$$

with $\Delta\nu$ the $\mathrm{FWHM}$ of the filter. This factor of $\pi/2$ is explained by the width of the Lorentzian filter. Previously the bandwidth of the filters was assumed to be negligible, resulting in an overestimation of the bunching. Because the photons that are impinging on the detector span a bigger bandwidth they bunch less.

The definition for the noise equivalent power $\mathrm{NEP}_{\tau=0.5s}$ means that it is defined at an integration time of $\tau = 0.5\ s$. For different integration times the $\mathrm{NEP}_\tau$ is defined as:

$$\mathrm{NEP}_\tau = \frac{1}{\sqrt{2\tau}}\mathrm{NEP}_{\tau=0.5\mathrm{s}} \tag{7.5}$$

However, this assumes that the integration time is much bigger than the coherence time of the detected photons $\tau \gg t_{\mathrm{coh}}$. Due to correlation of photons within the coherence time the $\mathrm{NEP}_\tau$ drops when the

integration time approaches and subceeds the coherence time.

Besides this algebraic result for a Lorentzian filter I have also modified the existing `deshima-sensitivity` [3] model to calculate the integral in eq. $(7.3)$ not just for mathematical filters, but for arbitrary filter shapes loaded in via a file. This allows researchers to compare the sensitivity of various designs in software.

To verify the changes to the model I have compared it with the old model and confirmed that in the case of perfect Lorentzian filter the latter overestimated the bunching noise by a factor of $\pi/2$, even on average for a non-flat $\mathrm{PSD}$. Other than this, the changes affect the power and noise in local extrema of the $\mathrm{PSD}$, where the old model didn't integrate over the full range of the filter and therefore took the $\mathrm{PSD}$ as a flat spectrum locally.

## The future of this research

Because the model now more closely resembles the physics that is occurring inside the filter section of a DESHIMA spectrometer, it can be used to compare different filter designs in the `deshima-sensitivity` package itself. This is an important tool to compare filter topologies differing from Lorentzian shapes. Paired with methods to accurately describe the coupling of a source to the detector it can be used to very accurately calculate the signal to noise ratio of a specific filter profile, aiding in the experimental design of different filter profiles. Such research is in progress and as such the model will immediately be put to use.

The improved accuracy of the approximation in the bunching term for a Lorentzian filter can prove useful when designing the DESHIMA spectrometer, as it gives a more physically rigorous target of the maximum sensitivity the DESHIMA spectrometer can strive towards.

Finally, this thesis gives a thorough overview of photon statistics in astronomical measurement and of photon bunching in particular and as such can be a great teaching tool. My thesis supervisor, dr. Akira Endo, has been very interested in using this as teaching material for courses he gives on the subject and I am looking forward to helping other students understand photon statistics and photon bunching better.

## Bibliography


1. [1]J. Zmuidzinas, “Thermal noise and correlations in photon detection,” *Applied Optics*, vol. 42, no. 25, p. 4989, 2003, doi: 10.1364/ao.42.004989.
2. [2]A. Endo *et al.*, “First light demonstration of the integrated superconducting spectrometer,” *Nature Astronomy*, vol. 3, no. 11, pp. 989–996, 2019, doi: 10.1038/s41550-019-0850-8.
3. [3]A. Endo and A. Taniguchi, “deshima-sensitivity v0.3.0,” *pypi.org*. Open Source, Jun-2021 [Online]. Available at: https://pypi.org/project/deshima-sensitivity/

# Appendix

Links to the model and a full bibliography

Jan 1, 2022 • 4 min read



## The model

The model can be found on my personal Github. An up to date version, that may have been changed since writing this report can be found at the deshima-sensitivity github and can be used via the python package installer `pip install deshima-sensitivity`.

## Bibliography


1. [1]E. Optics, "Introduction to Optical Prisms," *Edmund Optics*. [Online]. Available at: https://www.edmundoptics.eu/knowledge-center/application-notes/optics/introduction-to-optical-prisms/
2. [2]R. Nave, "Carbon Energy Levels," *hyperphysics.phy*. [Online]. Available at: http://hyperphysics.phy-astr.gsu.edu/hbase/Atomic/carbon.html
3. [3]A. Einstein, "Zur Elektrodynamik bewegter Körper," *Annalen der Physik*, vol. 322, no. 10, pp. 891–921, 1905, doi: 10.1002/andp.19053221004.
4. [4]V. M. Slipher, "Radial velocity observations of spiral nebulae," *The Observatory*, vol. 40, pp. 304–306, 1917, doi: 10.1002/andp.19053221004.
5. [5]B. L. Morgan and L. Mandel, "Measurement of Photon Bunching in a Thermal Light Beam," *Physical Review Letters*, vol. 16, no. 22, pp. 1012–1015, 1966, doi: 10.1103/physrevlett.16.1012.
6. [6]R. Meservey and P. M. Tedrow, "Measurements of the Kinetic Inductance of Superconducting Linear Structures," *Journal of Applied Physics*, vol. 40, no. 5, pp. 2028–2034, 1969, doi: 10.1063/1.1657905.
7. [7]P. L. Richards, "Bolometers for infrared and millimeter waves," *Journal of Applied Physics*, vol. 76, no. 1, pp. 1–24, 1994, doi: 10.1063/1.357128.
8. [8]G. P. Tozzi, P. D. Feldman, and M. C. Festou, "Origin and production of C( 1 D) atoms in cometary comae," *Astronomy and Astrophysics*, vol. 330, pp. 753–763, 1998.
9. [9]A. Blain, "Submillimeter galaxies," *Physics Reports*, vol. 369, no. 2, pp. 111–176, Jan. 2002, doi: 10.1016/s0370-1573(02)00134-5.
10. [10]J. Zmuidzinas, "Thermal noise and correlations in photon detection," *Applied Optics*, vol. 42, no. 25, p. 4989, 2003, doi: 10.1364/ao.42.004989.
11. [11]H. Paul, *Introduction to quantum optics: from light quanta to quantum teleportation*. Cambridge University Press, 2004, pp. 127–153.
12. [12]A. J. Baker, *From z-machines to ALMA: (sub)millimeter spectroscopy of galaxies: proceedings of a workshop held at the North American ALMA Science Center of the National Radio Astronomy Observatory in Charlottesville, Virginia, United States, 12-14 January 2006*. Astronomical Soc. of the Pacific, 2007, p. 375.
13. [13]S. Leclercq, "Discussion about Noise Equivalent Power and its use for photon noise calculation," 2007 [Online]. Available at: https://www.iram.fr/ leclercq/Reports/About_NEP_photon_noise.pdf

14. [14]C. S. Turner, “Johnson Nyquist noise - clay’s DSP Page,” *Johnson-Nyquist Noise*. Wireless Systems Engineering, Inc., Jan-2007 [Online]. Available at: http://www.claysturner.com/dsp/Johnson-Nyquist%20Noise.pdf
15. [15]G. B. Taylor, C. L. Carilli, and R. A. Perley, *Synthesis imaging in radio astronomy II: a collection of lectures from the Sixth NRAO/NMIMT Synthesis Imaging Summer School held at Socorro, New Mexico, USA, 17-23 June 1998*. Astronomical Society of the Pacific, 2008, pp. 671–688.
16. [16]D. R. Jacobsen, “Atacama Submillimeter Telescope Experiment complex, Chile.” English Wikipedia, 06-Jul-2008 [Online]. Available at: https://commons.wikimedia.org/w/index.php?curid=60009729
17. [17]H. Hahn, “Diagram Reflector Cassegrain.” Wikimedia, 01-Apr-2010 [Online]. Available at: https://nl.m.wikipedia.org/wiki/Bestand:Diagram_Reflector_Cassegrain.svg
18. [18]F. M. Dekking, C. Kraaikamp, L. H.P, and L. E. Meester, *A modern introduction to probability and statistics: Understanding why and how*. Springer-Verlag, 2011.
19. [19]J. Baselmans, “Kinetic inductance detectors,” *Journal of Low Temperature Physics*, vol. 167, no. 3-4, pp. 292–304, 2012, doi: 10.1007/s10909-011-0448-8.
20. [20]M. Krottenmüller, “Photon Statistics,” *Technische Universität München*. May-2013 [Online]. Available at: https://www.mpq.mpg.de/5020834/0508a_photon_statistics.pdf
21. [21]P. J. D. Visser, J. J. A. Baselmans, J. Bueno, N. Llombart, and T. M. Klapwijk, “Fluctuations in the electron system of a superconductor exposed to a photon flux,” *Nature Communications*, vol. 5, no. 1, 2014, doi: 10.1038/ncomms4130.
22. [22]P. J. de Visser, “Quasiparticle dynamics in aluminium superconducting microwave resonators,” Mar. 2014, doi: 10.4233/uuid:eae4c9fc-f90d-4c12-a878-8428ee4adb4c.
23. [23]D. R. Wilkins and S. J. Crass, “Institute of Astronomy,” *ALMA detects the most distant oxygen ever | Institute of Astronomy*. University of Cambridge, Jun-2016 [Online]. Available at: https://www.ast.cam.ac.uk/content/alma.detects.most.distant.oxygen.ever
24. [24]Y. Zhou *et al.*, “Superbunching Pseudothermal Light,” *Physical Review A*, vol. 95, no. 5, Mar. 2017, doi: 10.1103/physreva.95.053809.
25. [25]R. Garner, “Messier 16 (The Eagle Nebula),” *NASA*. NASA, Oct-2017 [Online]. Available at: https://www.nasa.gov/feature/goddard/2017/messier-16-the-eagle-nebula
26. [26]A. Endo *et al.*, “First light demonstration of the integrated superconducting spectrometer,” *Nature Astronomy*, vol. 3, no. 11, pp. 989–996, 2019, doi: 10.1038/s41550-019-0850-8.
27. [27]A. Endo *et al.*, “Wideband on-chip terahertz spectrometer based on a superconducting filterbank,” *Journal of Astronomical Telescopes, Instruments, and Systems*, vol. 5, no. 03, p. 1, 2019, doi: 10.1117/1.jatis.5.3.035004.
28. [28]E. et al. Huijten, “TiEMPO: Open-source time-dependent end-to-end model for simulating ground-based submillimeter astronomical observations,” *Millimeter, Submillimeter, and Far-Infrared Detectors and Instrumentation for Astronomy X*, 2020, doi: 10.1117/12.2561014.
29. [29]A. Lemke, “The visible light spectrum,” *Once Inc.* Aug-2020 [Online]. Available at: https://www.once.lighting/visible-light-spectrum/
30. [30]A. Endo, “Memo: Poisson limit and bunching limit of photon NEP: Deshima Kibela,” *Memo: Poisson limit and Bunching limit of Photon NEP*. Kibela, Nov-2020 [Online]. Available at: https://deshima.kibe.la/shared/entries/96349e15-acfa-474f-adf8-f21ebe25cda5
31. [31]T. Bakx and S. Brackenhoff, “galspec v0.2.6,” *pypi.org*. Open Source, Nov-2020 [Online]. Available at: https://pypi.org/project/opensimplex/
32. [32]A. Endo, “Session 2 | Line Emission and Cosmological Redshift ,” *EE3350TU Introduction to Radio Astronomy*. Nov-2020.
33. [33]A. Endo, “Session 4 | Photon Noise,” *EE3350TU Introduction to Radio Astronomy*. Dec-2020.

34. [34]M. Rybak *et al.*, “DESHIMA 2.0: Rapid redshift surveys and multi-line spectroscopy of dusty galaxies.” 2021.
35. [35]A. P. Laguna, K. Karatsu, D. Thoen, B. Murugesan rp, A. Endo, and J. Baselmans, “Terahertz Band-Pass Filters for Wideband Superconducting On-Chip Filter-Bank Spectrometers,” *IEEE Transactions on Terahertz Science and Technology*, vol. 11, no. 6, pp. 635–646, 2021, doi: 10.1109/tthz.2021.3095429.
36. [36]C. K. Alexander and M. N. Sadiku, *Fundamentals of Electric Circuits*, 7th ed. McGraw-Hill Education, 2021.
37. [37]A. Taniguchi *et al.*, “DESHIMA 2.0: development of an integrated superconducting spectrometer for science-grade astronomical observations.” 2021.
38. [38]A. Endo and A. Taniguchi, “deshima-sensitivity v0.3.0,” *pypi.org*. Open Source, Jun-2021 [Online]. Available at: https://pypi.org/project/deshima-sensitivity/
39. [39]K. Spencer and O. S. Community, “opensimplex v0.3,” *pypi.org*. Open Source, Dec-2021 [Online]. Available at: https://pypi.org/project/opensimplex/